

Wave-Mean Flow Interactions and Solar-Weather Effects

by

Alison F.C. Bridger

Department of Atmospheric Science
Colorado State University
Fort Collins, Colorado

**Colorado
State
University**

**Department of
Atmospheric Science**

Paper No. 334

WAVE-MEAN FLOW INTERACTIONS AND
SOLAR-WEATHER EFFECTS

by

Alison F.C. Bridger

Research supported by the
National Science Foundation
under Grant ATM 77-07096.

Department of Atmospheric Science
Colorado State University
Fort Collins, Colorado

April, 1981

Atmospheric Science Paper No. 334

ABSTRACT

A time-dependent, hemispheric, primitive-equation numerical model is constructed to test Hines' (1974) hypothesis that solar variations induce changes in the distributions of basic state variables at high levels in the atmosphere, and thus induce changes in planetary-scale wave structure at lower atmospheric levels. This mechanism was proposed to explain apparent atmospheric responses to solar activity. The changes are brought about by a diabatic heat source in the mesosphere or lower thermosphere. This is taken to be a simple representation of Joule dissipative heating in the atmosphere. We concern ourselves here with induced changes of the basic state zonal wind field.

Sensitivity studies reveal that planetary-scale wave structure is sensitive to the assumed initial basic state zonal wind distribution. The stratospheric sudden warming, which is driven by the interaction of such a large-scale wave with the zonally averaged flow, is therefore also sensitive to the initial basic state fields. The distributions of the latitudinal gradient of basic state potential vorticity, and the fields of wave energy flux at selected times, prove to be useful tools in diagnosing the atmosphere's response to forcing by a wave.

Lower atmospheric wave structure is found to be insensitive to solar-induced changes in the upper atmosphere. Such changes as do occur are limited to within about 30 kilometers below the level of maximum heating, and are also quite short-lived.

ACKNOWLEDGEMENTS

I should like to thank the members of my committee, Drs. R.E. Dickinson, W.H. Schubert, H. Frisinger and especially my advisors Drs. B. Haurwitz and D.E. Stevens for their guidance and assistance throughout my studies. I should also like to express my appreciation of all my friends, who have put up with my hermit-like existence over the past two months. Thanks are also due to Machel Sandfort (and her typewriter) for helping me to meet my deadline.

The work was sponsored by the National Science Foundation, Grant #ATM 77-07096. I should also like to acknowledge receipt of two Zonta International Amelia Earhart Fellowships. The computing work was done with the aid of the computing facilities at the National Center for Atmospheric Research.

TABLE OF CONTENTS

	<u>PAGE</u>
ABSTRACT.....	ii
ACKNOWLEDGEMENTS.....	iii
TABLE OF CONTENTS.....	iv
1. INTRODUCTION.....	1
2. NUMERICAL MODEL.....	14
2.1 Governing equations.....	14
2.2 The numerical model.....	19
2.3 Initial and boundary conditions.....	22
2.4 Diabatic forcing functions.....	23
2.5 Dissipation and diffusion.....	24
3. SENSITIVITY STUDIES	
3.1 Sensitivity to basic state wind.....	28
3.2 Sensitivity to amplitude of forcing function.....	70
3.3 Sensitivity to static stability parameter.....	80
4. THE SOLAR-WEATHER PROBLEM.....	83
4.1 Some remarks on the model.....	84
4.2 The nature of the forcing.....	86
4.3 The effect of heating on the basic state atmosphere.....	92
4.4 Joule heating and planetary wave structure.....	103
4.5 Experiments with a different wind profile.....	118
5. SUMMARY AND CONCLUSIONS.....	123
BIBLIOGRAPHY.....	129
APPENDIX I LIST OF SYMBOLS.....	134
APPENDIX II INDICES OF GEOMAGNETIC ACTIVITY.....	137
APPENDIX III ANALYSIS FOR BOUNDARY FORCING FUNCTION.....	139

1. INTRODUCTION

The possibility that "weather," or more specifically that atmospheric parameters such as pressure, wind and temperature vary in response to solar activity has been pursued for some time in the literature. Of course, the overall General Circulation is driven by differential solar heating. What is far less clear is whether or not variations in solar behavior can give rise to detectable variations in atmospheric behavior; variations which would otherwise not occur in the absence of solar variations. By solar variations, we may think of periodic events ranging from the rotation of the sun, with a period of about 27 days, to the cyclic occurrence of sun-spots, with a period of 11 years. There are also variations which do not occur regularly, such as the enhancement of the solar wind by solar flares, with subsequent terrestrial geomagnetic storms.

There are many reported relationships between solar activity and weather (henceforward, solar activity will be taken to mean temporal variations in solar activity i.e. deviations from the mean state). Some of the more recent reports of effects on time scales of 27 days or less are mentioned below. A more detailed survey may be found in Herman and Goldberg (1978).

An unequivocal influence of solar activity on the atmosphere is evident at thermospheric levels. For reference, Figure 1 shows the thermal structure of the atmosphere up to 150 km. Jacchia (1963) quotes the following results, derived from orbital variations of satellites. A 27 day periodicity was noted in density at heights of both 200 km

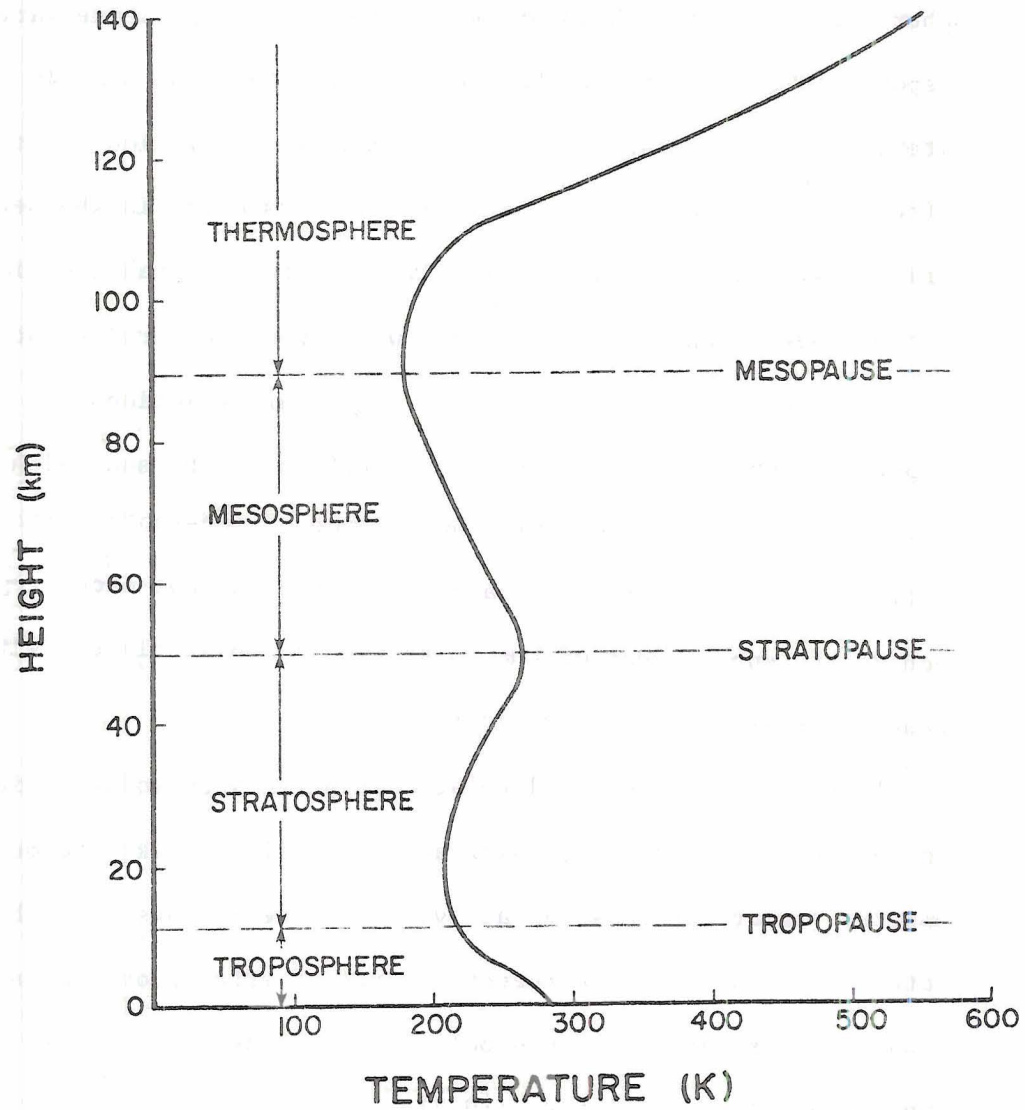


Figure 1 Temperature structure of the Atmosphere to 140 km and nomenclature (U.S. Standard Atmosphere, 1976).

and 650 km. Further satellite studies revealed the fluctuation to be of global extent. Evidence was also revealed of a variation of density in response to geomagnetic storms.

As we look at lower atmospheric levels, the evidence of a solar-weather link becomes less clear. Hicks and Justus (1970) analysed winds between 90 km and 140 km, as revealed by tracking rocket-borne chemical releases. A correlation was found between winds in the region and the index Kp. Definitions of various geomagnetic indices are given in Appendix II. Above 110 km, the Kp variations were observed to precede wind variations, suggesting that solar variations "drive" wind variations, whilst below 110 km wind variations preceded Kp variations, suggesting a dynamo-type interaction. This, incidentally, is a good example of the possible danger of taking an index such as Kp to be representative of solar variations (Hines, 1973; Shapiro, 1973).

Ramakrishna and Seshamani (1973) found a positive correlation between the 10.7 cm solar radio flux ($F_{10.7}$ index) and temperature in the equatorial mesosphere. They reported a one day time lag between $F_{10.7}$ increases and temperature increases. Ramakrishna and Seshamani (1976) found temperature increases in the 61-90 km region above Ft. Churchill in auroral latitudes to be correlated with changes in Kp, with a lag time of 12-15 hours, Kp variations preceding temperature variations. This lag time appears to be opposite that quoted by Hicks and Justus (1970) below 110 km. The different lag times quoted by Ramakrishna and Seshamani (one day at equatorial latitudes, 12 hours at auroral latitudes) are of interest, since they suggest that different mechanisms may be responsible for temperature variations at high vs. low latitudes. Richmond (1979), using a time dependent numerical model,

simulated high latitude auroral heating during a geomagnetic storm and found temperature increases at low latitudes. The auroral heating caused upward motion at high latitudes, a southward flow between 120 km and 150 km, sinking motion and consequent adiabatic heating at low latitudes and a return poleward flow in the lower thermosphere.

Although Richmond's model has a lower boundary at 80 km, nevertheless a mechanism such as this might explain the differing lag times discussed above.

Nastrom and Belmont (1978) correlated wind variations with the $F_{10.7}$ index for the period 1960-1976, using data in the range 25-65 km across the globe. A 27 day periodicity in zonal wind was found, with an amplitude of up to 2.5 ms^{-1} . As with the observations quoted above, a distinct causal relationship between wind speed and $F_{10.7}$ is not immediately obvious, since at around 50°N , wind maxima occur up to one week after $F_{10.7}$ maxima, whilst at low latitudes, wind maxima precede $F_{10.7}$ maxima by up to one week. Ebel and Bätz (1977) found a similar relationship between an index of circulation at 10 mb and the solar rotation. Noonkester (1967) reported that a change in the 100 mb circulation occurs about three days after a geomagnetic disturbance.

In the troposphere, Schuurmans (1979) found that the heights of both the 300 mb and 500 mb surfaces at various global locations changed in response to solar flare activity. Height rises and falls differed as a function of both latitude and longitude, suggesting a wave-like nature in the induced changes. Such changes occurred within a day of solar flares, although a later effect (after 2-4 days) was also noted. King et al. (1977) reported that the solar rotation gives rise to a 27 day wave in the 500 mb height statistics at 60°N . Schäfer (1979),

however, claimed that this correlation was not statistically significant. Whereas a periodicity of around 27 days can be found in 500 mb heights in middle-to-high latitudes, Schäfer claimed that it is the persistence of the disturbance (ranging up to 1 year) which will occasionally produce a coincidentally high correlation with the solar rotation. At other times the correlation will not be so good (Volland and Schäfer, 1979).

Finally there is the much heralded Vorticity Area Index phenomenon. Roberts and Olson (1973) studied the development of 300 mb troughs in the area delineated by 120°W and 180°W and by 40°N and 90°N . They found that troughs entering (or forming in) the area within 2-4 days of enhanced geomagnetic activity (measured by A_p) tended to be deeper than those entering (or forming in) the area during geomagnetically quiet times. The measure of trough intensity used, the Vorticity Area Index (VAI), was defined to be the area of the trough, over which the absolute vorticity exceeds $2 \times 10^{-4} \text{ S}^{-1}$, plus the area of the trough, over which the absolute vorticity exceeds $2.4 \times 10^{-4} \text{ S}^{-1}$. Wilcox et al. (1974) showed similar results, this time relating VAI to solar sector crossings (see Appendix II). Their Figure 5 shows that the VAI tends to decrease about two days before the sector crossing, reaching a minimum about one day after the sector crossing, and then increases again. Wilcox (1973, Figure 12) indicates that the K_p index of geomagnetic activity increases immediately following a sector crossing, but that it also decreases prior to the crossing; so, although the sector crossing provides an excellent temporal marker, since it is not subject to terrestrial influences, it is more likely to be the terrestrial geomagnetic effects, which the crossing presumably gives rise to both

before and after the event itself, which lead to meteorological changes. An obvious difficulty with VAI studies is that the quantity itself is not in common meteorological usage. Furthermore, in Wilcox et al. (1974), it is defined as a global parameter and is not particularly useful for forecast purposes.

The continuing dialogue over the existence or non-existence of solar-weather effects stems, in part, from the lack of conclusive observational evidence of such effects (although the VAI studies may have alleviated this to an extent). It is also due to a lack of understanding of how the lower atmosphere responds to solar activity. Although several mechanisms have been suggested, it remains to be demonstrated that any of them are valid.

Of the mechanisms proposed, one involves a solar modulation of ozone concentrations. Heath et al. (1977) have shown that zonally averaged O_3 amounts above 4 mb decreased by 20% following a major solar proton event (PCA) of August 1972. The event was characterised by an increased flux of solar protons and consequent production of NO_x , which in turn resulted in a catalytic destruction of O_3 . These results hold at $75^\circ-80^\circ N$, smaller changes being noted equatorward. The changes were not short lived, persisting several weeks. If these observations are representative of total depletion of O_3 in an atmospheric column, then it is reasonable to assume that reduced absorption of solar radiation in the stratosphere will result in lower stratospheric temperatures. There will also be an increased shortwave radiative flux into the troposphere. The resulting temperature modulations will depend on other radiatively-related factors (Ramanathan et al., 1976). Regardless of tropospheric effects, a reduction of O_3 in a given region of the

atmosphere and concomitant temperature changes should alter the temperature gradient and thus thermal wind, albeit locally.

Some numerical examinations of the effects of O_3 reduction are reported by Schoeberl and Strobel (1978). The reduction of O_3 on a global scale produced lower stratospheric and mesospheric temperatures and a weakened Polar Night Jet. They then performed additional experiments involving a local reduction of O_3 , representative of the kind of O_3 reductions noted by Heath et al. (1977). The global response to this perturbation was negligible, in terms of both temperature and polar night jet intensity. Similar experiments by Somerville et al. (1973), subjecting a General Circulation model to global-scale O_3 changes, yielded only minor changes in globally averaged temperature and in the development of the 500 mb flow pattern. However, the model top was at 10 mb and the vertical resolution was only about 110 mb, so that stratospheric changes were poorly handled.

Volland (1979) examined the effect of a 0.1% variation in the solar constant, with a 27 day periodicity. This effect was modelled through a variable forcing of planetary-scale Rossby waves. The results indicated that at 500 mb, a variation in height of about 0.5 gpm could be expected, clearly not particularly significant when compared to a longitudinal variation in the height of the 500 mb surface of, say, 500 gpm.

An overriding problem in finding a causal mechanism is that of energetics, namely that the deposition of energy due to a solar-related event is sufficiently small, compared to the energy associated with the General Circulation or even a part of the large scale circulation, that the effect is likely to be small. If we consider depositing a

given amount of energy (an amount consistent with, say, an auroral storm) into a volume of the atmosphere, the amplitude of the induced disturbance (measured, for example, in terms of a temperature perturbation and assuming all energy input is instantly converted to a temperature increase) will decrease exponentially as the height at which deposition occurs diminishes. The likelihood of direct forcing by solar activity on the lower atmosphere is therefore slim. Willis (1976) has examined this problem by comparing the energy typical of magnetospheric processes to that characteristic of the General Circulation. Table 1 is an adaptation of his Table 2, showing for example that the ratio of energy associated with a geomagnetic storm to that associated with the General Circulation is $O(10^{-5})$. There are instances when such a ratio may be larger, such as during high-latitude winter and at night. However the conclusion appears to be that solar activity will not directly affect the circulation at lower levels. Consequently, if observed effects are real, they must be induced via some indirect means.

Hines (1974) proposed a mechanism, whereby lower atmospheric variables might be modulated by solar events without invoking a direct transfer of energy from thermospheric to tropospheric heights.

The atmospheric circulation may be considered to comprise motions due to waves of wide-ranging temporal and spatial scales. Amongst these, the large-scale planetary waves comprise a fundamental part of the observed stratospheric and mesospheric structure, especially in winter. Large-scale (zonal wavenumbers 1 and 2) waves forced in the troposphere by orography and thermal gradients can propagate their

Table 1 Estimated energies (J) of certain meteorological and geomagnetic phenomena (adapted from Willis (1976), Table 2)

Phenomenon	Energy (J)
Total kinetic energy of the General Circulation of the Atmosphere	10^{21}
Frontal zone	10^{20}
Stratospheric warming	10^{19}
Extratropical cyclone	$10^{18} - 10^{19}$
Geomagnetic field external to the solid earth	10^{18}
Cold front	10^{17}
Geomagnetic storm	10^{16}
Magnetospheric substorm	10^{15}
Local thunderstorm	10^{14}
Local circulation cell without precipitation	$10^{10} - 10^{11}$

energy upward into the stratosphere, mesosphere and possibly the lower thermosphere. In an inviscid, adiabatic atmosphere with a resting basic state, the amplitude of such waves continues to grow with height approximately as $(\text{density})^{-1/2}$. However, in the real atmosphere where winds and stability vary with height, the wave energy may be reflected at a certain level, thus creating a standing wave below. Hines (1974) suggested that the effect of a solar disturbance might be to alter the reflective properties of the atmosphere at large heights, thereby altering the nature of the wave pattern below. In addition to being reflected, wave energy may also be absorbed and this mechanism in turn can be influenced by solar effects. This is further discussed below. The mechanism does not therefore require a large energy input but rather a reasonable input into relatively tenuous regions.

There is theoretical evidence that planetary-scale wave structure is quite sensitive to the wind and stability profiles of the basic state flow. Simmons (1974) studied the structure of stationary waves forced from below in a quasi-geostrophic, β -plane model. The mean wind was assumed to be linearly sheared in the vertical and to have a sinusoidal latitudinal dependence. His Figure 2 shows the variation of amplitude with height for three different values of (constant) vertical shear. He also noted that varying horizontal profiles of mean wind can influence the vertical penetration of wave energy. Matsuno (1970) and Dickinson (1968a) showed that the 2-dimensional, quasi-geostrophic wave geopotential equation contains a term, analagous to refractive index squared, which is proportional to the latitudinal gradient of mean potential vorticity. This in turn is a function of the wind, its

first and second vertical and horizontal derivatives and of static stability. Wave propagation is favoured in regions where this quantity is (relatively) large and positive, whilst waves are "guided" away from regions of small positive or negative refractive index squared. It follows that a change in distribution of this quantity might change the structure of a forced wave. Schoeberl and Geller (1976), via numerical solutions of a stationary forced wave in a spherical, quasi-geostrophic model, have further indicated the sensitivity of wave structure to the basic state. Taking two profiles of basic state zonal wind, varying essentially only in the maximum strength of the polar night jet, they showed quite different resultant wave structures. The question of wave structure is further discussed below, in the context of sensitivity studies for the model we have used.

An encouraging aspect of Hines' proposal is that it involves planetary-scale waves, which only propagate into the stratosphere in winter (Charney and Drazin, 1961; Dickinson, 1968). A recurrent theme in solar-weather observations is that they are most noticeable during winter, if not entirely absent in summer. There are drawbacks to the theory, however, as Hines himself pointed out. Specifically, dissipative effects (thermal and mechanical) can be expected to attenuate waves as they propagate into the mesosphere. Observations of long wave structure above the mesopause are still scant, and it is not clear whether or not significant wave amplitudes extend to these altitudes. Green (1972) indicated that there is a marked decrease of wave energy between 50 km and 80 km, whilst Hirota and Barnett (1977) showed evidence of waves extending to 85 km. Although their amplitudes were

seen to decline above the stratopause, they were nevertheless present at the mesopause.

A study of the viability of Hines' suggestion was performed by Geller and Alpert (1980). Using a quasi-geostrophic, hemispheric, numerical model, the structure of planetary-scale waves forced at the surface was examined in the presence of varying basic state winds. Variations in wind were introduced by reductions of a "control" wind profile, the maximum reduction of 20% being at the latitude of the polar night jet maximum and at a given height, with lesser changes away from these levels. The authors did not generate the basic state wind changes by a specific solar-related mechanism; rather, such changes were imposed. They found it necessary to make these reductions below a height of about 35 km in order to produce a change in the tropospheric wave pattern. Typical height changes of the 500 mb pressure surface of 20 m were generated by the model in response to mean wind changes, centred at 30 km. The study seemed to indicate that any solar-induced modulation must occur at relatively low levels.

A similar study was done by Schmitz and Greiger (1980), although it was not specifically concerned with Hines' mechanism. They too utilized a quasi-geostrophic, hemispheric, numerical model, to test the sensitivity of wave structure to mean zonal wind changes. Again, their wind changes were imposed, rather than internally generated by some means, however winds were changed through a rather deep layer of the atmosphere from 20 km to the upper boundary at 100 km. They then found that wave amplitudes in the 5-20 km height range varied with different mean wind profiles and that, as with Geller and Alpert (1980), the effect was largest at high latitudes.

Neither study discussed above addressed the problem of how wind changes in a relatively shallow (Geller and Alpert) or deep (Schmitz and Greiger) layer of the atmosphere could be induced. In his paper, Hines (1974) referred to a solar-induced modulation at relatively large heights due perhaps to aurorally-generated heating. We propose here to examine the possibility that a high level heating associated with a geomagnetic storm can induce wind changes, which in turn can modify wave structure below, bearing in mind that at such an altitude (around 100-120 km), the density is sufficiently small that relatively large wind (and temperature) deviations can be induced. It is not suggested that there is any particular significance to this mode of forcing; it merely serves in an exemplary capacity. As mentioned above, it is not clear that wave energy associated with large-scale, tropospherically forced waves can propagate to such heights, but we consider the most optimistic situation, where the wave makes its presence felt, at least to some degree, at large heights. As in Geller and Alpert (1980), only the modification of winds will be considered; the effect of altered static stability will be ignored.

Briefly, our procedure will be to simulate a geomagnetic storm-induced heating in the auroral oval. This will be prescribed simply as a diabatic heat source. The forcing will be projected onto both the zonal flow and onto wave motions, since the auroral oval is centred about the geomagnetic pole. In the context of a numerical model (hemispheric, primitive equation), the temporal behavior of planetary long waves forced at the tropopause will be examined, to see what, if any, effects can be produced by the storm.

2. NUMERICAL MODEL

2.1 Governing equations

The model used is an adaptation of that introduced by Holton (1976). It is based on the primitive equations of Meteorology and allows for interactions between a single Fourier component and the basic state (zonally averaged) flow.

Following Holton (1975), we may write the primitive equations for the zonally averaged flow as:

$$\frac{d\bar{u}}{dt} = f\bar{v} + \bar{u}\bar{v} \frac{\tan\theta}{a} - \bar{F}_x, \quad (2.1)$$

$$\frac{d\bar{v}}{dt} = -f\bar{u} - \bar{u}^2 \frac{\tan\theta}{a} - \frac{\partial\bar{\Phi}}{\partial y} - \bar{F}_y, \quad (2.2)$$

$$\frac{d}{dt} \left(\frac{\partial\bar{\Phi}}{\partial z} \right) = -N^2\bar{w} + \bar{Q} - \bar{G}, \quad (2.3)$$

$$\frac{1}{\cos\theta} \frac{\partial}{\partial y} (\bar{v}\cos\theta) + \frac{\partial\bar{w}}{\partial z} - \frac{\bar{w}}{H} = 0, \quad (2.4)$$

with:

$$\frac{d}{dt} = \frac{\partial}{\partial t} + \bar{v} \frac{\partial}{\partial y} + \bar{w} \frac{\partial}{\partial z}.$$

In (2.4), we have assumed a density-like function of the form $\rho_0(z) = \rho_0(0)e^{-z/H}$, where H is some arbitrary, constant scale height. All symbols are defined in Appendix I and we note that $\bar{\Phi}$ is defined as the deviation of the zonal mean geopotential from its global average at a constant height; it is not the total zonally averaged geopotential. A prescribed function, $\Phi_0(z)$, represents the globally averaged geopotential; it remains constant in time, and defines the static stability, N^2 , thus:

$$N^2 = \frac{d^2\Phi_0}{dz^2} + \frac{\kappa}{H} \frac{d\Phi_0}{dz}. \quad (2.5)$$

The discussion in Holton (1975) indicates that, in order to have a consistent set of energy equations for the model, N^2 must be assumed constant. This is discussed further in Section 3.3.

The eddy equations are obtained by subtracting (2.1) - (2.4) from the original primitive equations, giving

$$\frac{du'}{dt} = fv' + \bar{u}v' \frac{\tan\theta}{a} + \bar{v}u' \frac{\tan\theta}{a} - v' \frac{\partial \bar{u}}{\partial y} - w' \frac{\partial \bar{u}}{\partial z} - \frac{\partial \Phi'}{\partial x} - \bar{F}_x', \quad (2.6)$$

$$\frac{dv'}{dt} = -fu' - 2\bar{u}u' \frac{\tan\theta}{a} - v' \frac{\partial \bar{v}}{\partial y} - w' \frac{\partial \bar{v}}{\partial z} - \frac{\partial \Phi'}{\partial y} - \bar{F}_y', \quad (2.7)$$

$$\frac{d}{dt} \left(\frac{\partial \Phi'}{\partial z} \right) = -v' \frac{\partial}{\partial y} \left(\frac{\partial \bar{\Phi}}{\partial z} \right) - w' \frac{\partial}{\partial z} \left(\frac{\partial \bar{\Phi}}{\partial z} \right) - w' N^2 + Q' - \bar{G}', \quad (2.8)$$

$$\frac{\partial u'}{\partial x} + \frac{1}{\cos\theta} \frac{\partial}{\partial y} (v' \cos\theta) + \frac{\partial w'}{\partial z} - \frac{w'}{H} = 0, \quad (2.9)$$

with

$$\frac{d}{dt} \equiv \frac{\partial}{\partial t} + \bar{u} \frac{\partial}{\partial x} + \bar{v} \frac{\partial}{\partial y} + \bar{w} \frac{\partial}{\partial z}.$$

Equations (2.6) - (2.9) describe the behavior of the flow, which is a deviation from the zonal mean. We have not yet restricted ourselves to a single Fourier mode.

The eddy flux terms in (2.1) - (2.3) are defined as:

$$\bar{F}_x = \frac{1}{\cos^2\theta} \frac{\partial}{\partial y} (\overline{u'v'} \cos^2\theta) + \left(\frac{\partial}{\partial z} - \frac{1}{H} \right) (\overline{u'w'}), \quad (2.10)$$

$$\bar{F}_y = \frac{1}{\cos\theta} \frac{\partial}{\partial y} (\overline{v'^2} \cos\theta) + \left(\frac{\partial}{\partial z} - \frac{1}{H} \right) (\overline{v'w'}) + \overline{u'^2} \frac{\tan\theta}{a}, \quad (2.11)$$

$$\bar{G} = \frac{1}{\cos\theta} \frac{\partial}{\partial y} (\overline{v'\Phi'_z} \cos\theta) + \left(\frac{\partial}{\partial z} - \frac{1}{H} \right) (\overline{w'\Phi'_z}), \quad (2.12)$$

and in the eddy equations we have:

$$\begin{aligned} \mathcal{F}_x' &= \frac{\partial}{\partial x} (u'^2) + \frac{1}{\cos^2\theta} \frac{\partial}{\partial y} [(u'v' - \overline{u'v'}) \cos^2\theta] \\ &+ \left(\frac{\partial}{\partial z} - \frac{1}{H} \right) (u'w' - \overline{u'w'}), \end{aligned} \quad (2.13)$$

$$\begin{aligned} \mathcal{F}_y' &= \frac{\partial}{\partial x} (u'v') + \frac{1}{\cos\theta} \frac{\partial}{\partial y} [(v'^2 - \overline{v'^2}) \cos\theta] \\ &+ (u'^2 - \overline{u'^2}) \frac{\tan\theta}{a} + \left(\frac{\partial}{\partial z} - \frac{1}{H} \right) (v'w' - \overline{v'w'}), \end{aligned} \quad (2.14)$$

$$\begin{aligned} \mathcal{G}' &= \frac{\partial}{\partial x} (u'\phi'_z) + \frac{1}{\cos\theta} \frac{\partial}{\partial y} [(v'\phi'_z - \overline{v'\phi'_z}) \cos\theta] \\ &+ \left(\frac{\partial}{\partial z} - \frac{1}{H} \right) (w'\phi'_z - \overline{w'\phi'_z}). \end{aligned} \quad (2.15)$$

The equations are now scaled, using the following scaling parameters (Holton, 1975):

$$(x, y) \sim L$$

$$(\bar{u}, u', v') \sim U$$

$$t \sim L/U$$

$$z \sim D$$

$$\bar{v} \sim R_0 U$$

$$\bar{w} \sim R_0 UD/L$$

$$w' \sim UD/L$$

$$\phi', \bar{\phi} \sim 2\Omega UL$$

$$\bar{Q}, Q' \sim 2\Omega U^2/D$$

where L, U, D are typical length, velocity and depth scales for stratospheric motions and $R_0 = U/2\Omega L$ is a Rossby number. Using $L \sim 10^6$ m and $U \sim 15 \text{ ms}^{-1}$ gives $R_0 \sim 0.1$. The time scale is reasonable for the problem we are considering, in which a diabatic heating is applied for

a relatively short time. A longer time scale (L/R_0U) is appropriate for studies of the seasonally varying stratospheric circulation.

Using this scaling and throwing out higher order terms yields:

$$\frac{\partial \bar{u}}{\partial t} = f\bar{v} + \bar{u}\bar{v} \frac{\tan\theta}{a} - \bar{F}_x, \quad (2.16)$$

$$\frac{\partial \bar{v}}{\partial t} = -f\bar{u} - \bar{u}^2 \frac{\tan\theta}{a} - \frac{\partial \bar{\Phi}}{\partial y}, \quad (2.17)$$

$$\frac{\partial}{\partial t} \left(\frac{\partial \bar{\Phi}}{\partial z} \right) = -N^2 \bar{w} + \bar{Q} - \bar{G}, \quad (2.18)$$

$$\frac{1}{\cos\theta} \frac{\partial}{\partial y} (\bar{v}\cos\theta) + \frac{\partial \bar{w}}{\partial z} - \frac{\bar{w}}{H} = 0. \quad (2.19)$$

The $\tan\theta$ terms have been retained since they become important near the pole. Following Holton (1976), we retain the $\partial \bar{v}/\partial t$ term, although it is $O(R_0^2)$ smaller in the scaling than the coriolis and geopotential terms.

Scaling the eddy equations similarly gives:

$$\frac{du'}{dt} = fv' - \frac{\partial \Phi'}{\partial x} - \frac{v'}{\cos\theta} \frac{\partial}{\partial y} (\bar{u}\cos\theta), \quad (2.20)$$

$$\frac{dv'}{dt} = -fu' - 2\bar{u}u' \frac{\tan\theta}{a} - \frac{\partial \Phi'}{\partial y}, \quad (2.21)$$

$$\frac{d}{dt} \left(\frac{\partial \Phi'}{\partial z} \right) = -v' \frac{\partial}{\partial y} \left(\frac{\partial \bar{\Phi}}{\partial z} \right) - w'N^2 + Q', \quad (2.22)$$

$$\frac{\partial u'}{\partial x} + \frac{1}{\cos\theta} \frac{\partial}{\partial y} (v'\cos\theta) + \frac{\partial w'}{\partial z} - \frac{w'}{H} = 0. \quad (2.23)$$

Again the $\tan\theta$ terms have been retained. Following Holton (1976), we neglect vertical advection by the eddy motions. In addition, we neglect eddy interaction terms, which will vanish when we restrict attention

to a single wave. The behaviour of stratospheric waves is found to be well approximated by linear theory (the scaled eddy equations are now linear).

We now restrict attention to a single wave by making the following assumption:

$$\begin{pmatrix} u' \\ v' \\ \phi' \end{pmatrix} = \begin{pmatrix} u \\ v \\ \phi \end{pmatrix} e^{is\lambda + z/2H}. \quad (2.24)$$

The introduction of the $e^{z/2H}$ term is a standard procedure; for a problem in which the eddy equations are separable in y and z , the Vertical Structure Equation will then be cast in canonical form.

Eliminating w' and including mechanical and thermal dissipation (parameterized by Rayleigh friction, α_R , and Newtonian cooling, α_N , respectively), we have:

$$\frac{\partial u}{\partial t} = fv - im\bar{u} - im\bar{\phi} - \frac{v}{\cos\theta} \frac{\partial}{\partial y} (\bar{u}\cos\theta) - \alpha_R u, \quad (2.25)$$

$$\frac{\partial v}{\partial t} = -fu - im\bar{v} - \frac{\partial \bar{\phi}}{\partial y} - 2\bar{u} \frac{\tan\theta}{a} - \alpha_R v, \quad (2.26)$$

$$\begin{aligned} \frac{\partial}{\partial t} \left(\frac{\partial^2 \bar{\phi}}{\partial z^2} - \frac{\bar{\phi}}{4H^2} \right) &= N^2 \left[im\bar{u} + \frac{1}{\cos\theta} \frac{\partial}{\partial y} (v\cos\theta) \right] \\ &- \left(\frac{\partial}{\partial z} - \frac{1}{2H} \right) \cdot \left[(\alpha_N + im\bar{u}) \left(\frac{\partial \bar{\phi}}{\partial z} + \frac{\bar{\phi}}{2H} \right) + v \frac{\partial}{\partial y} \left(\frac{\partial \bar{\phi}}{\partial z} \right) - Q' e^{-z/2H} \right], \end{aligned} \quad (2.27)$$

where $m = s/a\cos\theta$.

Similarly, assuming

$$\begin{pmatrix} \bar{u} \\ \bar{v} \\ \bar{\phi} \end{pmatrix} = \begin{pmatrix} U \\ V \\ \Psi \end{pmatrix} e^{z/2H}$$

we have:

$$\frac{\partial U}{\partial t} = fV + UVe^{z/2H} \frac{\tan\theta}{a} + \mathcal{F}, \quad (2.28)$$

$$\frac{\partial V}{\partial t} = -fU - \frac{\partial \Psi}{\partial y} - U^2 e^{z/2H} \frac{\tan\theta}{a}, \quad (2.29)$$

$$\begin{aligned} \frac{\partial}{\partial t} \left(\frac{\partial^2 \Psi}{\partial z^2} - \frac{\Psi}{4H^2} \right) &= \frac{N^2}{\cos\theta} \frac{\partial}{\partial y} (\bar{v} \cos\theta) \\ &- \left(\frac{\partial}{\partial z} - \frac{1}{2H} \right) \cdot \left[\alpha_N \left(\frac{\partial}{\partial z} + \frac{1}{2H} \right) (\Psi - \Psi^*) + \mathcal{G} - \bar{Q} e^{-z/2H} \right]. \end{aligned} \quad (2.30)$$

In (2.27), Newtonian cooling acts to relax the temperature perturbation to its initial value of zero. In (2.30) it acts to relax $\bar{\Phi}$ to its initial value of $\bar{\Phi}^*$ ($\bar{\Phi}^* \equiv \bar{\Phi}(t=0) \equiv \Psi^* e^{z/2H}$).

In (2.28) and (2.30), the eddy forcing terms are now

$$\mathcal{F} = - \frac{e^{-z/2H}}{\cos^2\theta} \frac{\partial}{\partial y} (\overline{u'v'} \cos^2\theta) \quad (2.31)$$

and

$$\mathcal{G} = \frac{e^{-z/2H}}{\cos\theta} \frac{\partial}{\partial y} \left(\overline{v' \frac{\partial \Phi'}{\partial z}} \cos\theta \right). \quad (2.32)$$

For quasi-geostrophic motions when the length scale assumed is $O(R_0 a)$, the vertical flux terms in $\bar{\mathcal{F}}$ and $\bar{\mathcal{G}}$ are small compared to the horizontal flux terms; although we are using the primitive equations, the same assumption is made here. Bates (1980) however indicates that when scaling length by a , the vertical flux terms must be retained.

2.2 The numerical model

Equations (2.25) - (2.30) are cast in finite - difference form in the $y - z$ plane. We take a staggered grid in the y - direction with $\Delta\theta = 5^\circ$ ($y = a\theta$) and $\Delta z = 2.5$ km. The distribution of variables on the

grid is shown schematically in Figure 2. We employ a simple leapfrog scheme to calculate time derivatives. Consequently, (2.28) becomes:

$$\frac{U_{j,k}^{n+1} - U_{j,k}^{n-1}}{2\Delta t} = f_j V_{j,k}^n + V_{j,k}^n U_{j,k}^n e^{z_k/2H} \frac{\tan\theta_j}{a} + \mathcal{F}_{j,k}^n \quad (2.33)$$

with

$$\mathcal{F}_{j,k} = -e^{z_k/2H} \left[\delta(\overline{u v}) - \frac{2 \langle \overline{u v} \sin\theta \rangle}{\langle \overline{\cos\theta} \rangle} \right] . \quad (2.34)$$

The index n represents the time step. In addition,

$$\langle \overline{u v} \rangle = \frac{(\overline{u v})_{i-1,k} + (\overline{u v})_{i,k}}{2} \quad (2.35)$$

is an averaging operator (Holton, 1976) and

$$\delta(\overline{u v}) = \frac{(\overline{u v})_{i-1,k} - (\overline{u v})_{i,k}}{\Delta y} \quad (2.36)$$

is a differencing operator (Holton, 1976).

The other equations are written in finite difference form in a similar manner. To avoid swamping the reader with endless finite-differenced equations and discussions on the handling of certain terms, we have omitted detailed descriptions. The reader is referred to Holton and Wehrbein (1979) for additional information.

To prevent decoupling between odd and even time step solutions as the integration proceeds, we apply an Asselin time filter to every field at every time step. The filter is given by:

$$\overline{X(t)} = X(t) + \nu/2 \left[\overline{X(t-1)} - 2X(t) + X(t+1) \right] , \quad (2.37)$$

where we use $\nu = .02$ (Asselin, 1972). The time step used is 8 minutes.

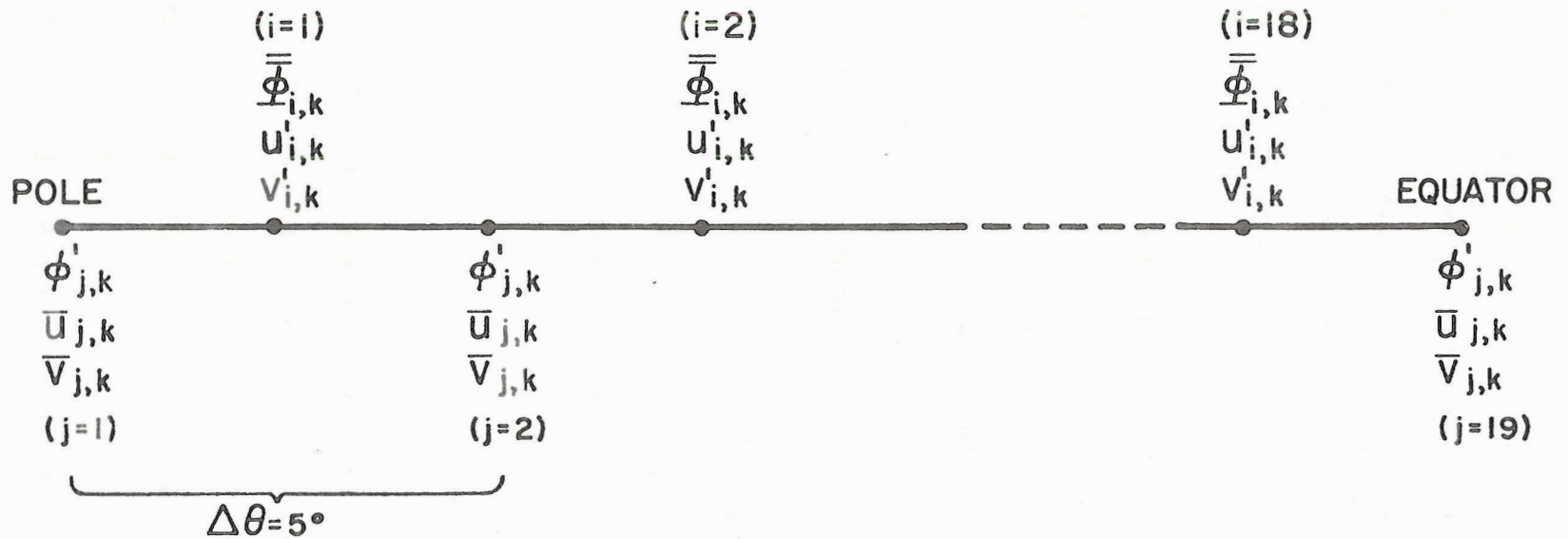


Figure 2 Schematic arrangement of variables on model staggered grid. i and j are the y indices, k is the vertical index.

Note that in order to avoid computational instability, all dissipative terms (Rayleigh friction, Newtonian cooling and 4th order diffusion) are evaluated using the fields at time step $(n - 1)$, rather than at n .

Provided we specify initial and boundary conditions, and the forcing functions \bar{Q} and Q' , we can numerically solve the system (2.25) - (2.30).

2.3 Initial and boundary conditions

We assume that the wave fields are zero initially and that there is a prescribed initial zonal flow and concomitant temperature field to support this flow. The procedure for creating the initial zonal flow is outlined in Chapter 3. Given $\bar{u}(t = 0)$, we can solve for $\bar{\Phi}(t = 0)$ by assuming the flow to be in gradient wind balance:

$$f\bar{u} + \bar{u}^2 \frac{\tan\theta}{a} = - \frac{\partial\bar{\Phi}}{\partial y} . \quad (2.38)$$

Finite - differencing (2.38) gives us 18 equations in 19 unknowns. To close the system, we use the definition of $\bar{\Phi}$:

$$\int_{\text{pole}}^{\text{equator}} \bar{\Phi} \cos\theta d\theta = 0 .$$

Fields at $t = \Delta t$ are calculated using a forward time step.

We assume that $\phi' = 0$ at the pole and at the equator. We further assume that $\partial\bar{\Phi}/\partial y = 0$ at the pole and equator. At the upper boundary, we take $\phi' = 0$ and $\bar{\Phi}(t) = \bar{\Phi}(t = 0)$. At the lower boundary (10 km), we again set $\bar{\Phi}(t) = \bar{\Phi}(t = 0)$ and ϕ' is specified to simulate a wave propagating up from the troposphere. We take a forcing function of the form:

$$\phi' = \left\{ \begin{array}{ll} gh_T \sin^s \left[\frac{\pi(\theta - 30^\circ)}{60^\circ} \right] & , \quad 30^\circ < \theta \leq 90^\circ \\ 0 & , \quad 0^\circ \leq \theta \leq 30^\circ . \end{array} \right\} \quad (2.39)$$

Holton (1976) used this form with $s = 2$ whilst Matsuno (1971) used it with $s = 1$. The analysis in Appendix III shows that the following is true for the wave:

$$\left. \begin{array}{l} \text{for } s > 1: \quad u' = v' = \frac{\partial \phi'}{\partial y} = 0 \quad \text{at } \theta = \pi/2 , \\ \text{for } s = 1: \quad \frac{\partial u'}{\partial y} = \frac{\partial v'}{\partial y} = \frac{\partial^2 \phi'}{\partial y^2} = 0 \quad \text{at } \theta = \pi/2 . \end{array} \right\} \quad (2.40)$$

Clearly, the form assumed in (2.39) satisfies (2.40) whilst those employed by Matsuno (1971) and Holton (1976) are suitable for only wavenumbers 1 or 2 respectively.

The forcing is turned on slowly, with the following time dependence: $(1 - \exp(-t/2.5 \times 10^5 \text{s}))$.

2.4 Diabatic forcing functions

In Chapter 3, the sensitivity of the numerical model is discussed, in terms of the stratospheric sudden warming. For this problem, the only forcing is through the lower boundary condition; thus Q' and \bar{Q} are zero. In the solar-weather experiments, discussed in Chapter 4, we will introduce a diabatic heat source in the mean flow and wave equations. The form of this forcing is given by:

$$Q' \text{ (or } \bar{Q}) = A \operatorname{sech} \left(\frac{z - z_F}{z_E} \right) \operatorname{sech} \left(\frac{y - y_F}{y_E} \right) , \quad (2.41)$$

where (y_F, z_F) are the latitude and height of the maximum forcing and (y_E, z_E) are distances, over which the forcing decays.

Consider the response of an atmosphere that is heated directly by a diabatic forcing, Q' , without any circulation. Then:

$$\frac{\partial}{\partial t} \left(\frac{\partial \Phi'}{\partial z} \right) = Q' = \frac{\kappa J'}{H}, \quad (2.42)$$

where J' has units Joules/sec. Using the hydrostatic relation, we have:

$$\frac{\partial T'}{\partial t} = \frac{J'}{c_p}. \quad (2.43)$$

If we let the diabatic forcing have a heating rate of X deg/day, we get

$$\bar{A} = \frac{RX}{H.86400}. \quad (2.44)$$

Representative values for z_F , z_E , y_F , y_E and \bar{A} are discussed in Chapter 4.

2.5 Dissipation and diffusion

Mechanical dissipation is modelled simply using a Rayleigh friction coefficient given by

$$\alpha_R(z) = \frac{1}{80 \text{ days}} + \frac{1}{4 \text{ days}} \left[1 + \tanh \left(\frac{z - 71 \text{ km}}{10 \text{ km}} \right) \right] \text{sec}^{-1}. \quad (2.45)$$

The large values at high levels effectively act as a sponge to prevent reflections at the upper boundary from ruining the solution.

Thermal dissipation is represented by Newtonian cooling with the following distribution:

$$\alpha_N(z) = \left[1.5 + \tanh \left(\frac{z - 35 \text{ km}}{7 \text{ km}} \right) \right] 10^{-6} \text{ sec}^{-1}. \quad (2.46)$$

The forms for α_R and α_N are taken from Holton and Wehrbein (1979) and Holton (1976), respectively. In Figure 3 we show the e-folding times for α_R and α_N as a function of z .

We include a 4th order diffusion in the equations, without which fields become contaminated with small scale noise (2 - Δy grid noise) after 10-20 days. The noise obscures the larger scale nature of the

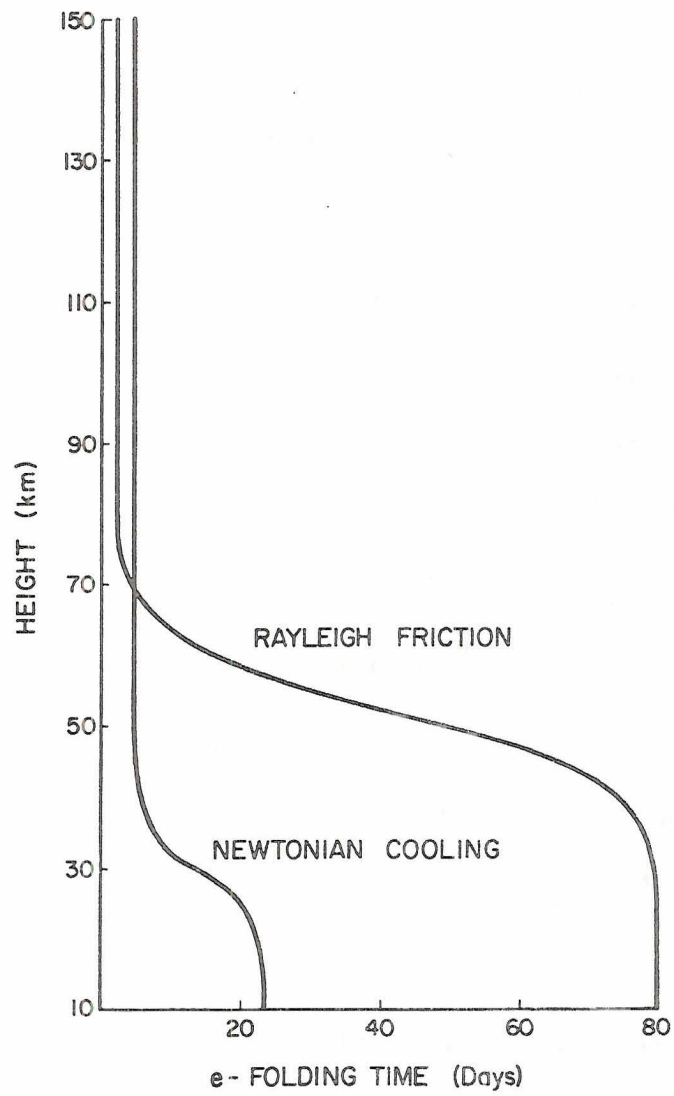


Figure 3 Height distribution of e-folding times due to Rayleigh friction and Newtonian cooling.

wave solution and the integration eventually "blows up." The diffusion operator is:

$$D(\chi) = - \frac{K}{\cos\theta} \frac{\partial^4 \chi}{\partial y^4} \quad (2.47)$$

for $\chi = \bar{v}$, $\partial\bar{\phi}/\partial z$, u' , v' and $\partial\phi'/\partial z$ whilst we use;

$$D(\chi) = - \frac{K}{\cos^2\theta} \frac{\partial^4}{\partial y^4} \left(\frac{\chi}{\cos\theta} \right) \quad (2.48)$$

for $\chi = \bar{u}$ (Holton and Wehrbein, 1979).

The scheme is extremely scale selective. If we consider the simple diffusion equation:

$$\frac{\partial \chi}{\partial t} = - K \frac{\partial^4 \chi}{\partial y^4}$$

and assume $\chi = \tilde{\chi} e^{\sigma t + imy}$ we have:

$$\sigma = - Km^4 \text{ sec}^{-1} .$$

Substituting $m = 2\pi/L$ with $L = \rho\Delta y$, we have:

$$\sigma = - \frac{K}{\Delta y^4} \left(\frac{2\pi}{\rho} \right)^4 \text{ sec}^{-1} .$$

$$= (\text{dissipative e-folding time})^{-1} .$$

We find it necessary to use a value of $K/\Delta y^4 = 5 \times 10^{-7} \text{ m}^4 \text{ s}^{-1}$ and, taking $\Delta y = \pi a/36$, we construct Table 2, indicating how scale selective the procedure is.

ρ	σ^{-1} (days)
2	0.24
4	3.80
6	19.25
8	60.84
10	148.52

Table 2 Variation of dissipative e-folding time with scale of disturbance ($\rho = 2$ indicates a $2 - \Delta y$ wave).

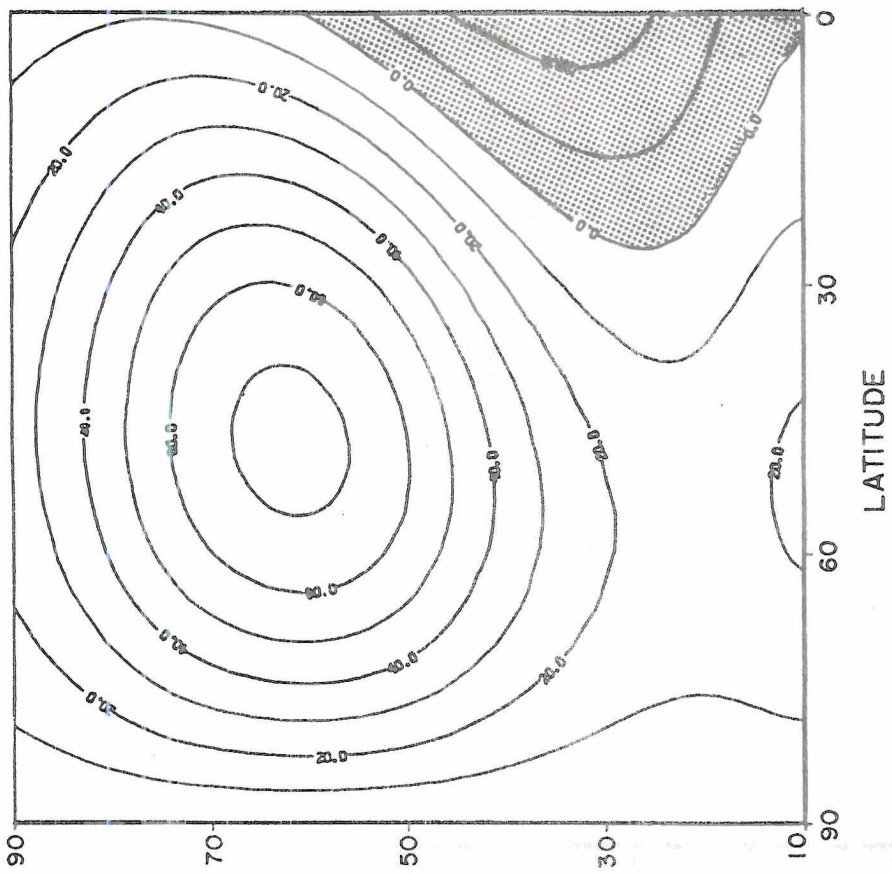
3. SENSITIVITY STUDIES

Since the numerical model (i.e. equations (2.25)-(2.30) and the finite difference scheme) was originally set up by Holton (1976) to study the stratospheric sudden warming problem, hereafter referred to as the SSW, it seemed appropriate initially to attempt to reproduce his results, as a check of the model. This was done and in addition, some sensitivity studies regarding the numerical modelling of the SSW were performed. Although these studies, reported in this chapter, have no direct bearing on the solar-weather problem, they are interesting in their own right and provide a useful insight into the solar-weather problem.

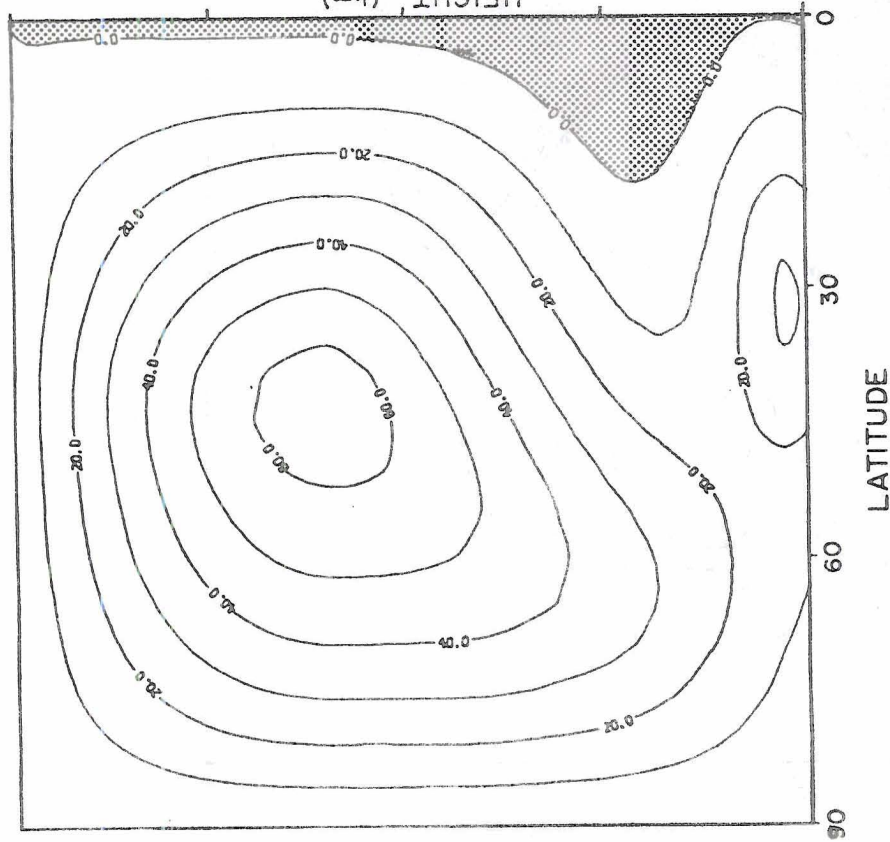
3.1 Sensitivity to basic state wind

A set of experiments was performed to gauge the importance of the initial zonally averaged wind (\bar{u}) in determining the course of the SSW event. Three wind profiles were used. The first is that used by Holton (1976) (data kindly provided by J. Holton) and is shown in Figure 4(a). The second was constructed using the scheme given in Lindzen and Hong (1974) and is representative of solstice conditions. It is shown in Figure 4(b), and in Figure 4(c) we show the third wind profile, constructed using the expression in Tung and Lindzen (1979). The three profiles are hereafter referred to as H, LH, and T.

The three profiles are qualitatively similar, having a polar night jet at about 60 km and from 45° - 60° in latitude. Of the three, H has the weakest jet maximum of about 65 ms^{-1} . The three all have a low level, sub-tropical jet, although that in LH is at a higher latitude than in either H or T. In each there is also a region of easterly winds near the equator.



4 (b)



4 (a)

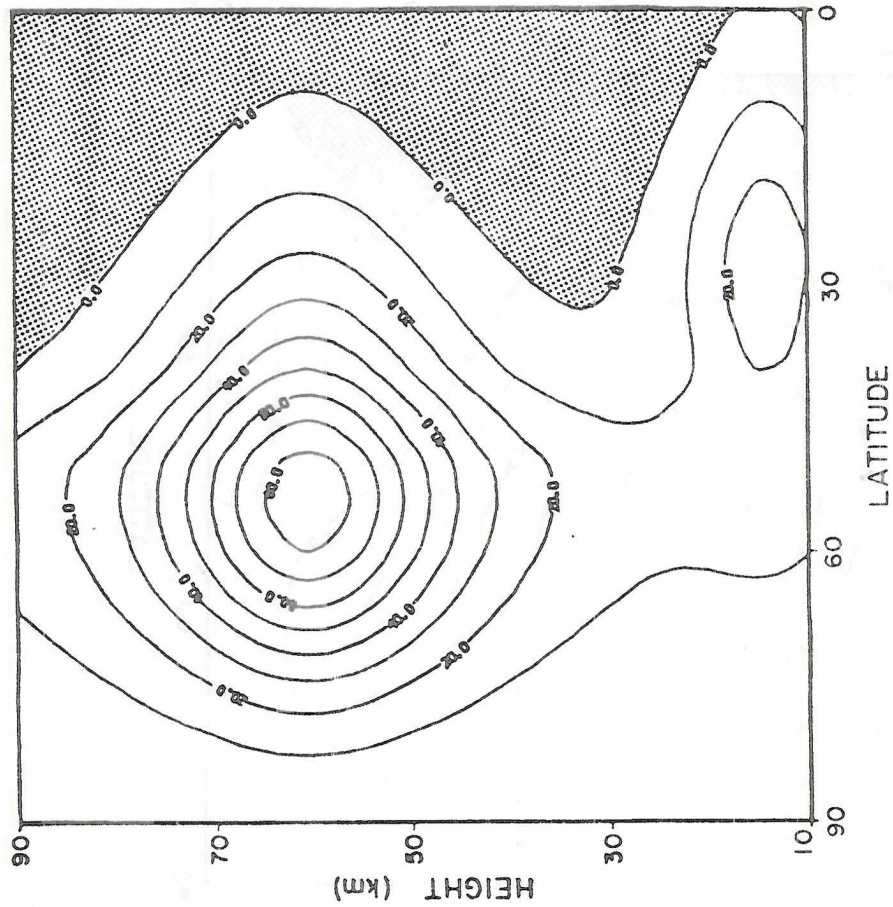


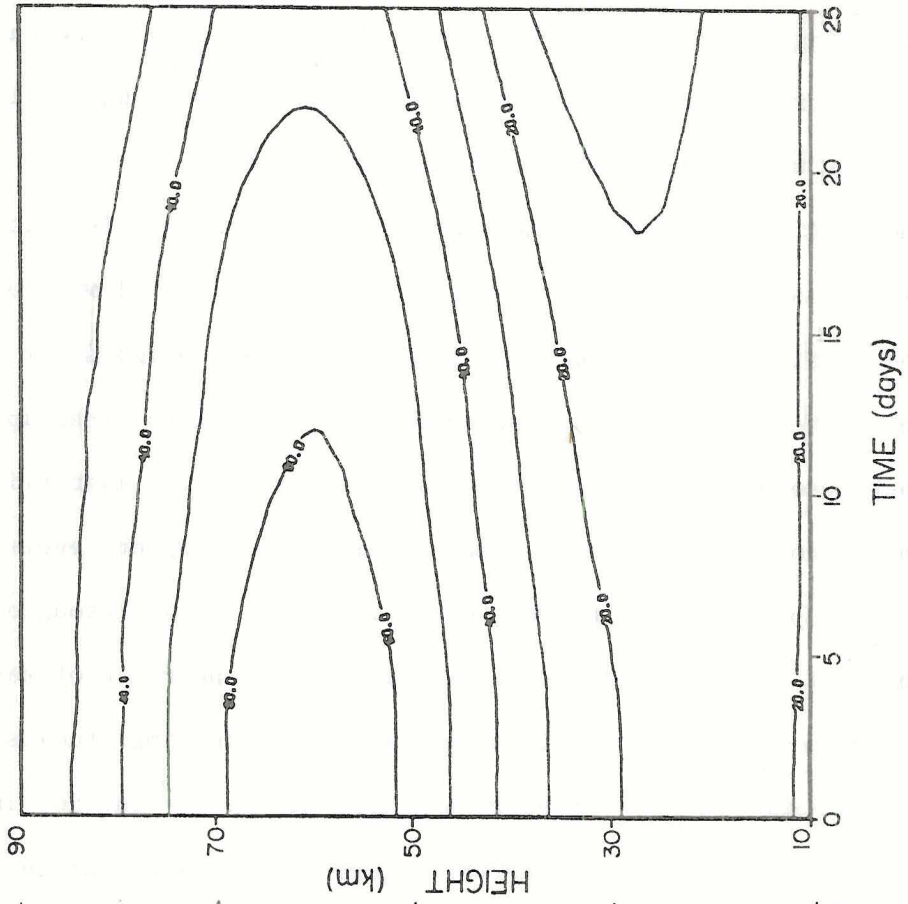
Figure 4 Latitude-height sections of the three initial mean zonal wind profiles used (a) from Holton (1976); (b) from Lindzen and Hong (1974); (c) from Tung and Lindzen (1979). Units are m/s. Stippled areas denote regions of easterly winds.

4 (c)

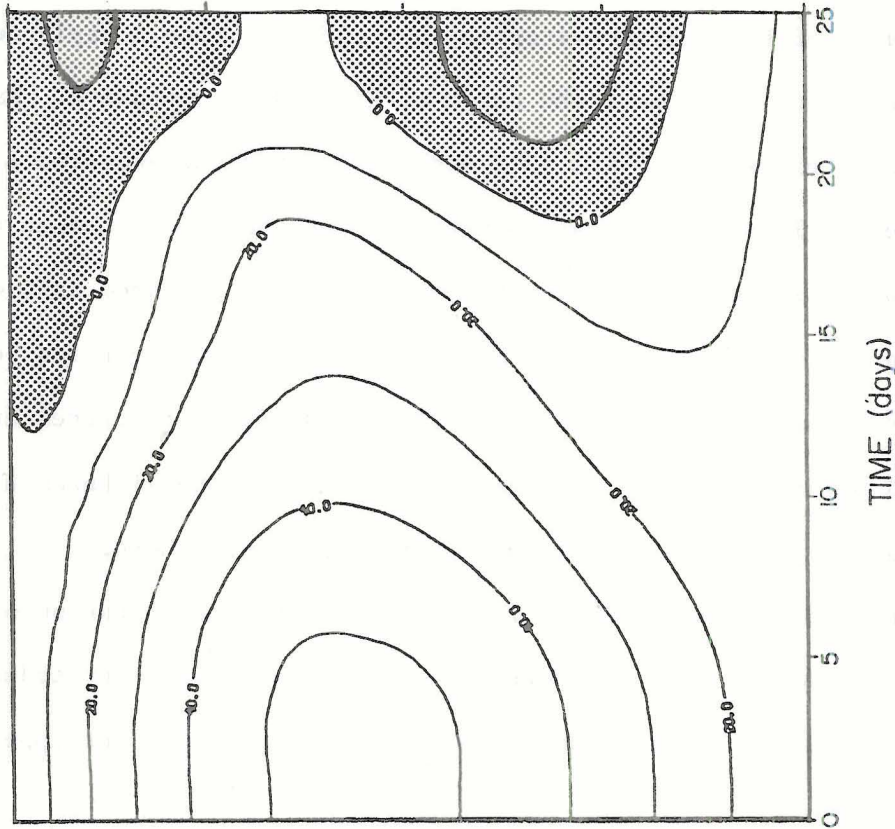
For each profile, we ran the model for 25 days with the forcing at 10 km reaching a maximum of 300 m after about five days. The cases discussed here are all for wavenumber one. Figure 5 shows the evolution of the three \bar{u} fields at 60° over the 25 day period.

The most striking difference between the three runs is that at 60° , easterly winds do not develop over the period with the LH wind profile. For wind profile H, winds diminish gradually at all heights for about two weeks after the forcing is switched on. Easterlies first appear in the upper mesosphere and migrate downward. A region of easterlies also appears at around 30 km about a week after those at upper levels and propagate both up and down. Between days 17 and 19, winds throughout the atmosphere at high latitudes reverse sign. The appearance of easterlies at two levels has been noted in some numerical modelling studies of the SSW (e.g., Matsuno, 1971; Schoeberl and Strobel, 1980) but not in others (Lordi *et al.*, 1981). Holton (1976; Figure 2) indicates the initial appearance of high level easterlies but there is then a rapid deceleration of winds throughout the depth of his model atmosphere. Kanzawa (1980), in his study of the 1973 warmings, noted the appearance of high level easterlies in association with a minor warming, although the circulation at lower levels did not reverse. It is presumed that differences between the numerical model in Holton (1976) and this version (e.g., different forcing functions, explicit time-differencing, greater diffusion, Rayleigh friction formulation) account for the differences between the results presented by Holton and those presented here.

For the LH wind profile, there is a gradual deceleration of winds at all heights at 60° and indeed at all extra-tropical latitudes, but the deceleration never becomes rapid and easterlies do not appear.



5 (a)



5 (b)

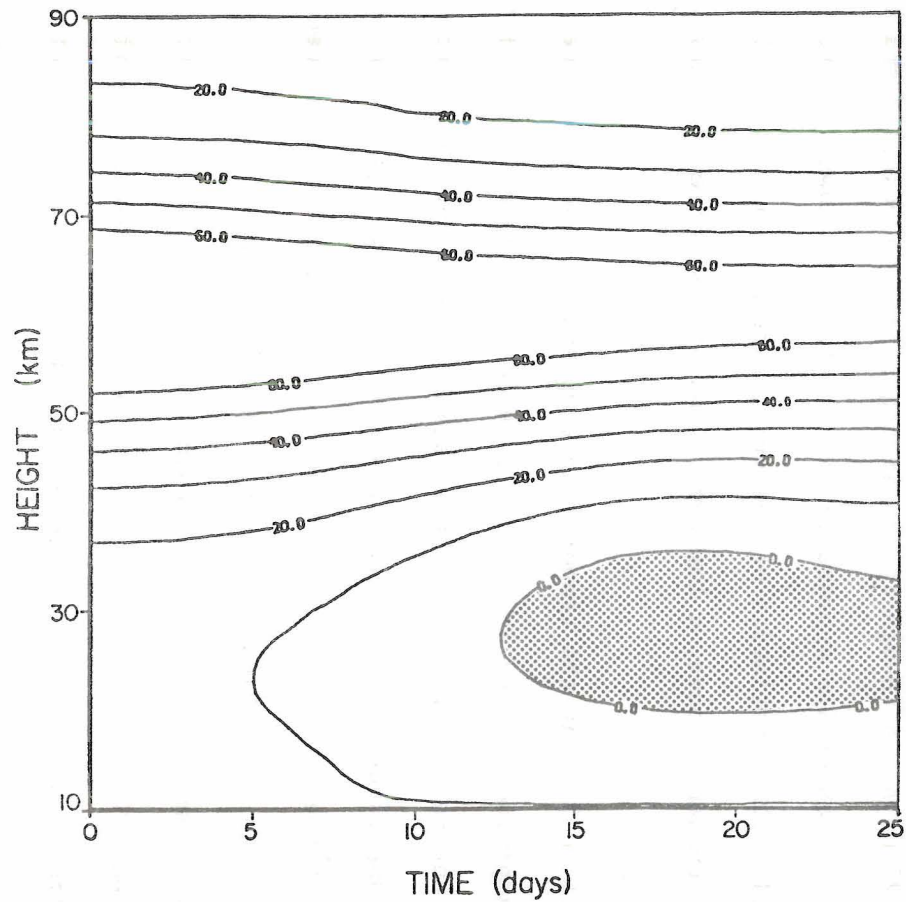


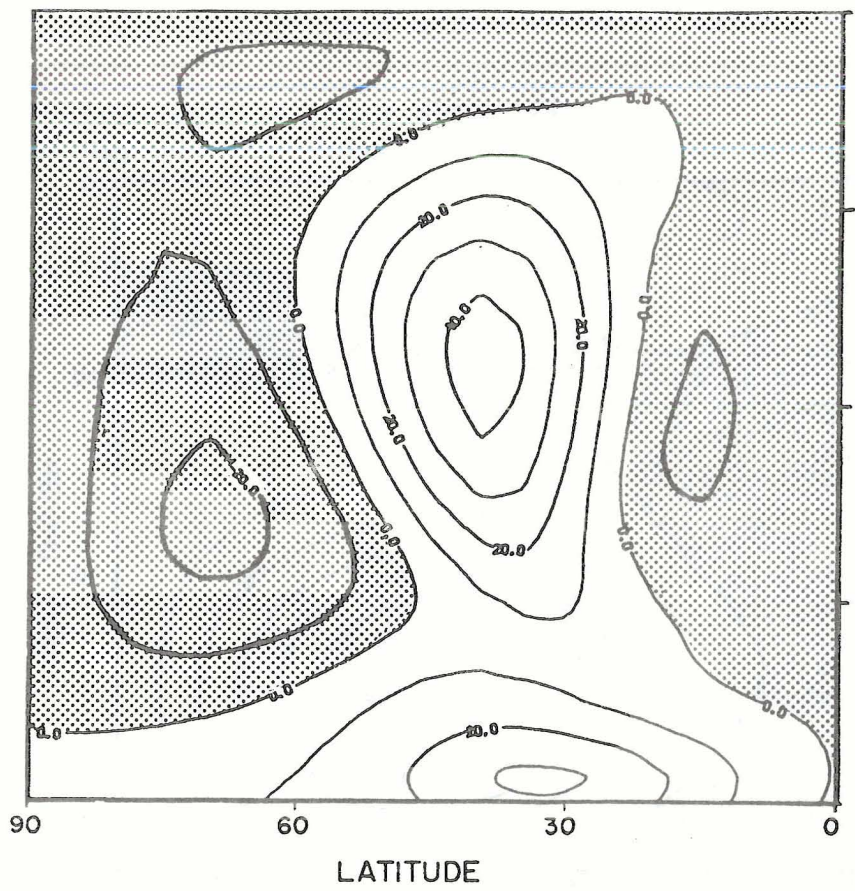
Figure 5 Time-height diagrams of basic state zonal wind at 60° for wind profiles (a) H, (b) LH, and (c) T. Stippled areas denote regions of easterly winds.

5 (c)

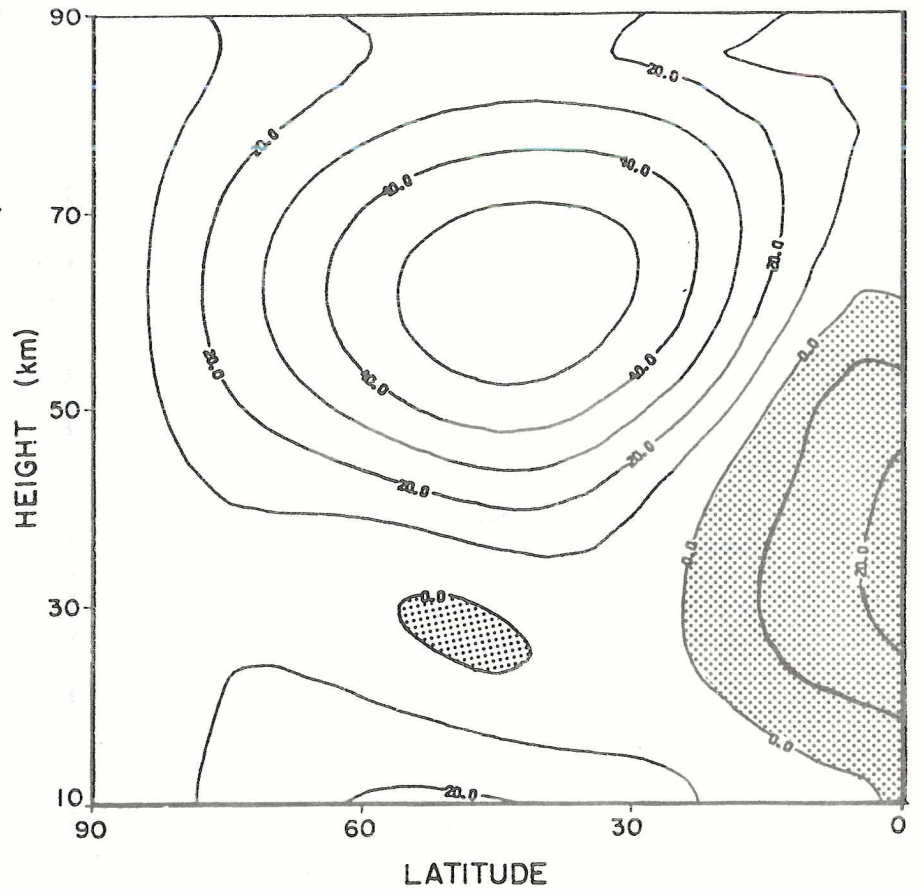
The situation with profile T is quite similar, in that although easterlies do appear after about 13 days, they are confined to a relatively shallow layer, centred just below 30 km and poleward of 55° . By day 20, they have spread equatorwards to join up with low latitude easterlies and form a band of easterlies from pole to equator.

Figure 6 shows the basic state zonal wind fields that have evolved after 25 days. For profile H, the original westerly jet has decreased in amplitude and is confined to the mid-latitudes. Poleward of 50° - 60° , easterly winds have developed, attaining a maximum of -22 ms^{-1} at 70° and 40 km. There has also been a poleward expansion of the tropical easterlies. The wave forcing has left profile LH relatively untouched after 25 days. Although the polar night jet has weakened and a small region of easterlies appears in the mid-latitude lower stratosphere, the essential characteristics of the profile remain unchanged. For profile T, as mentioned above, a low-level band of easterlies has developed after 25 days.

If we look at the temporal development of wavenumber one geopotential amplitude, shown in Figure 7, we can gain some insight into the different behaviour of the three warmings. Only for the H profile do large amplitudes develop, with rapid amplification following the initiation of the forcing. It is noted that the differences between Figure 7(a) and Holton's Figure 2 (1976) arise from the different forcing functions employed. Figure 8 indicates the two different functions involved. The one used here is latitudinally broader than that used by Holton. When we run the model with Holton's forcing function (for wavenumber one), the time-height development of wave geopotential amplitude is like that shown by Holton, although the amplitude maxima

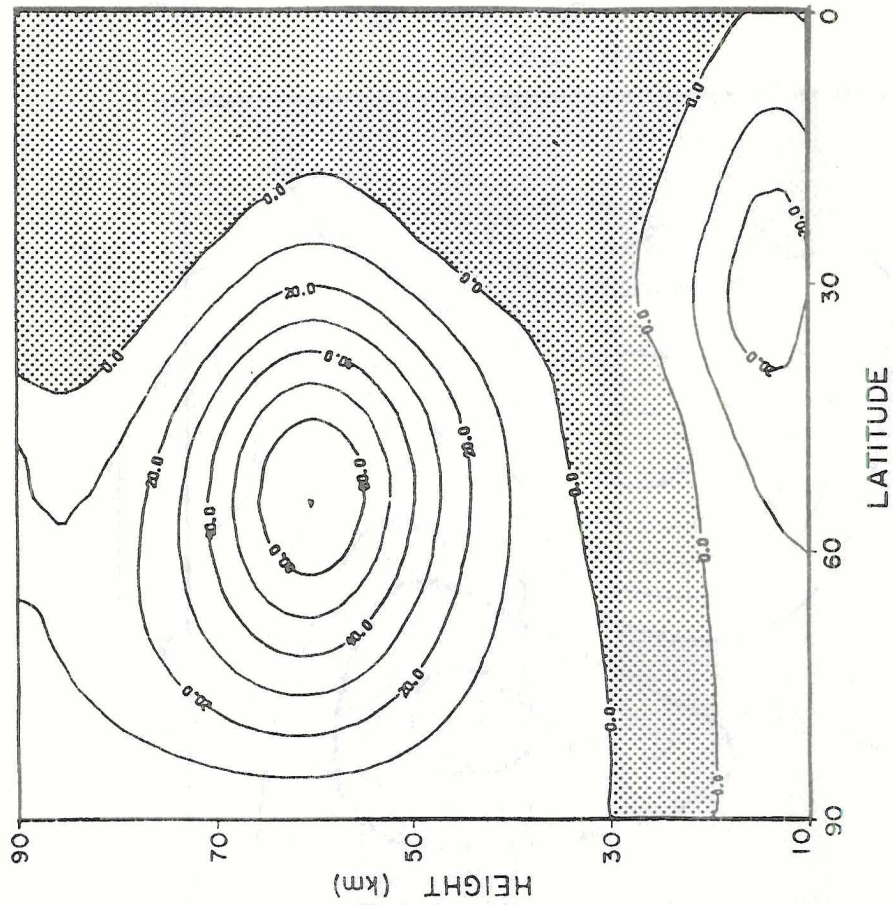


6 (a)

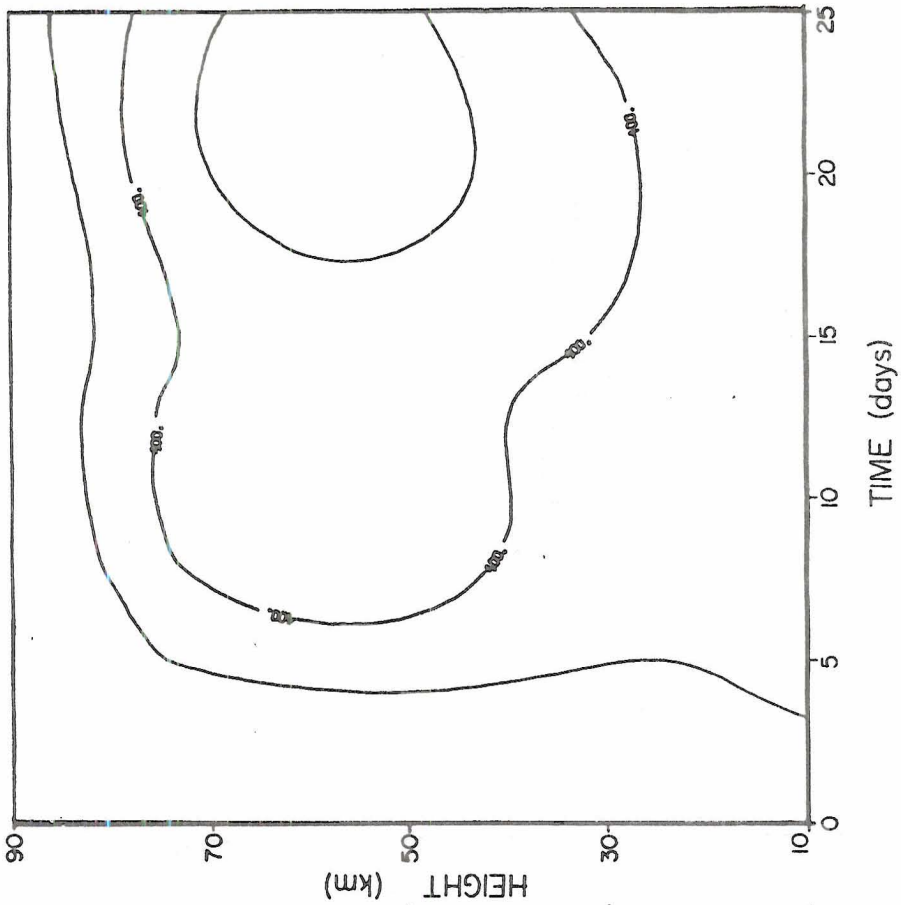


6 (b)

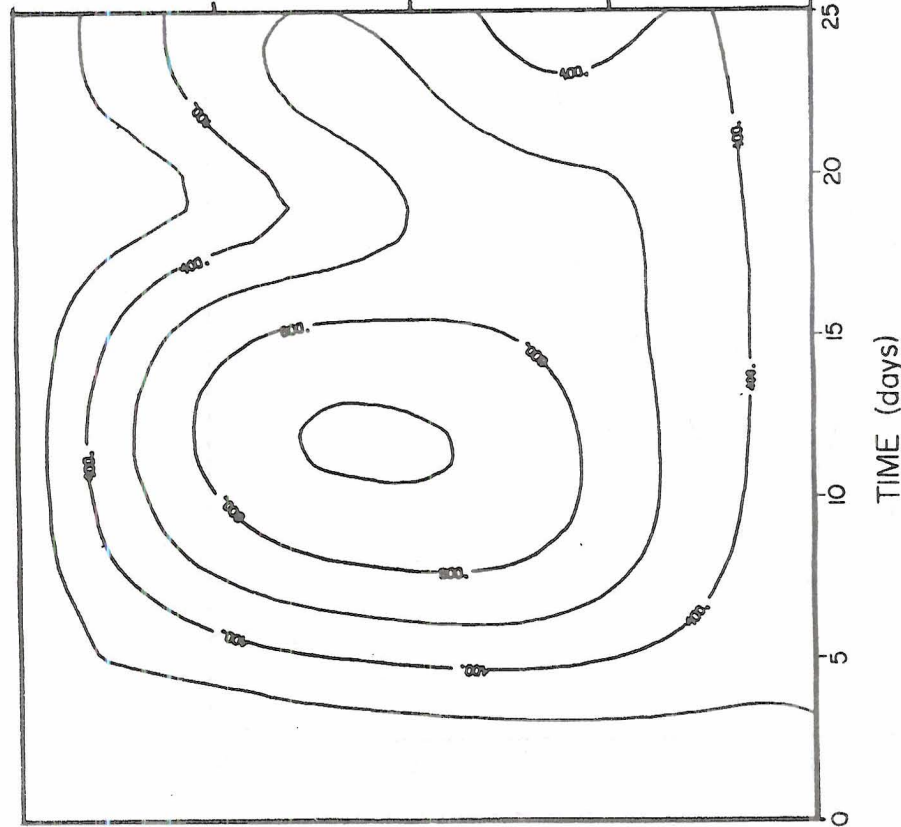
Figure 6 Latitude-height sections of basic state zonal wind after 25 days for initial wind profiles (a) H, (b) LH, and (c) T. Stippled areas denote regions of easterly winds.



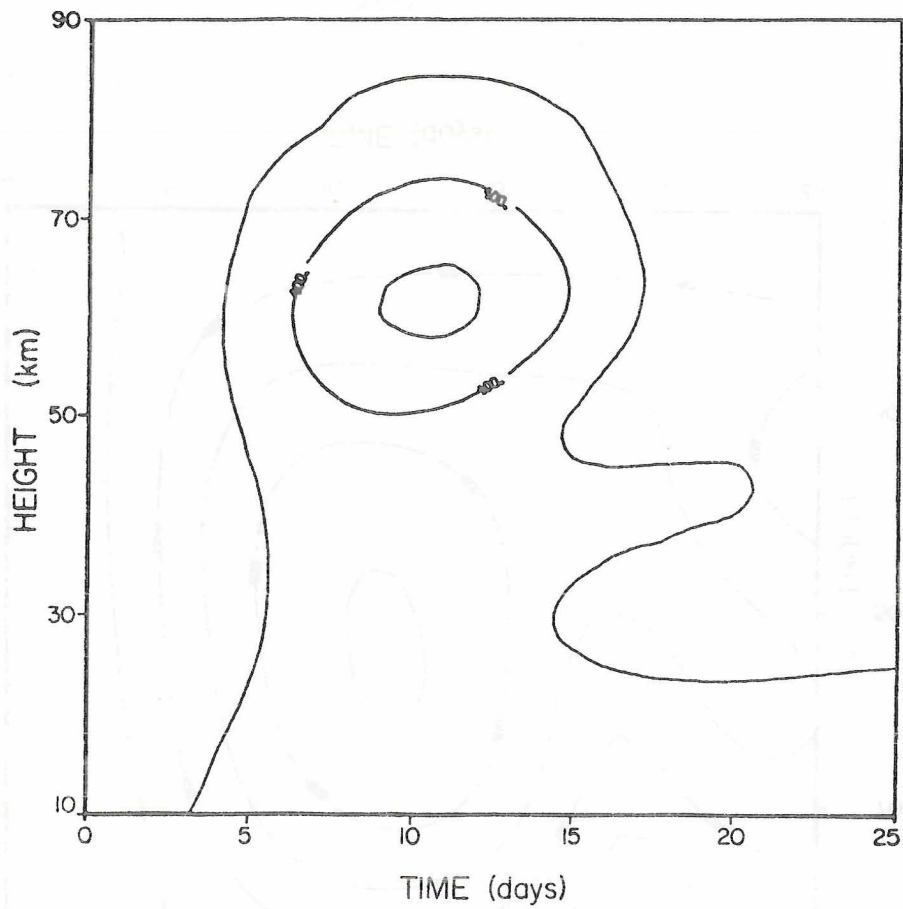
6(c)



7 (a)



7 (b)



7(c)

Figure 7 Time-height development of wavenumber 1 geopotential amplitude for the three wind profiles (a) H, (b) LH, and (c) T. Contour intervals are 200 m.

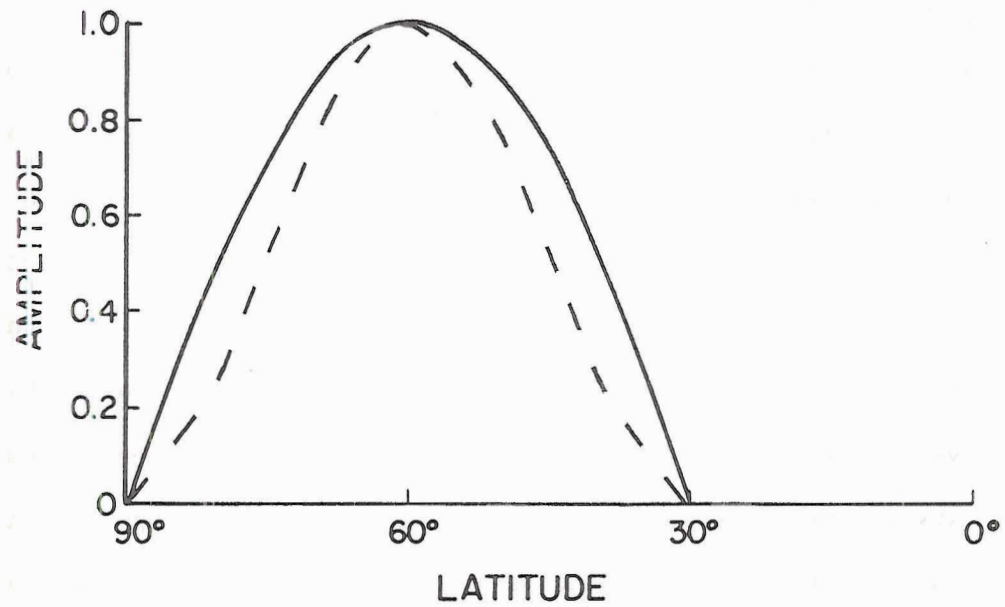


Figure 8 Latitudinal distribution of amplitude of forcing functions (for wavenumber one) used in the SSW studies. Solid line: this study; dashed line: Holton (1976). Refer to (2.39) for formulae.

attained are a little weaker. This point is alluded to further in Section 3.2. Wave development is slower for the LH profile, with amplitudes still increasing after 20 days, whilst for profile T, a peak of 700 m is attained at 10 days, after which amplitudes diminish. This reduction occurs as low level easterlies form and block further upward propagation of wave energy.

We may seek the reason for these differences in the theory of wave propagation and wave-mean flow interaction. The vertical propagation of waves was examined by Charney and Drazin (1961). Using a quasi-geostrophic, mid-latitude, β -plane model, they showed that stationary waves can only propagate energy vertically when the basic state zonal wind (assumed constant) is (i) westerly, and (ii) weaker than a critical value, determined by the scale of the waves. The theory thus explains why we only observe long waves in the winter stratosphere (since in summer, stratospheric winds are easterly) and also why wavenumbers one and two predominate (the critical wind value decreases with increasing wavenumber). The theory was refined by Dickinson (1968), who indicated that the critical wind value increases when the earth's sphericity is accounted for. Dickinson (1969) also showed that wave propagation is affected by thermal damping in the mesosphere.

In the simple Charney-Drazin theory, we may separate the equations of motion and arrive at a vertical structure equation of the following form:

$$\frac{d^2\psi}{dz^2} + n^2\psi = 0. \quad (3.1)$$

Here, n^2 can be regarded as an (index of refraction)² and depends upon the scale of the disturbance, on the basic state wind strength and on

temperature through N^2 , the static stability. Only when $n^2 > 0$ can energy propagate vertically, the solution to (3.1) taking the form $\Psi \sim e^{inz}$. For $n^2 < 0$, the solution is of the form $\Psi \sim e^{-nz}$ and wave energy is trapped. The wave is then said to be evanescent.

For realistic wind profiles, lateral and vertical wind shears play an important role in wave energy propagation. Matsuno (1970) looked at this problem using a quasi-geostrophic model in spherical geometry. He reduced the governing equations to a single equation for the wave geopotential of the form:

$$\mathcal{L}_z \Psi + \mathcal{L}_y \Psi + Q_s \Psi = 0, \quad (3.2)$$

where \mathcal{L}_z and \mathcal{L}_y are vertical and horizontal operators and Q_s can be thought of as a (refractive index)². Q_s is written as:

$$Q_s = \frac{\partial \bar{q}}{\partial \theta} \frac{1}{\bar{u} \cos \theta} - \frac{s^2}{\cos^2 \theta} - \frac{\lambda^2 \sin^2 \theta}{4H^2}, \quad (3.3)$$

where $\bar{u} = \frac{\bar{u}}{a \cos \theta}$, $s = \text{wavenumber}$, $\lambda^2 = \frac{(2 \Omega a)^2}{N^2}$

and

$$\frac{\partial \bar{q}}{\partial \theta} = \left[2(\Omega + \bar{\omega}) - \frac{\partial^2 \bar{\omega}}{\partial \theta^2} + 3 \tan \theta \frac{\partial \bar{\omega}}{\partial \theta} - \frac{4\Omega^2 a^2 \sin^2 \theta}{p} \frac{\partial}{\partial z} \left(\frac{p}{N^2} \frac{\partial \bar{\omega}}{\partial z} \right) \right] \cos \theta. \quad (3.4)$$

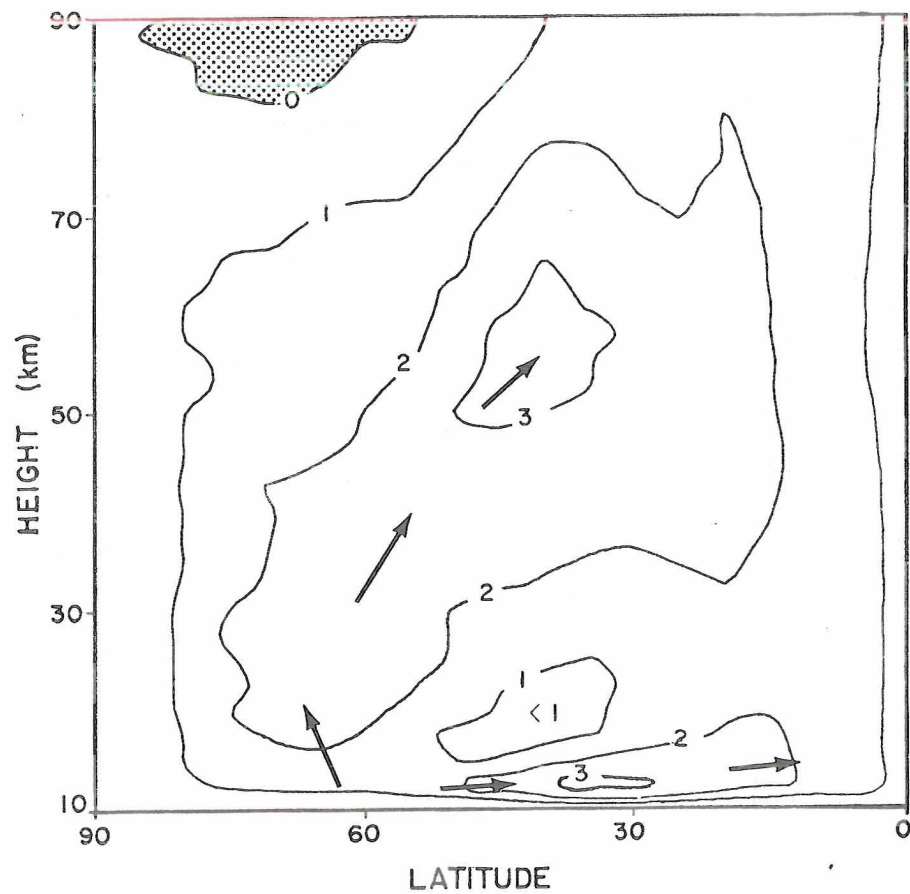
Here, $p = \text{pressure}$. $\partial \bar{q} / \partial \theta$ is the latitudinal gradient of basic state potential vorticity and clearly is influenced by the shear and curvature of the basic state wind and by temperature via N^2 . When $\bar{u} = \text{constant}$, as in Charney and Drazin's analysis, the distribution of $\partial \bar{q} / \partial \theta$ is the same as the distribution of β .

Given a wind profile, we can construct $\partial \bar{q} / \partial \theta$ and thus Q_0 and Q_s . This allows us to see in what regions of the atmosphere wave propagation

is favoured. Wavenumber s will be evanescent where Q_s is negative. Examination of (3.3) shows that this will be the case when: (a) $\partial\bar{q}/\partial\theta$ is small or negative, (b) when θ is large (near the pole), or (c) when s is large. For a given wavenumber, we can therefore use the distribution of $\partial\bar{q}/\partial\theta$ as a guide to wave propagation.

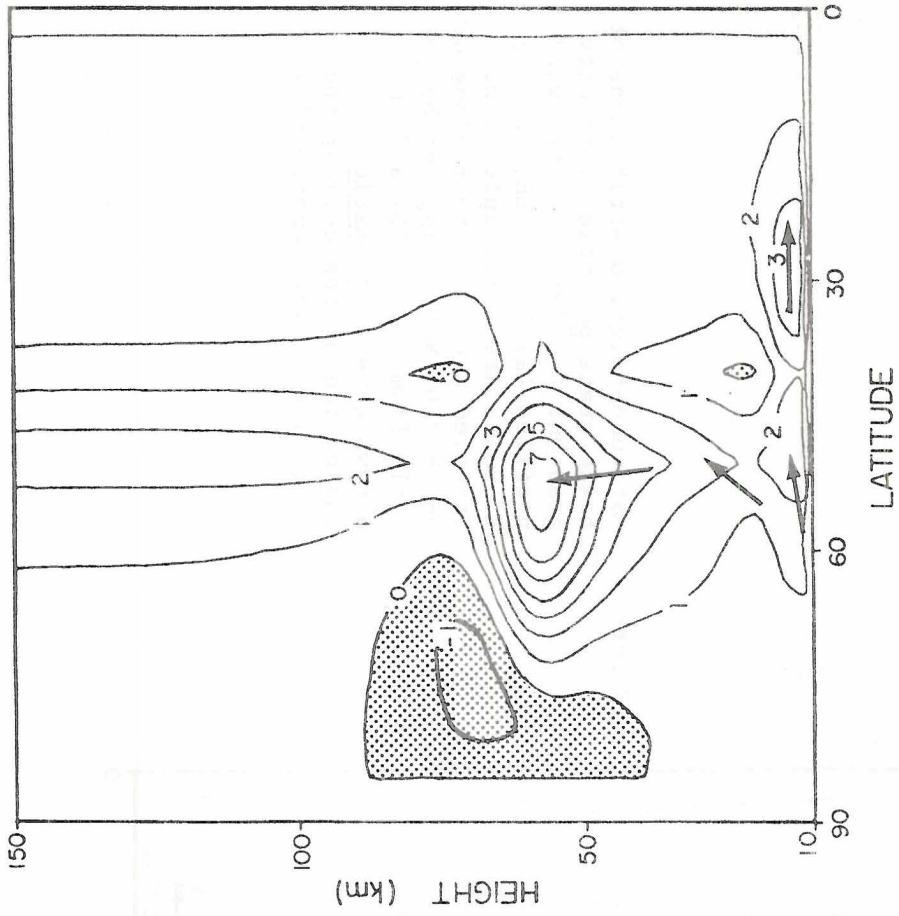
Figure 9 shows the initial distributions of $\partial\bar{q}/\partial\theta$ corresponding to the three wind profiles. Bearing in mind the tendency for wave energy flow to avoid areas of small or negative $\partial\bar{q}/\partial\theta$, the arrows indicate schematically the general paths of energy propagation. There are certain elements common to all three profiles. Each has a region of negative $\partial\bar{q}/\partial\theta$ at high latitudes around 90 km. This barrier to propagation will be an important factor in the studies discussed in Chapter 4. Each also has a maximum in the regions of both the polar night and sub-tropical jets. However, we note the tongue of relatively high values extending to 10 km at high latitudes for profile H. In the other two profiles, values here are small. Using Matsuno's (1970) terminology, we can thus expect waves to be "guided" up to the polar night jet region in all three cases, but for profiles LH and T the energy is guided in a more southerly direction, reducing the likelihood of wave propagation into high latitude regions with concomitant easterly acceleration and warming.

For the T profile, the extent of the low-latitude easterlies effectively confines the wave to a relatively small latitudinal band. Since the low-level, mid-latitude winds for this profile are weaker than those for the other two profiles, the winds are decelerated to become easterly sooner, thus blocking further upward propagation of the wave.

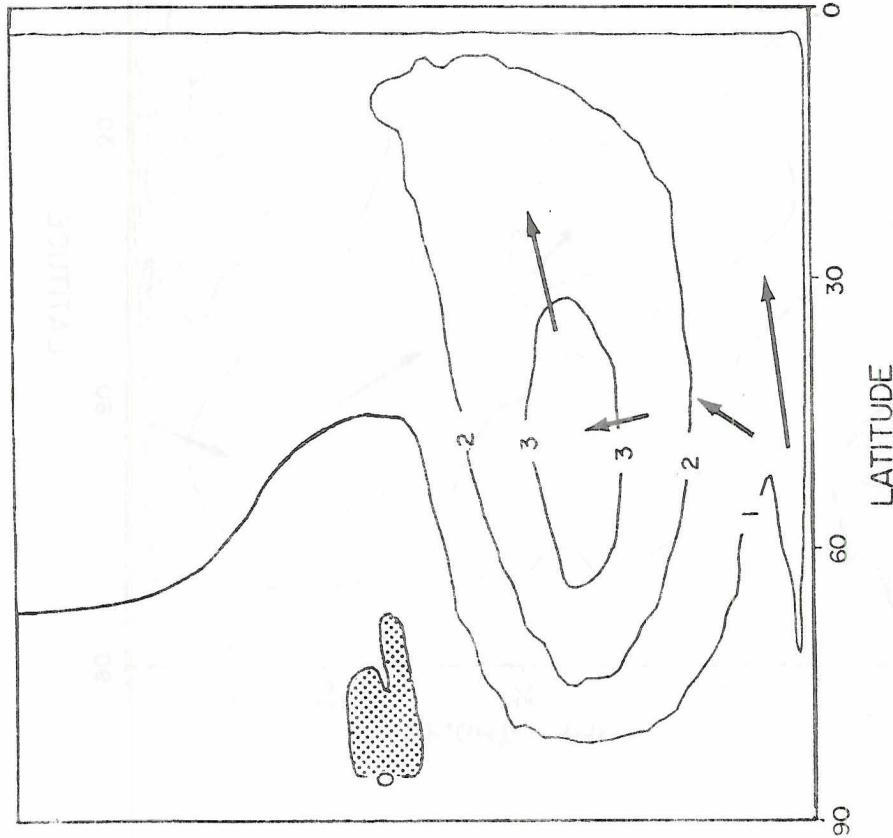


9 (a)

Figure 9 Latitude-height distributions of basic state potential vorticity gradient ($\partial\bar{q}/\partial\theta$) for the wind profiles (a) H, (b) LH, and (c) T. Units are a multiple of Ω . Stippled areas denote regions of $\partial\bar{q}/\partial\theta < 0$. Note change of height scale from (a) to (b) and (c). Arrows give a schematic indication of the anticipated direction of wave energy flow.



9(c)



9(b)

The development of the $\partial\bar{q}/\partial\theta$ field at selected days, along with the mean zonal wind field, for profile H is shown in Figure 10. By day 13, the "tongue" of high $\partial\bar{q}/\partial\theta$ values at low-levels and high-latitudes has receded as the mean zonal winds in that region have decreased (compare with Figures 4(a) and 9(a)). This explains the decay of wave geopotential amplitude seen at 60° , beginning around day 13 (Figure 7(a)). By day 18, as easterlies first appear around 40 km in polar latitudes, values of $\partial\bar{q}/\partial\theta$ poleward of 60° are small, further blocking wave propagation into this region. A day later, $\partial\bar{q}/\partial\theta$ has become negative here, reflecting the presence of the zero wind line.

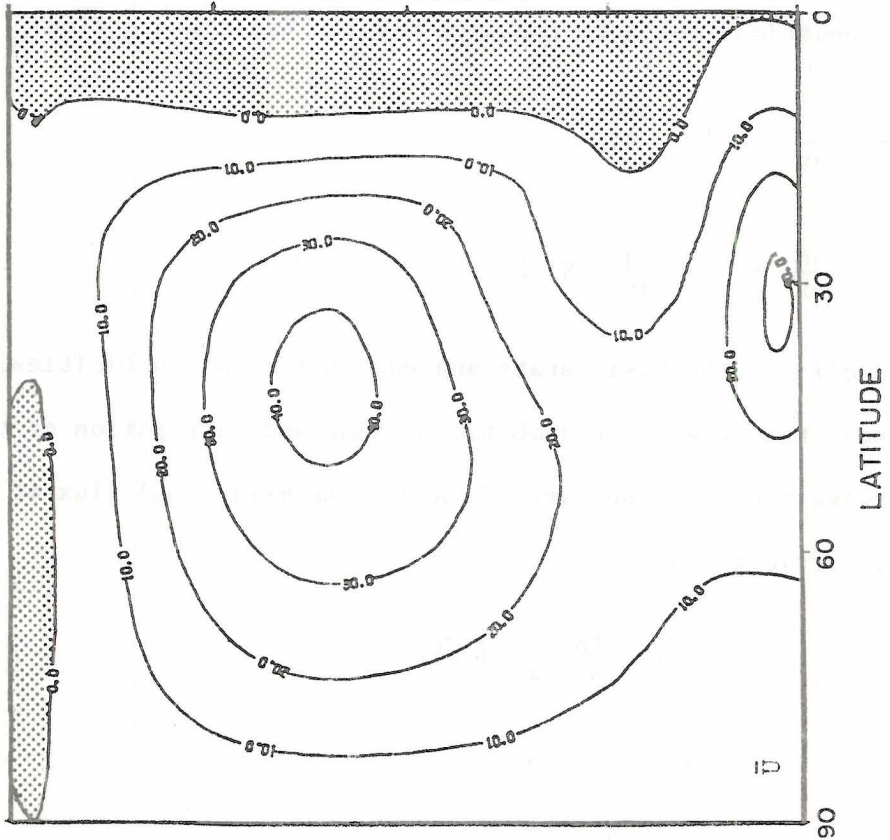
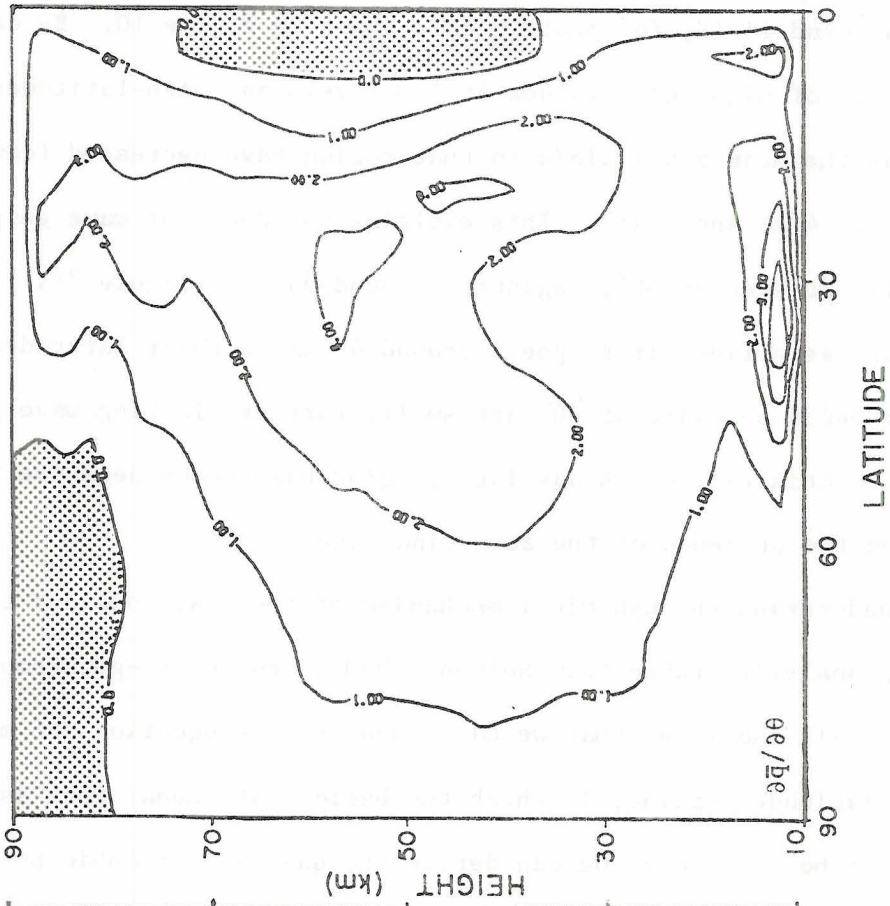
To understand the dynamical mechanism of the SSW, consider the following analysis, taken from Holton (1980). For quasi-geostrophic motions (small enough so that we can linearise the equations of motion) on a mid-latitude β -plane, in which the basic state zonal flow is a function of both y and z , we can derive the quasi-geostrophic potential vorticity equations for both the wave and the basic state flow:

$$\frac{\partial\bar{q}}{\partial t} = - \frac{\partial}{\partial y} (\overline{v'q'}) - \bar{S}, \quad (3.5)$$

$$\frac{\partial q'}{\partial t} + \bar{u} \frac{\partial q'}{\partial x} = - v' \frac{\partial \bar{q}}{\partial y} - S', \quad (3.6)$$

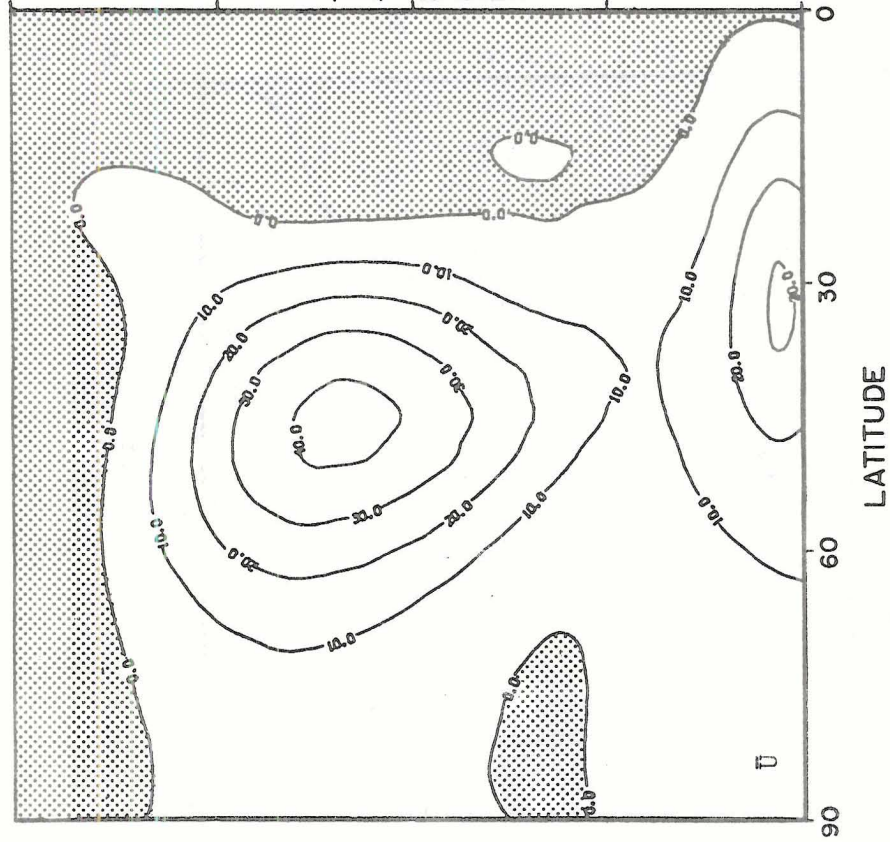
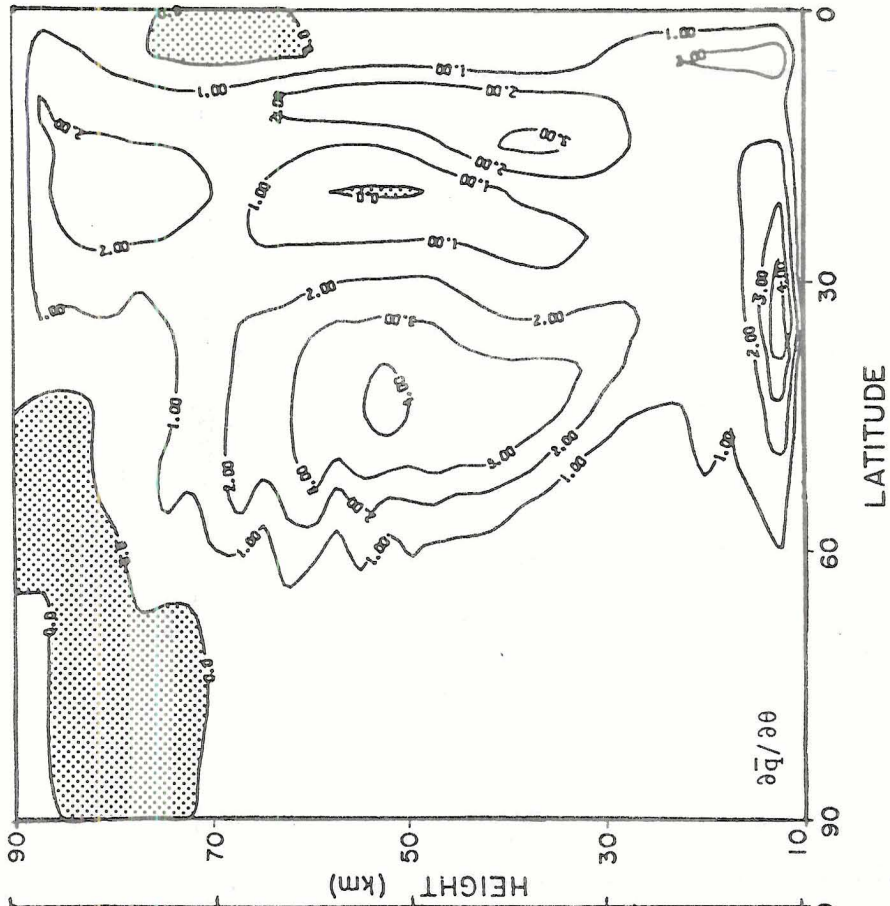
where (\bar{q}, q') are the basic state and eddy potential vorticities. \bar{S} and S' represent the effects of diabatic heating and dissipation of the mean and wave flows, respectively. Also, the meridional flux of eddy potential vorticity is:

$$\overline{v'q'} = - \frac{\partial}{\partial y} (\overline{u'v'}) + \frac{f_0}{N^2} \frac{\partial}{\partial z} (\overline{v'\theta'}) \quad (3.7)$$



DAY 13

10 (a)



DAY 18

10 (b)

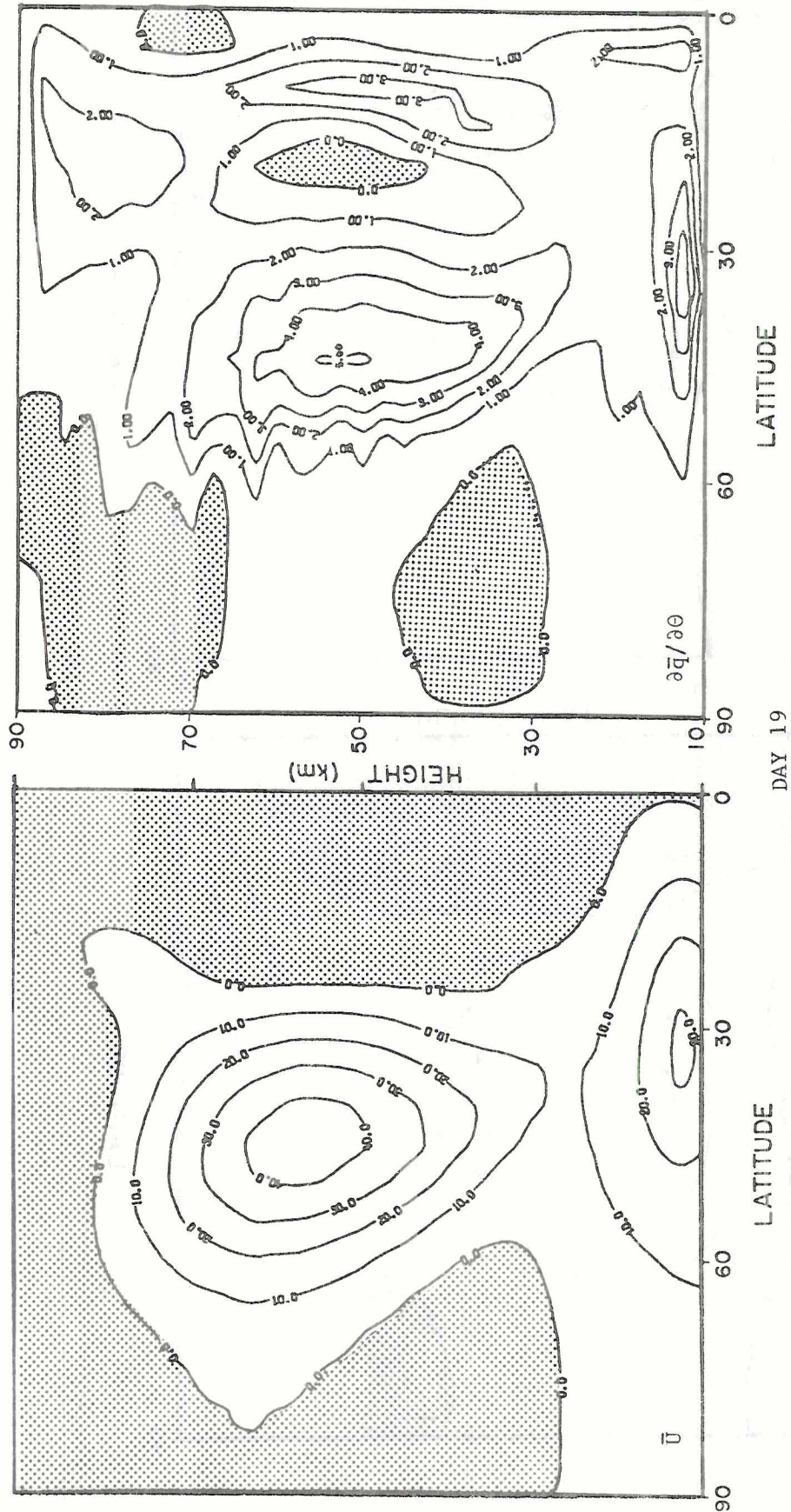


Figure 10 Latitude-height distribution of basic state zonal wind, \bar{u} (m/s), and $\partial \bar{q} / \partial \theta$ (in units of Ω) for wind profile H at (a) 13 days, (b) 18 days, and (c) 19 days. Stippling denotes regions of negative \bar{u} and $\partial \bar{q} / \partial \theta$.

and

$$\frac{\partial \bar{q}}{\partial y} = \beta - \frac{\partial^2 \bar{u}}{\partial y^2} - \frac{f_0^2}{N^2} \frac{\partial^2 \bar{u}}{\partial z^2}. \quad (3.8)$$

f_0 is a constant value of f on the β -plane, and θ' is analogous to potential temperature; so eddy potential vorticity flux is due to eddy heat and momentum fluxes. $\partial \bar{q}/\partial y$ is analogous to Matsuno's (1970) $\partial \bar{q}/\partial \theta$, discussed above.

In the SSW, basic state winds and temperatures are being changed by the wave; so we ask under what conditions is $\partial \bar{q}/\partial t \neq 0$? (From the definition of \bar{q} , if \bar{q} is independent of t , then so are \bar{u} and $\bar{\theta}$). Ignoring the zonal mean diabatic terms, as we do in the SSW problem, from (3.5) we see that when $\overline{v'q'} = 0$, then $\partial \bar{q}/\partial t = 0$; so we now seek conditions under which $\overline{v'q'} = 0$. (Even if $\overline{v'q'} \neq 0$ somewhere in the domain, it will vanish at the boundaries, so that its derivative will be non-zero; thus we need only look at whether or not $\overline{v'q'}$ itself is non-zero somewhere).

Multiplying (3.6) by q' and zonally averaging gives:

$$\overline{v'q'} = - \left[\frac{1}{2} \frac{\partial}{\partial t} (\overline{q'^2}) + \overline{S'q'} \right] / \frac{\partial \bar{q}}{\partial y}. \quad (3.9)$$

Hence, for $\partial \bar{q}/\partial y \neq 0$, $\overline{v'q'}$ and thus $\partial \bar{q}/\partial t$ will be non-zero only where there is (a) transience (i.e., the wave amplitude is growing/decaying with time) or (b) dissipation (such as Newtonian cooling).

On the other hand, if we neglect transience and assume a stationary wave (so $\partial q'/\partial t = 0$) and also neglect dissipation ($S' = 0$), (3.6) becomes:

$$\bar{u} \frac{\partial q'}{\partial x} = - v' \frac{\partial \bar{q}}{\partial y} \quad (3.10)$$

Taking v' to be geostrophically determined by

$$v' = \frac{1}{f} \frac{\partial \phi'}{\partial x},$$

if we multiply (3.10) by Φ' and zonally average, we have:

$$\bar{u} \overline{v'q'} = 0. \quad (3.11)$$

Thus $\overline{v'q'} = 0$, unless $\bar{u} = 0$.

Thus, there are three conditions, under which the wave can interact with the basic state and change it, viz: (a) transience, (b) dissipation, and (c) critical levels ($\bar{u} = 0$ for stationary waves). Although Matsuno (1970) originally explained the mechanism of the SSW in terms of critical levels causing mean flow deceleration, observations indicate that the warmings happen in the absence (initially) of a critical level, and it is clear now that the dominant of the three mechanisms for the SSW is wave transience.

Consider now the simplified equations (2.16) and (2.18) to see how the warming "works":

$$\frac{\partial \bar{u}}{\partial t} = f\bar{v} + \mathcal{F}, \quad (3.12)$$

$$\frac{\partial}{\partial t} \left(\frac{\partial \bar{\Phi}}{\partial z} \right) = -N^2 \bar{w} - \mathcal{G}, \quad (3.13)$$

with

$$\mathcal{F} = \frac{-1}{\cos^2 \theta} \frac{\partial}{\partial y} (\overline{u'v'} \cos^2 \theta)$$

and

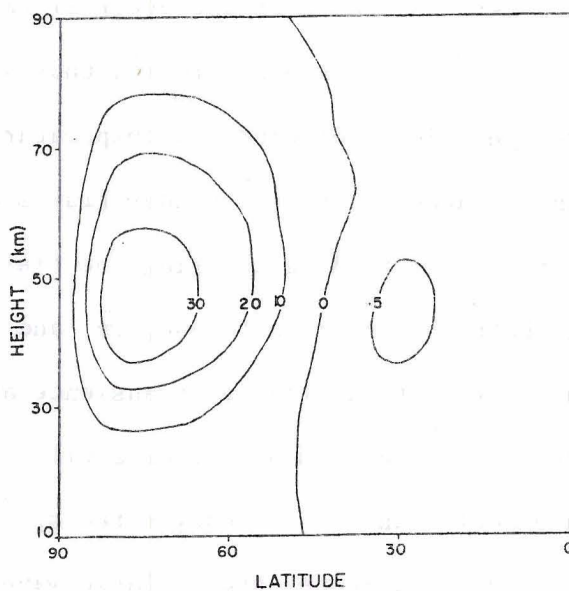
$$\mathcal{G} = \frac{1}{\cos \theta} \frac{\partial}{\partial y} \left(\overline{v' \frac{\partial \Phi'}{\partial z}} \cos \theta \right).$$

As the wave grows and propagates its influence vertically and horizontally, heat and momentum fluxes (i.e., potential vorticity fluxes) develop. Since the wave is transient, there is a region sufficiently far beyond the origin of the forcing where there is no such

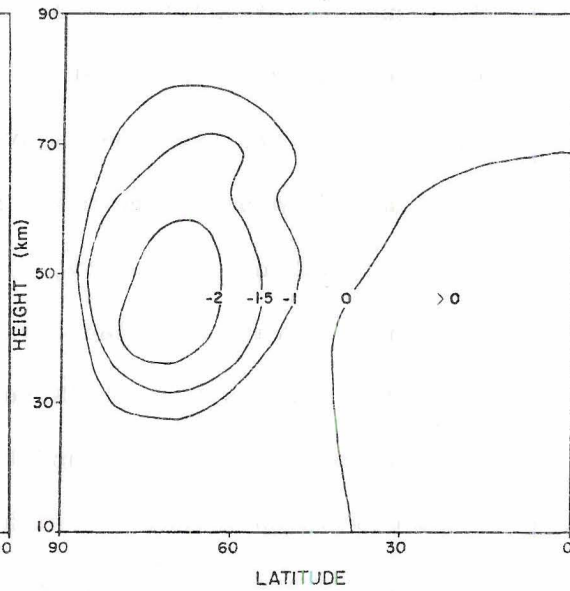
potential vorticity flux; the wave's influence has yet to arrive. Consequently, \mathcal{F} and \mathcal{G} must be non-zero and so $\partial\bar{u}/\partial t$ and $\partial(\partial\bar{\phi}/\partial z)/\partial z$ must be non-zero. Alternatively, $\partial(\overline{v'q'})/\partial y$ is non-zero and thus so is $\partial\bar{q}/\partial t$. However, the zonally averaged fields of wind and temperature are constrained to be in thermal wind balance, so that the eddy fluxes cause a mean meridional motion (\bar{v}, \bar{w}) to arise, tending to bring the fields back into a state of balance via both the coriolis torque, $f\bar{v}$, and adiabatic warming. In the absence of critical levels, transience and dissipation, steady waves and their heat and momentum fluxes will induce a mean meridional motion, which exactly cancels the eddy effects, leaving the basic state unchanged. With wave transience, when a large wave propagates up from the troposphere, it is the small imbalance between the eddy forcing terms and the mean meridional motion terms which results in the SSW (i.e., the temperature and wind changes).

In Figure 11, we show for each wind profile the following, all at day 12: (i) the distribution of eddy momentum flux convergence, \mathcal{F} ; (ii) the distribution of wave-induced meridional flow, \bar{v} ; (iii) the latitudinal distribution of eddy momentum flux convergence and coriolis torque, $f\bar{v}$, at 45 km; and (iv) the distribution of eddy heat flux. As expected, for profile H the fluxes are larger than with profiles LH and T, since the wave amplitude is less in the latter two cases. We can also see from Figure 11 (iii) the near cancellation of the twin driving terms of $\partial\bar{u}/\partial t$.

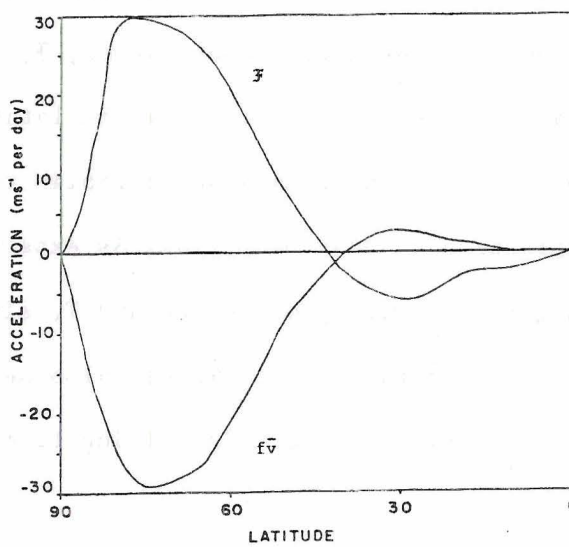
Customarily, the eddy heat and momentum fluxes have been considered separately in discussions of the SSW. The previous analysis shows that it is their combined effect, through $\overline{v'q'}$, which generates the warming and that therefore they should be considered in tandem (Holton, 1980).



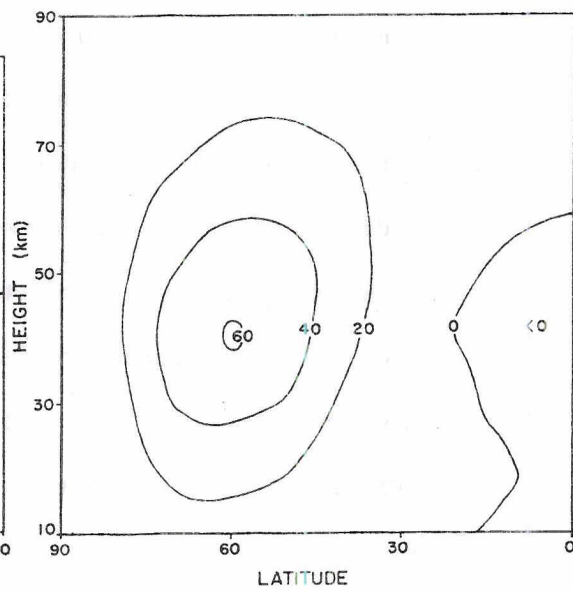
(i) \bar{F}



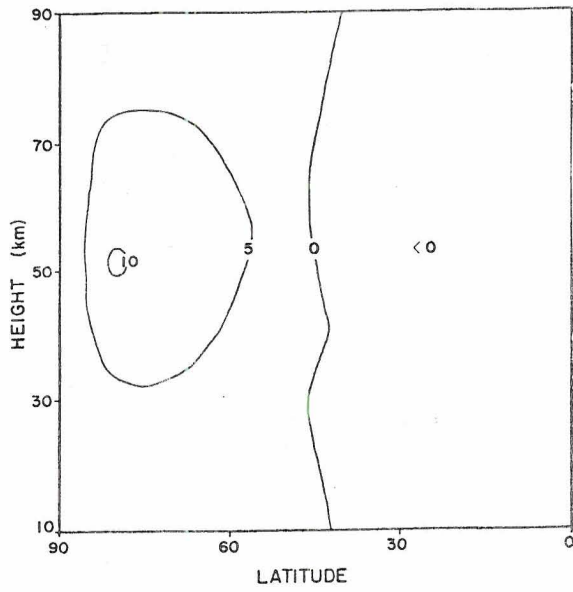
(ii) \bar{v}



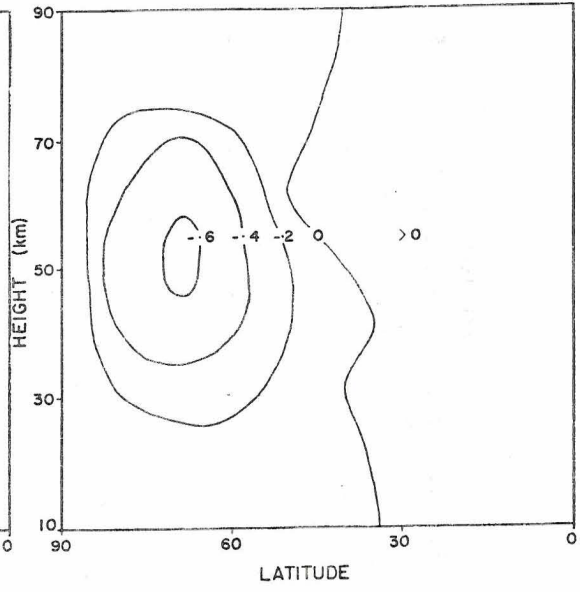
(iii) \bar{F} vs $f\bar{v}$



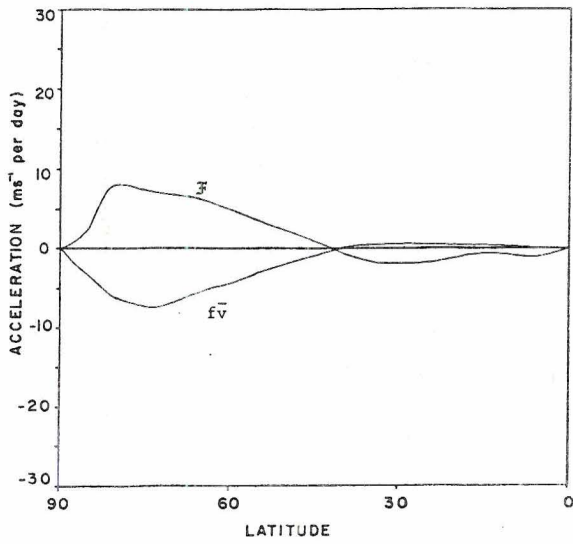
(iv) $\overline{v'T'}$



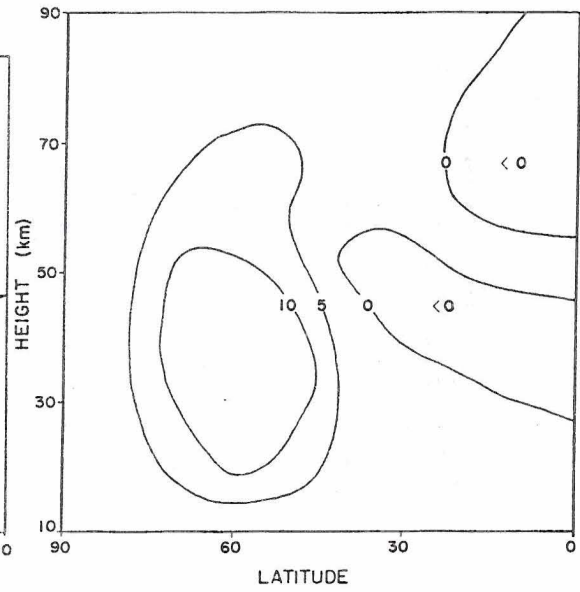
(i) \mathcal{F}



(ii) \bar{v}



(iii) \mathcal{F} vs \bar{v}



(iv) $\overline{v'T'}$

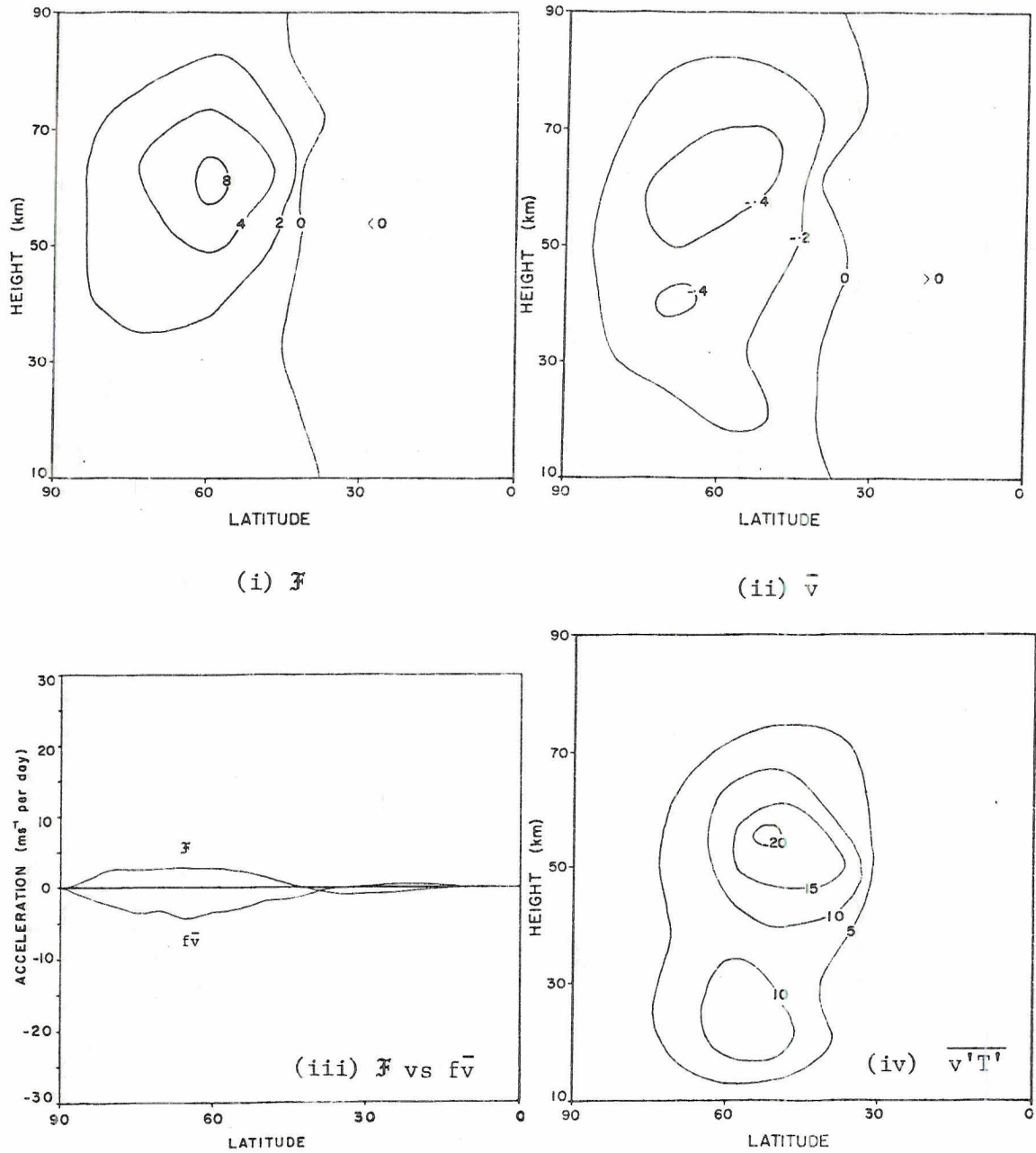


Figure 11 For wind profiles (a) H, (b) LH, and (c) T, we show: (i) the distribution of momentum flux convergence, \bar{F} ($\times 10^{-5} \text{ ms}^{-2}$); (ii) the distribution of mean meridional wind, \bar{v} (ms^{-1}); (iii) the latitudinal distributions of eddy momentum flux convergence, \bar{F} , and the coriolis torque, $\bar{f}v$, at height 45 km. (units are ms^{-1} per day); and (iv) the distribution of eddy heat flux, $\overline{v'T'}$ $\cos\theta$ (units of k ms^{-1}). All are for conditions at day 12. Note change of contour intervals between the three cases.

Since the net mean zonal wind acceleration and the net temperature change are the small residuals of two larger terms, we define a residual mean meridional circulation, following Holton (1980, 1981):

$$\bar{w}^* = \bar{w} + \frac{1}{\cos\theta} \frac{\partial}{\partial y} \left(\frac{\mathfrak{H}}{N^2} \right), \quad (3.14)$$

$$\bar{v}^* = \bar{v} - \frac{1}{\cos\theta} \left(\frac{\partial}{\partial z} - \frac{1}{H} \right) \left(\frac{\mathfrak{H}}{N^2} \right), \quad (3.15)$$

where \mathfrak{H} is defined by

$$\begin{aligned} \mathfrak{G} &= \frac{1}{\cos\theta} \frac{\partial \mathfrak{H}}{\partial y} \\ \text{i.e.,} & \\ \mathfrak{H} &= \overline{v' \frac{\partial \Phi'}{\partial z}} \cos\theta. \end{aligned} \quad (3.16)$$

Substituting (3.14) and (3.15) back into (3.12) and (3.13), we have:

$$\frac{\partial \bar{u}}{\partial t} = f \bar{v}^* + \bar{P}, \quad (3.17)$$

$$\frac{\partial}{\partial t} \left(\frac{\partial \bar{\Phi}}{\partial z} \right) = -N^2 \bar{w}^*, \quad (3.18)$$

where

$$\begin{aligned} \bar{P} &= \mathfrak{F} + \frac{f}{\cos\theta} \left(\frac{\partial}{\partial z} - \frac{1}{H} \right) \left(\frac{\mathfrak{H}}{N^2} \right) \\ &= -\frac{1}{\cos^2\theta} \frac{\partial}{\partial y} (\overline{u'v'} \cos^2\theta) + \frac{f}{\cos\theta} \left(\frac{\partial}{\partial z} - \frac{1}{H} \right) \left(\overline{v' \frac{\partial \Phi'}{\partial z}} \frac{\cos\theta}{N^2} \right) \end{aligned} \quad (3.19)$$

$$\equiv \frac{1}{\rho_0 \cos\theta} \nabla \cdot \rho_0 \underline{F}, \text{ defining } \underline{F}. \quad (3.20)$$

Since now \bar{v}^* and \bar{w}^* are small quantities, the distribution of \bar{P} provides a useful diagnosis of the distribution of $\partial \bar{u} / \partial t$, and we note now that in looking at \bar{P} , we are looking at both eddy momentum and heat fluxes. In the β -plane analysis discussed earlier, \bar{P} reduces to $\overline{v'q'}$.

From (3.20), we can see that \bar{P} in turn can be written in terms of the divergence of the quantity $\rho_0 \underline{F}$. Holton and Wehrbein (1980) indicate that \underline{F} is approximately the Eliassen-Palm flux of wave energy.

The quantities, which Eliassen and Palm (1961) refer to as wave energy flux, are $\overline{v' \phi'}$ and $\overline{w' \phi'}$ in the horizontal and vertical, respectively. They showed that for long waves:

$$\overline{v' \phi'} = \bar{u} \left[\frac{1}{N^2} \frac{\partial \bar{u}}{\partial z} \overline{v' \frac{\partial \phi'}{\partial z}} - \overline{u' v'} \right] \quad (3.21)$$

and

$$\overline{w' \phi'} = \bar{u} \left[\frac{1}{N^2} \left(f - \frac{\partial \bar{u}}{\partial y} \right) \overline{v' \frac{\partial \phi'}{\partial z}} - \overline{u' w'} \right]. \quad (3.22)$$

For quasi-geostrophic waves, (3.21) and (3.22) reduce to:

$$\overline{v' \phi'} = - \bar{u} \overline{u' v'} \quad (3.23)$$

and

$$\overline{w' \phi'} = \frac{\bar{u} f}{N^2} \overline{v' \frac{\partial \phi'}{\partial z}} \quad (3.24)$$

i.e., they are just the momentum and heat fluxes due to the wave. From (3.24), we see that a poleward heat flux is associated with an upward energy flux, and (3.23) indicates that a poleward momentum flux corresponds to an equatorward energy flux. A poleward heat flux is in turn associated with a westward tilt of the wave with increasing height, whilst a westward tilt with decreasing latitude is indicative of poleward momentum flux. Both these tilts result in the model (not shown).

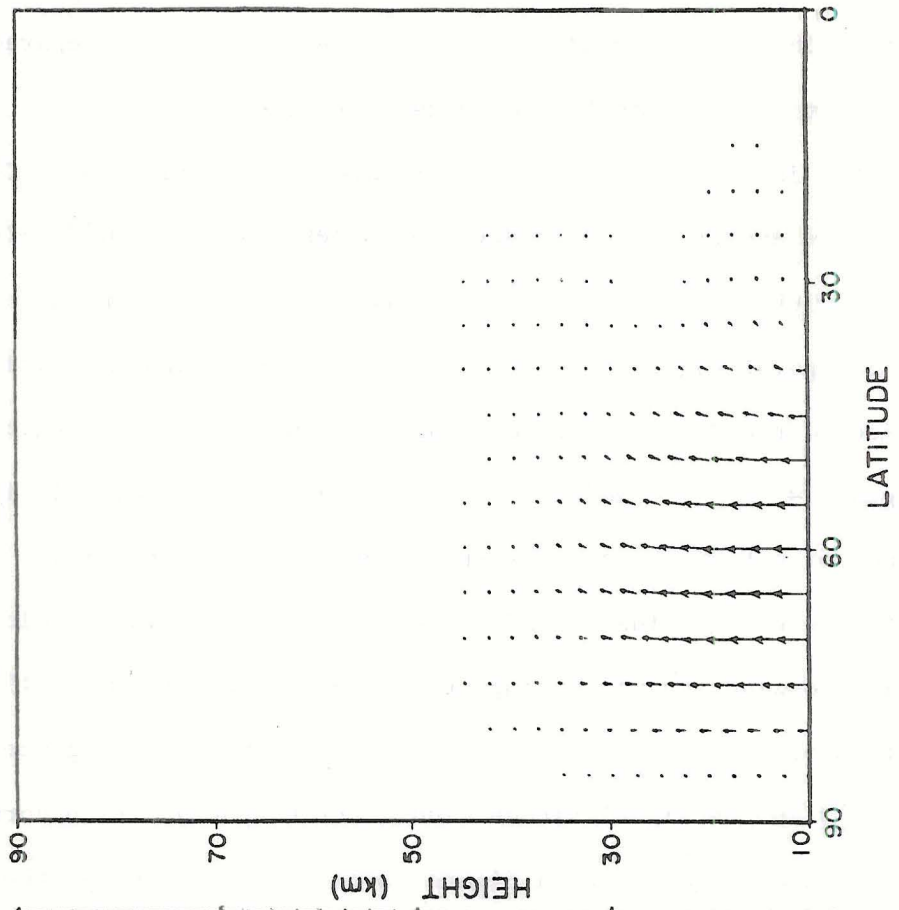
Thus, \underline{F} is analogous to $(\overline{v' \phi'}, \overline{w' \phi'})$ in a quasi-geostrophic system and thus is analogous to wave energy flux. Also therefore, \bar{P} is analogous to the divergence of the Eliassen-Palm wave energy flux. Matsuno (1970) plotted the vector quantity $(\overline{v' \phi'}, \overline{w' \phi'})$ in his study of long wave structure.

In Figure 12, we show the distribution of (a) \underline{F} , (b) $\rho_{\underline{O}}\underline{F}$, and (c) \bar{P} after 18 days for wind profile H. These should be compared with the distributions of \bar{u} at 18 and 19 days (Figure 10 (b, c)).

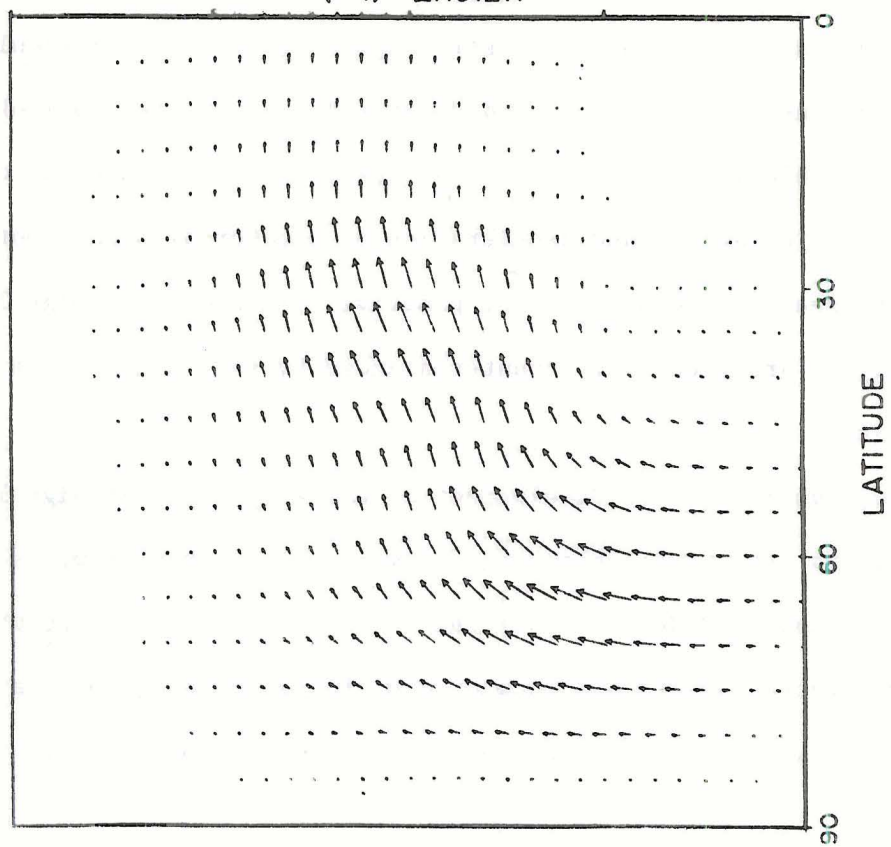
Figure 12(a) indicates an upward and equatorward energy flux. Convergence of wave energy (\underline{F}) is apparent at upper levels at middle-to-high latitudes, with divergence just above the forcing level and also equatorward of the polar night jet. The convergence at equatorial latitudes gives rise to the deceleration of mean zonal winds in this region (convergence $\Rightarrow \bar{P} < 0 \Rightarrow \partial\bar{u}/\partial t < 0$ and vice versa), although it is the divergence of $\rho_{\underline{O}}\underline{F}$ which actually should be equated with $\partial\bar{u}/\partial t$. We note decay of wave energy flux beyond the equatorial wind line, indicating that the zero-wind line is an important energy sink (Matsuno, 1970).

Examination of Figure 12(b) reveals more clearly the convergence of the quantity $\rho_{\underline{O}}\underline{F}$ in the high-latitude middle stratosphere, which corresponds to the region of negative \bar{P} in Figure 12(c). Unfortunately, the quantity $\rho_{\underline{O}}\underline{F}$ is so small above the lower stratosphere that it is difficult to detect regions of convergence and divergence; so we need to look at both \underline{F} and $\rho_{\underline{O}}\underline{F}$ fields. Figure 12(c) also indicates a strengthening of the polar night jet at 45° and deceleration of equatorial winds, both of which are seen in the model. The positive values of \bar{P} at high latitudes around 50 km are presumably counterbalanced by $f\bar{v}^*$, since winds here decelerate.

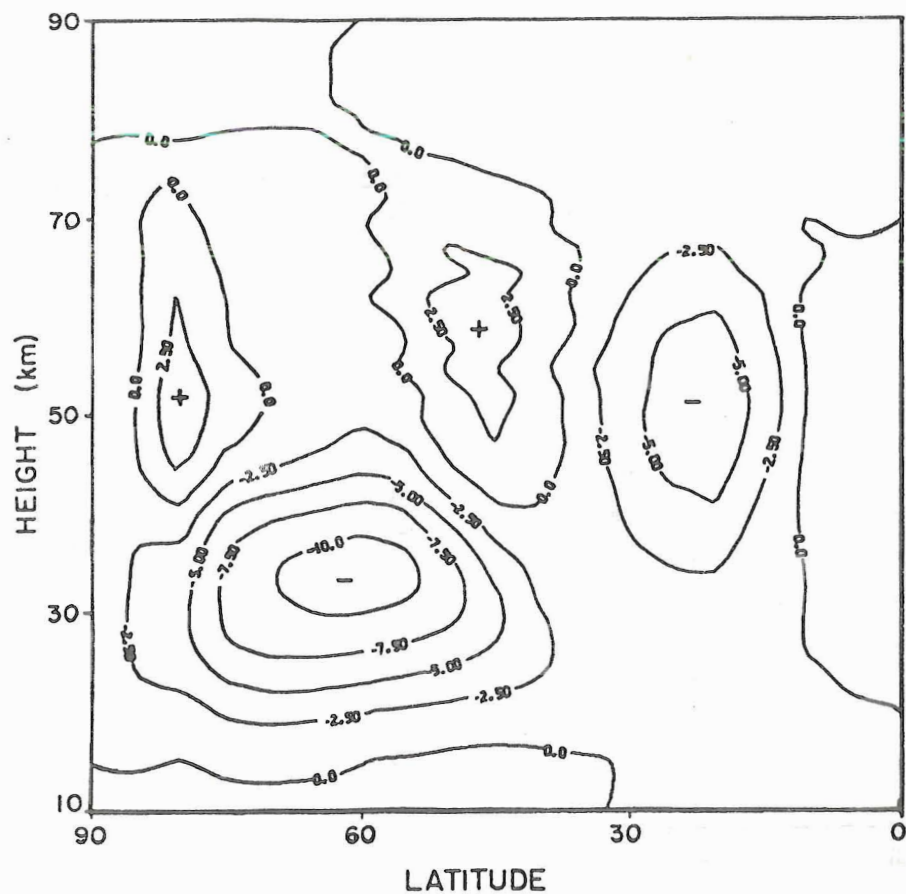
Two days later, the development of easterly winds at high latitudes has begun to effectively block equatorward wave energy flow, as Figure 13 shows. O'Neill (1981) has shown that the vector \underline{F} , which is usually directed upward and equatorward, turns to become poleward in association with the SSW. This only occurs in the model above the polar



12(b) $p_0 \bar{F}$



12(a) \bar{F}



12(c) \bar{P}

Figure 12 Latitude-height distribution of (a) \underline{F} , (b) $\rho_0 \underline{F}$, and (c) \bar{P} at day 18 for wind profile H. The units of \bar{P} are ms^{-1} per day. In (c), areas marked + or - show where the effect of \bar{P} is to accelerate or decelerate the mean zonal wind. The vertical component of \underline{F} in this, and subsequent Figures showing the distribution of \underline{F} , has been multiplied by $\Delta y/\Delta z$ for plotting.

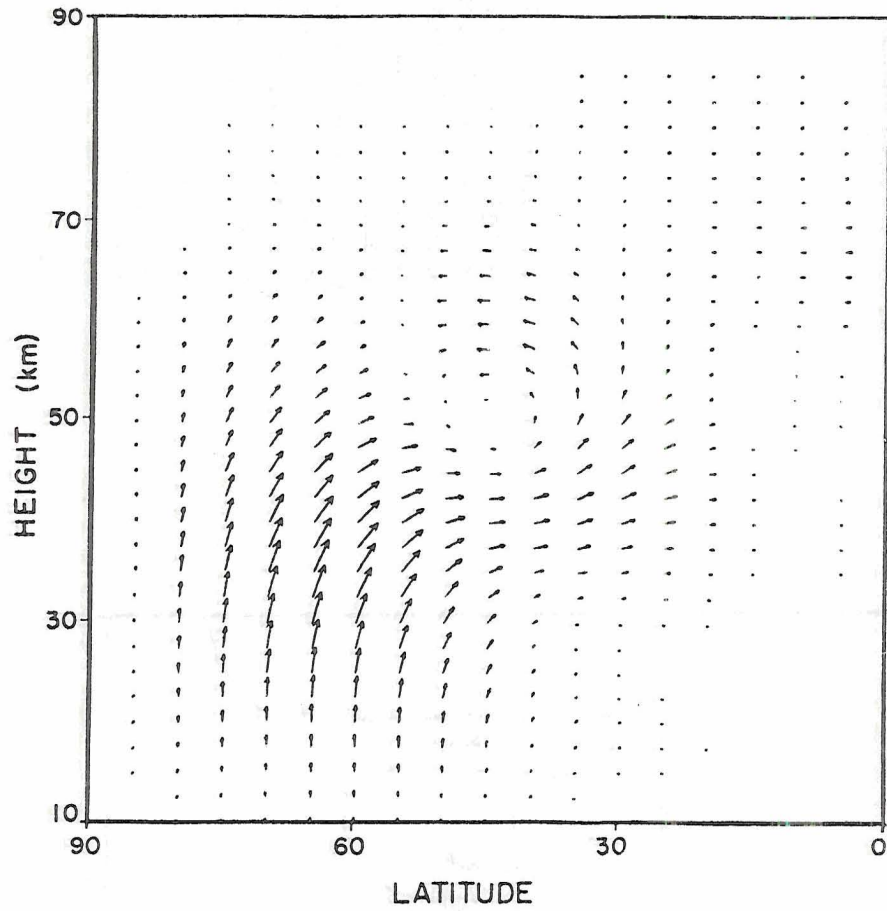
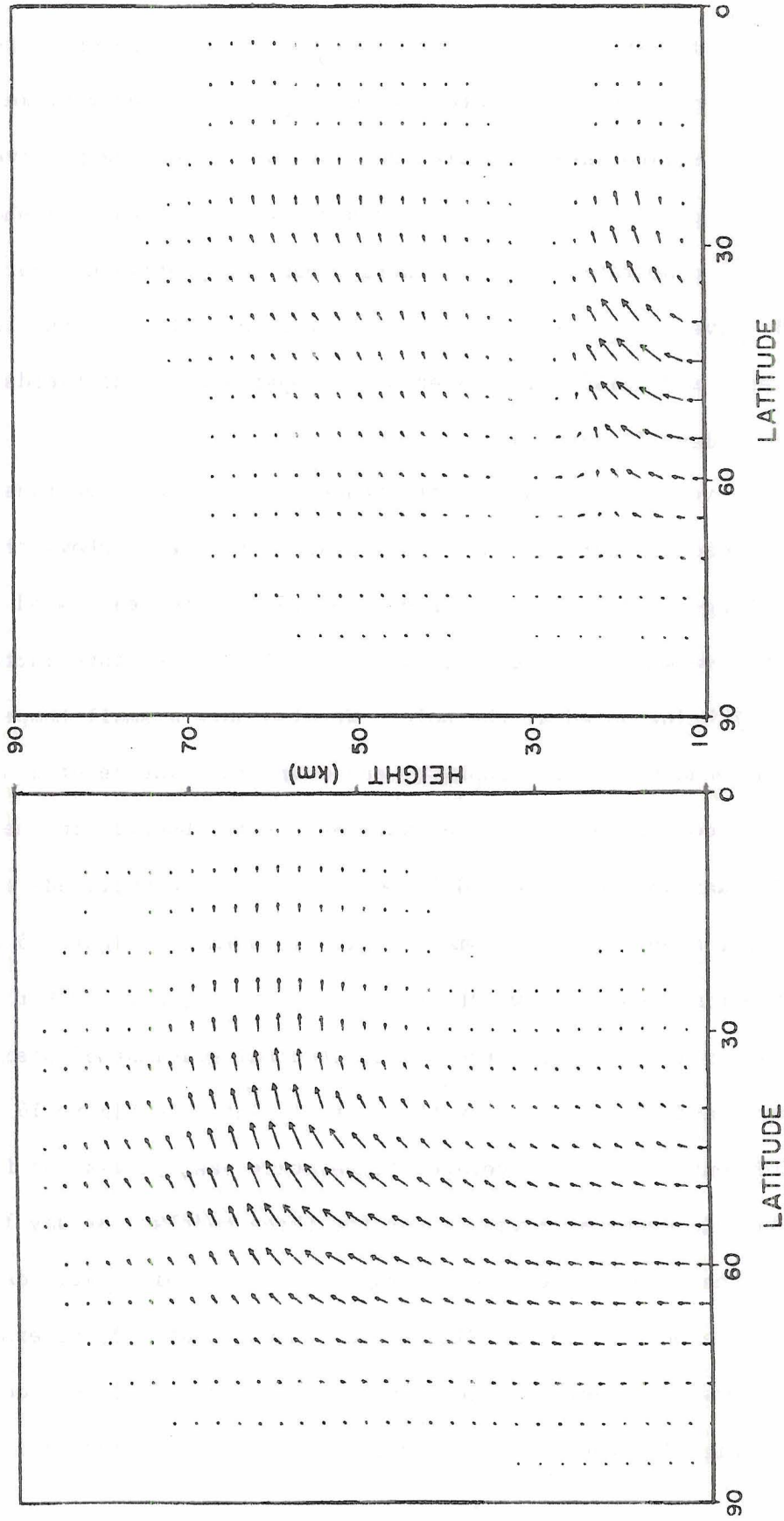


Figure 13 Latitude-height distribution of F at day 20 for wind profile H.

night jet after the high-latitude deceleration has occurred. Sato (1980) has shown the January average vector $\rho_0 \underline{F}$ for seven different years. He shows both poleward and equatorward directed wave energy fluxes and thus both equatorward and poleward momentum fluxes, respectively.

For wind profiles LH and T, the distribution of \underline{F} and $\rho_0 \underline{F}$ show less vertical penetration of wave energy than for profile H. For profile T, wave energy flux is cut off by the easterlies in the lower stratosphere, and this is indicated by a comparison of the fields of \underline{F} at 10 and 22 days (Figure 14).

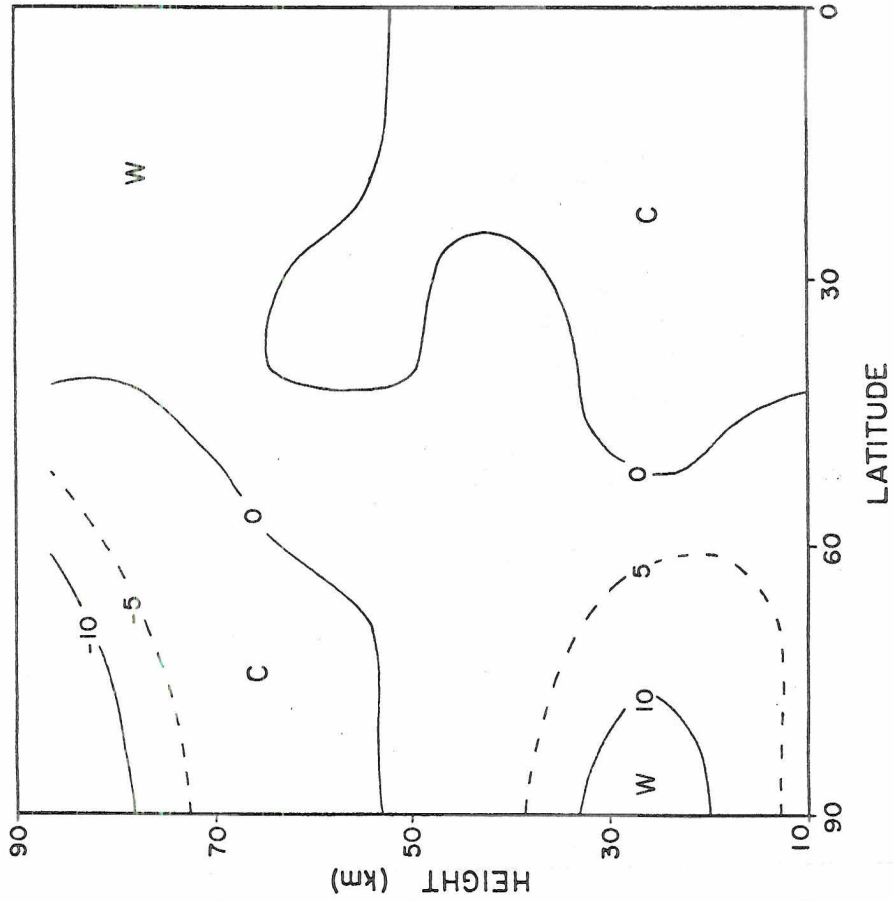
We have yet to discuss the difference between the three runs in terms of the actual warming that takes place. Figure 15 shows the temperature changes which have occurred after 25 days for each wind model. Clearly, the warming in model H is largest, with temperature increases of over 35 K being noted at the pole. We also note a small temperature fall in the equatorial stratosphere, and there is evidence of a high level polar cooling and equatorial warming, as is observed in the atmosphere. The warming for wind models LH and T reach an amplitude of only 10 K, and for model T, only a small region is warmed. Figure 15 reveals neither the time scale, on which the warming occurs, nor whether the warming is sufficient to reverse the latitudinal gradient of basic state temperature, and thus to destroy the westerly jet. In Figure 16 we show the development of zonally averaged temperature (as a deviation from the hemispheric mean) at 26.25 km for the three models. By day 17 for profile H, the temperature gradient has reversed at high latitudes, which we may expect since, as Figure 5(a) shows, the winds reverse here shortly afterwards. For profile LH, the temperature gradient does not reverse at high latitudes until later, and indeed it is not until day 25



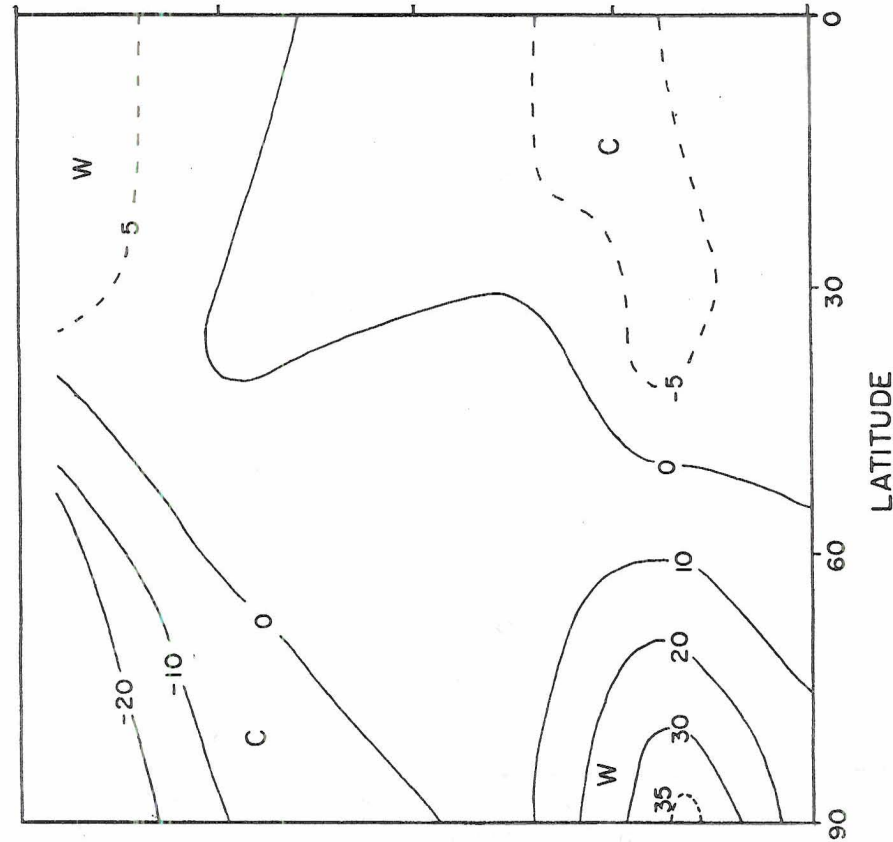
(a) 10 days

(b) 22 days

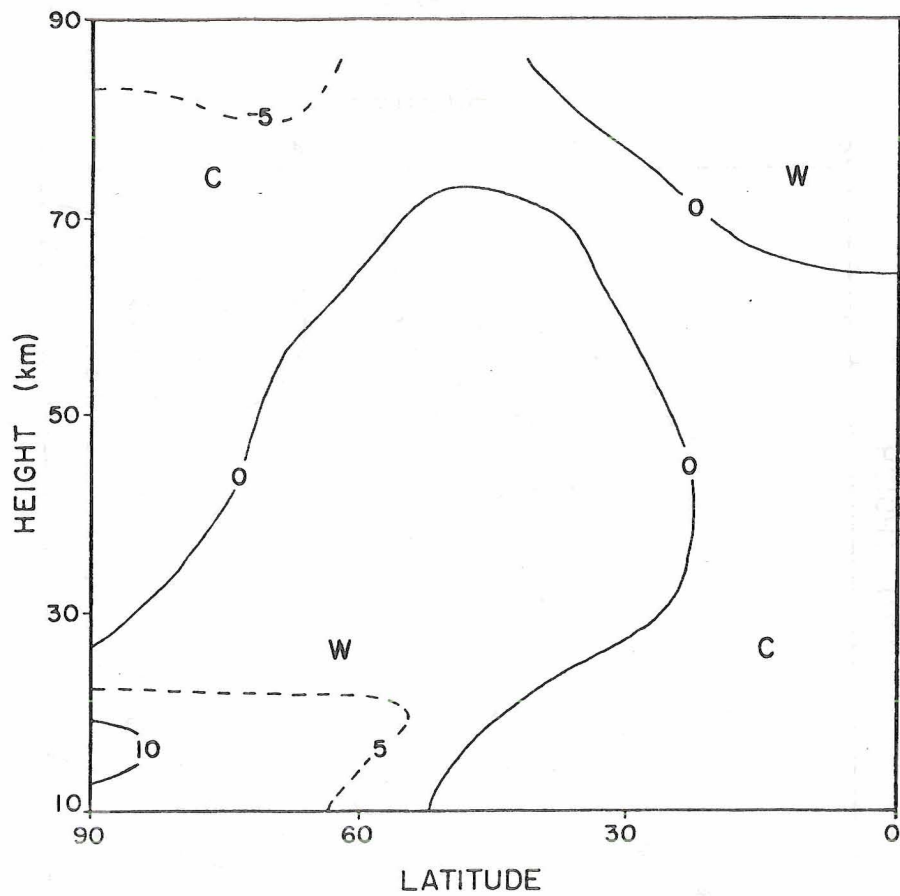
Figure 14 Latitude-height distribution of \underline{F} at (a) 10 days, and (b) 22 days for wind profile T.



15 (b)

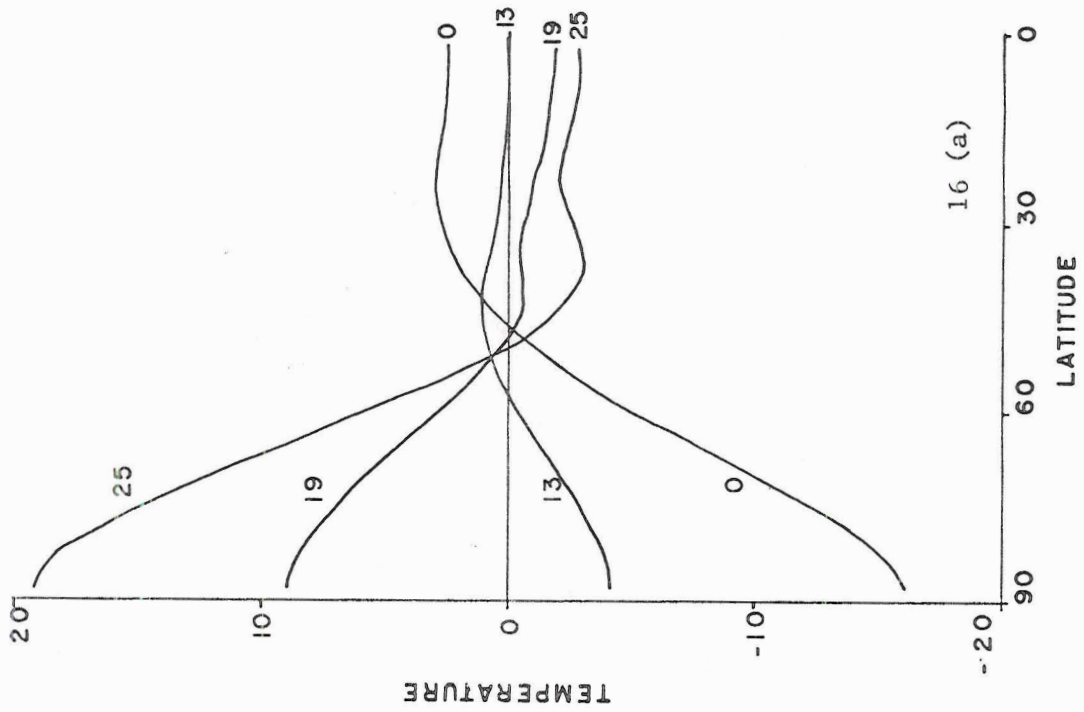
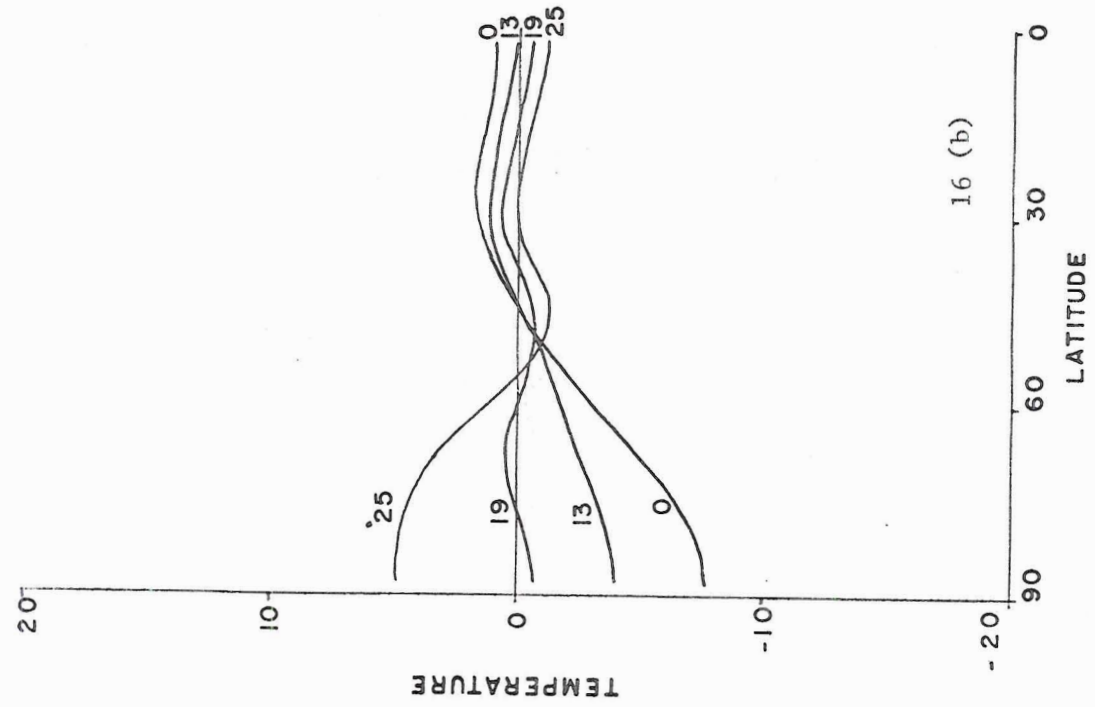


15 (a)



15 (c)

Figure 15 For wind profiles (a) H, (b) LH, and (c) T: the latitude-height distribution of the zonal mean temperature changes after 25 days. Areas of warming and cooling are indicated by W and C, respectively.



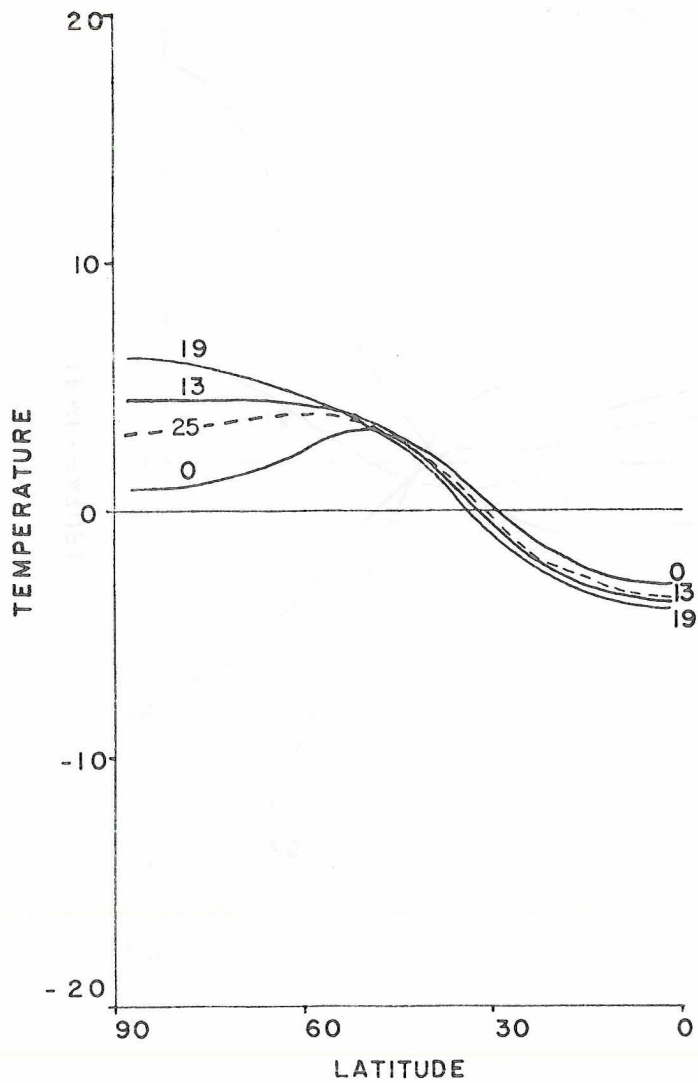


Figure 16 Zonal mean temperature (departure from hemispheric mean) as a function of latitude at selected days for profiles (a) H, (b) LH, and (c) T. All profiles are at altitude 26.25 km.

that the temperature maximum appears at the pole. In fact, at day 17, the warming appears to begin at about 65° . For profile T, the gradient of temperature does reverse near the pole between days 17 and 21, but it is always only slightly positive. Furthermore, after day 21, the temperature falls at the pole; so the negative temperature gradient is re-established.

Finally, we briefly discuss how well the model SSW compares with observed warmings. It is important to bear in mind that only one wave is allowed in the model, whereas both wavenumbers one and two are observed to play an important role in the real (atmospheric) SSW. This is seen in Kanzawa (1980, Figure 5) where, as the mean zonal wind becomes easterly, the amplitude of wavenumber one falls and at the same time wavenumber two amplitude increases. J.P. Koerner (private communication) has also reported that the sudden reversal of mean zonal wind tends to occur when the amplitudes of wavenumbers one and two are decreasing and increasing, respectively. Whilst wavenumber two has not been observed to be capable of producing a major warming by itself, it often plays an important role.

The warming at the pole at 26.25 km for wind model H is consistent with observations, although more dramatic temperature increases have been observed (Schoeberl, 1978: Table 1). The concomitant warming/cooling pattern away from polar regions and in the mesosphere (cf. Figure 15) has also been observed. McInturff (1978) has noted that the region of maximum warming can occur in the upper stratosphere, rather than the lower stratosphere. In some cases, the warming is seen to begin in mid-latitudes and migrate poleward. Holton (1976) showed

this to be a characteristic of wavenumber two, indicating the need for both waves in the model. However, we noted a similar warming beginning at 65° and moving poleward for wavenumber one with the LH wind profile. The warming has also been observed to propagate downward, but this may be due to a misinterpretation of the data. The apparent downward propagation may be a result of the westward propagation of a thermal wave, which tilts westward with increasing height (McInturff, 1978).

For the warming studied by Kanzawa (1980), easterlies appeared almost simultaneously at 72° and 52° in the upper stratosphere and then appeared to propagate both down and up. In the warming with wind model H, we also noted the spreading up and down of the zero wind line.

The review of McInturff (1978) indicates that the SSW does not follow one set pattern; many variations are possible regarding the location of maximum warming and where the easterlies first appear. There are also, of course, major and minor warmings. A major warming is defined to be one in which (a) the latitudinal gradient of the zonally averaged temperature and (b) the zonal wind reverse below 10 mb (c. 35 km) at high latitudes. Often, temperature gradient reversals are seen but without a circulation reversal. This is especially true in the southern hemisphere.

The warming of model H clearly fits into the category of a major SSW. In model LH, there was indeed a warming, but no circulation reversal, whilst for model T, the latitudinal gradient of zonal mean temperature barely changed sign and, although easterlies did appear at high latitudes, by no means can we say that the polar night jet broke down entirely. It may be claimed therefore that by using different initial

wind profiles, we have succeeded in reproducing major and minor warmings (within the limitations of the model).

Warmings are not observed to occur in isolation. Kanzawa (1980) studied a pair of warmings, separated by about two weeks. He noted that spectacular major warmings are always preceded by smaller major or minor warmings. It appears that the first of the two warmings produces conditions more favourable for the second, larger warming. For example, his Figures 4 and 5(a) show that the first warming produced easterlies in the high latitude mesosphere, but did not cause a circulation breakdown. It did however leave an area of weak westerlies in mid-latitudes, and weak latitudinal shears to the north and south, where the circulation reversal associated with the second warming began. The sensitivity studies in this section give an indication of the importance of this mechanism, whereby one event can make conditions for a major warming more favourable. It was noted that for wind profile T, the weak westerlies in the mid-latitude lower stratosphere, combined with the distribution of refractive index, allowed the mean zonal winds to reverse there after only 13 days. The fact that warming events appear to be separated in time by about two weeks suggests the importance of travelling planetary-scale waves in the stratosphere, which interfere constructively and destructively with the orographically forced, stationary waves to produce fluctuations in mean zonal wind and temperature. These fluctuations may make the atmosphere more susceptible to the influence of a particularly large amplitude wave, propagating up from the troposphere.

The warmings should therefore not, in general, be treated in isolation but as one (perhaps the final one) in a series of events throughout the winter stratosphere. The model used here is only a mechanistic one, designed to investigate a particular scenario, but it might be of interest to see whether or not a similar sequence of events could be reproduced. Nevertheless, the sensitivity to the basic state profiles provides an interesting insight into the differing behaviour of atmospheric SSW's. The distribution of basic state zonal wind and thus of refractive index is obviously of key importance to the SSW. It is also seen that the distribution of $\partial \bar{q} / \partial \theta$, \bar{P} and \bar{F} (or $\rho_0 \bar{F}$) are good diagnostic guides to what we can expect to happen in the atmosphere, given a large wave forcing from below.

3.2 Sensitivity to amplitude of forcing function

In the runs reported in Section 3.1, we used a forcing amplitude of 300 m. Although others have reported on the sensitivity of the results to the forcing amplitude (Matsuno, 1971; see also Holton and Mass, 1976), we do so here for the following reason. Since we are going to use the model with a long wave propagating up from below subject to high-altitude forcing, we do not wish our results to be construed as an examination of the effect of geomagnetic activity on the SSW. It is necessary to find a forcing amplitude, which will not lead to the relatively catastrophic changes noted in the previous section. It also affords us an opportunity to examine the importance of the wave-mean flow interaction mechanism to the development of the wave.

In Figure 1.7 we show the temporal development of wavenumber one geopotential amplitude at 60° , when interaction is suppressed, with

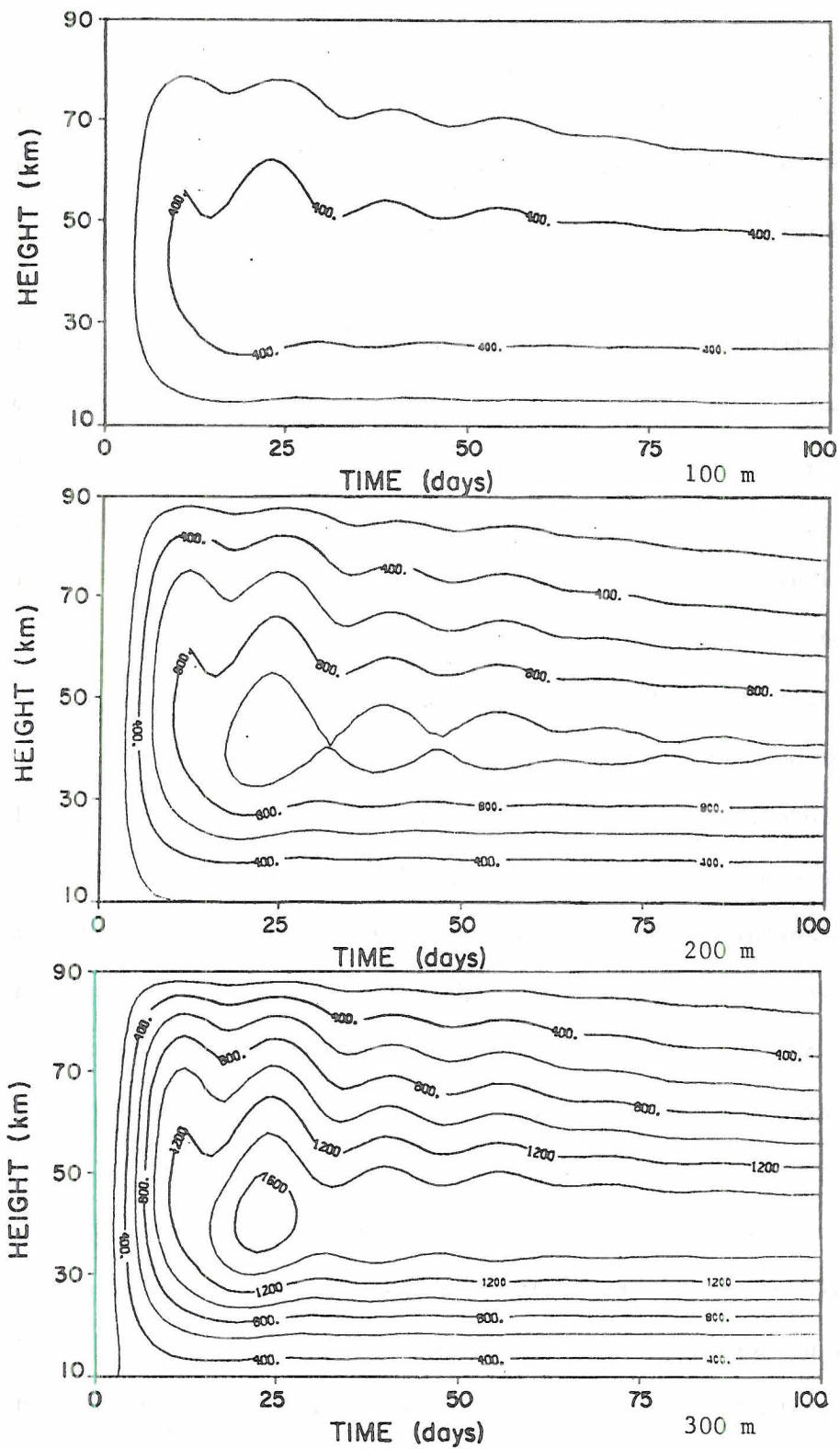


Figure 17 Time-height development of wavenumber 1 geopotential amplitude at 60° for 100 m, 200 m, and 300 m forcing. Wave-mean flow interaction is suppressed.

forcing amplitudes of 100 m, 200 m, and 300 m. Unless otherwise stated, the experiments reported here are with wind profile H. The response appears to be linear, as it should be, with the response to a 300 m forcing (applied throughout the period) three times as big as the response to a 100 m forcing. After the onset of forcing, the atmosphere appears to settle into a quasi-steady state, although a gradual loss of energy is noted. We note also the quasi-periodic oscillations in all three cases, also decaying in amplitude with time. The period of the oscillations is about 15 days in all cases. Schoeberl and Strobel (1980) noted a similar oscillation in their quasi-geostrophic model of the SSW and attributed it to a travelling free mode of the model, excited by the lower boundary forcing. The travelling mode periodically reinforces and reduces the standing wave amplitude to produce the oscillations. These numerical oscillations agree well with observations of oscillations in planetary wave amplitude in the stratosphere with a period of about two weeks (Hirota, 1968). Madden (1978) argued that the oscillations were due to a combination of the quasi-stationary wave and a westward propagating free mode with a period of 16 days, rather than a quasi-periodic forcing.

In Figure 18, we show the same wave development but now the wave is allowed to interact with the basic state flow. The alert reader will notice that the distributions in Figure 7(a) and 18 (300 m) are not quite the same, in that a larger amplitude is evident between days 20 and 25 in Figure 18. This is due entirely to the fact that in the computer runs, from which Figure 7 was constructed, we used an earlier version of the model with the coefficient of Rayleigh friction given by:

$$\alpha_R = \exp \left((z - 90 \text{ km}) / 15 \text{ km} \right) \cdot 10^{-5} \text{ s}^{-1}.$$

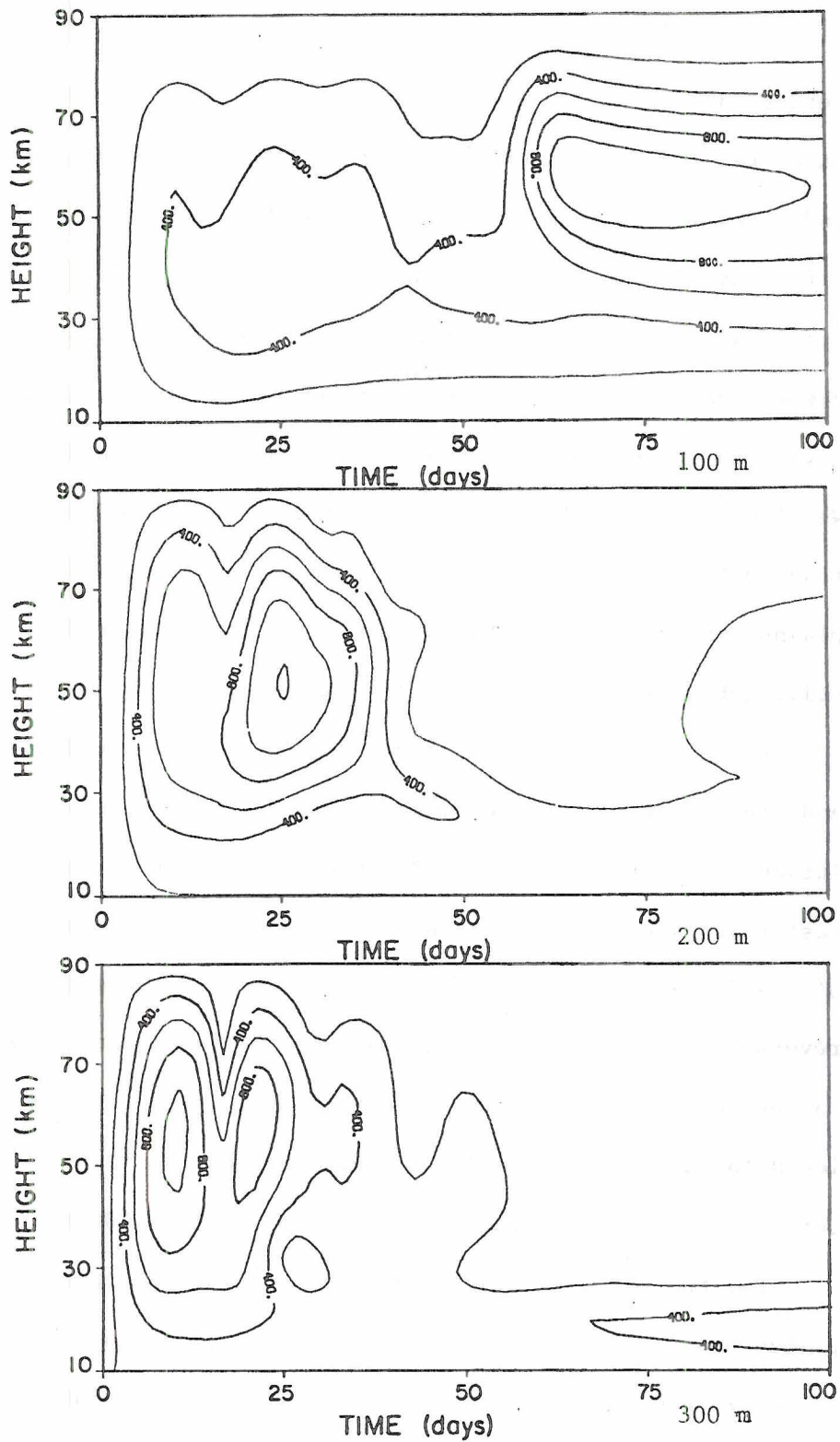


Figure 18 As Figure 17 but now wave-mean flow interaction is allowed.

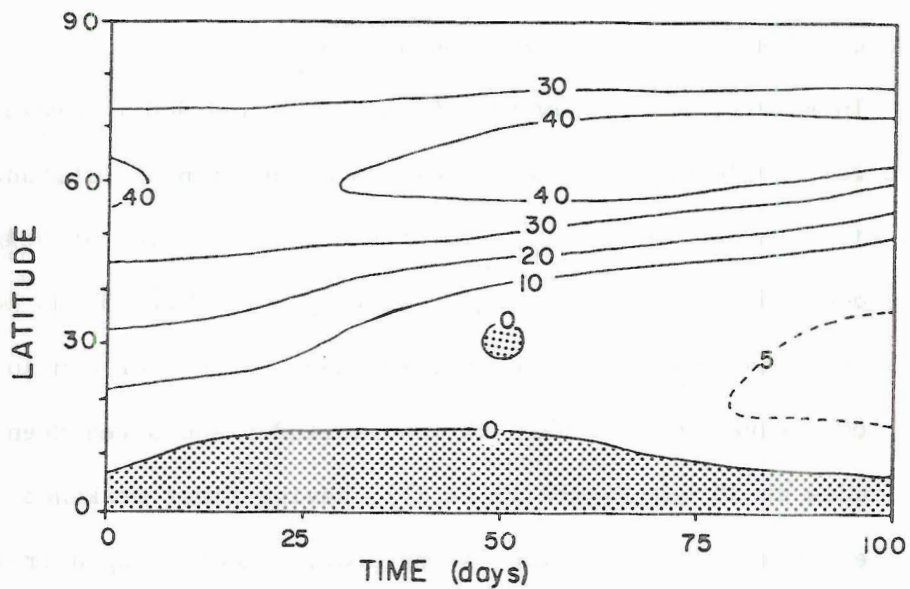
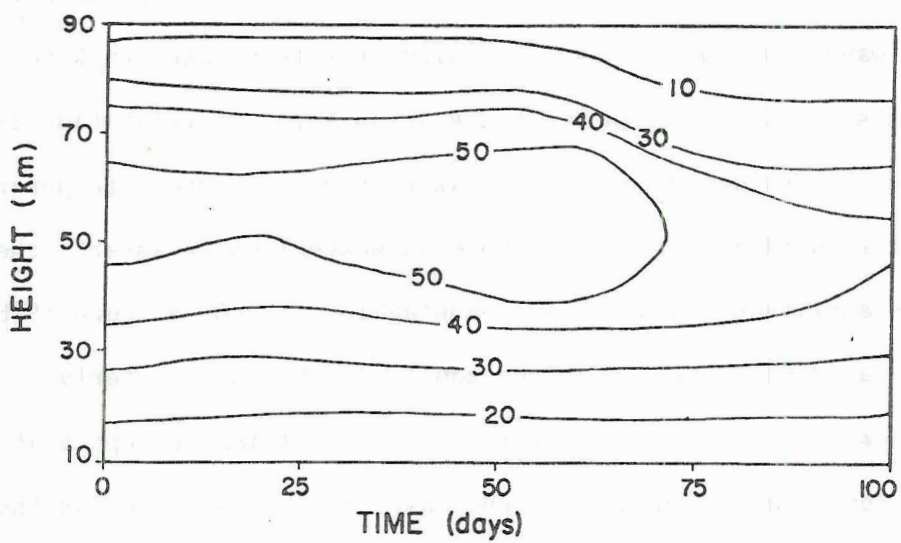
Between 30 and 70 km, the damping rate due to this formulation is larger than that shown in Figure 3; so it is reasonable that smaller wave amplitudes develop. Since the object of Section 3.1 was a comparison between different wind profiles, and due to financial considerations, it was deemed unnecessary to repeat the experiments of that section with the newer formulation of α_R . The differences do however indicate a sensitivity to the parameterization of mechanical dissipation in the model. We also note that the damping rate due to the above formulation is faster than that given by Holton's (1976) equation for α_R . This therefore explains why, when we use the same forcing function as Holton (1975), we still get smaller wave amplitudes than he did.

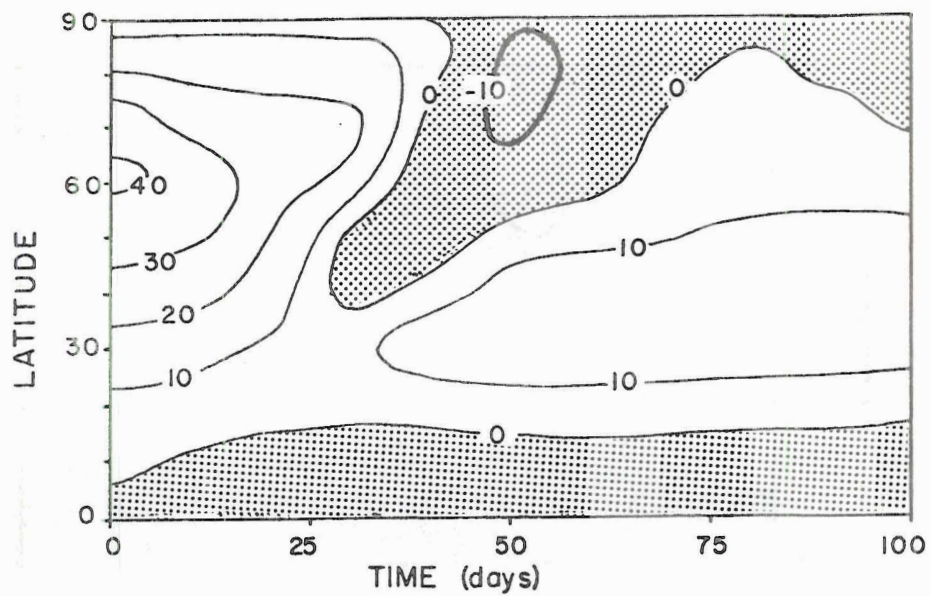
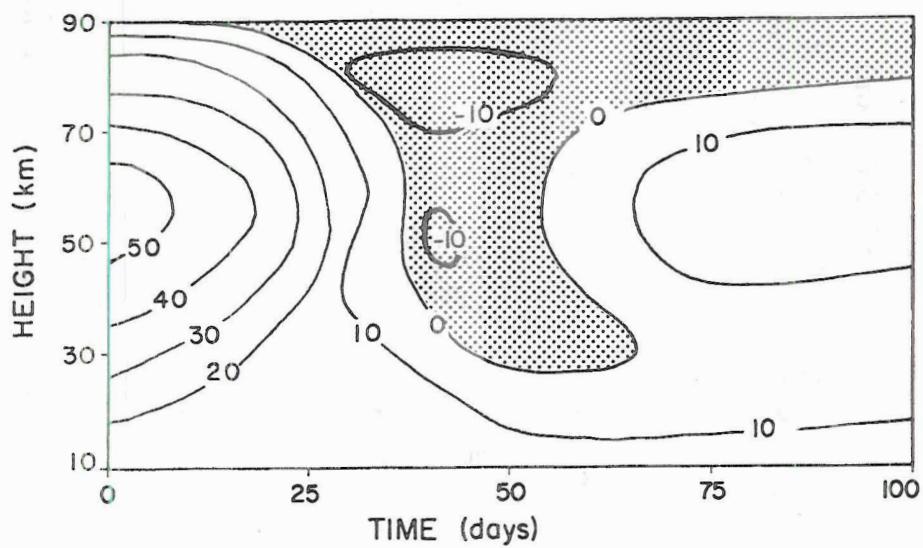
For both the 200 m and 300 m forcings, the wave initially amplifies and then decays, as easterly winds appear. The quasi-bi-weekly oscillation is again apparent in all three cases, but for a 300 m forcing, easterlies appear sooner than for the 200 m forcing case. As Figures 5(a) and 6(a) showed, by day 25 the high latitude circulation has reversed with a 300 m forcing, but for the 200 m case this does not happen until between 30 and 40 days. Hence, the wave amplitude is allowed to build up in the 200 m case; the maximum is over 1200 m whilst for the 300 m forcing the maximum is only about 1000 m.

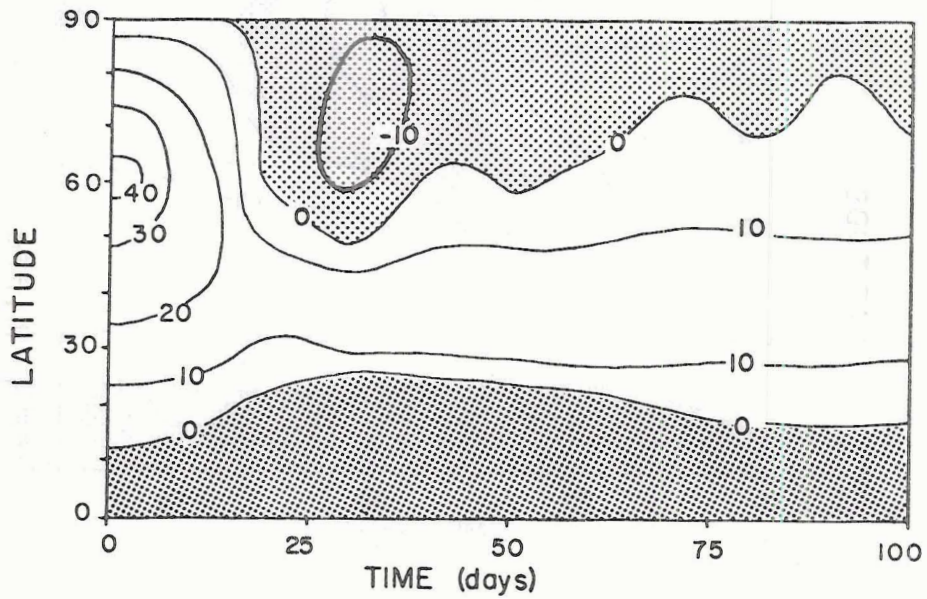
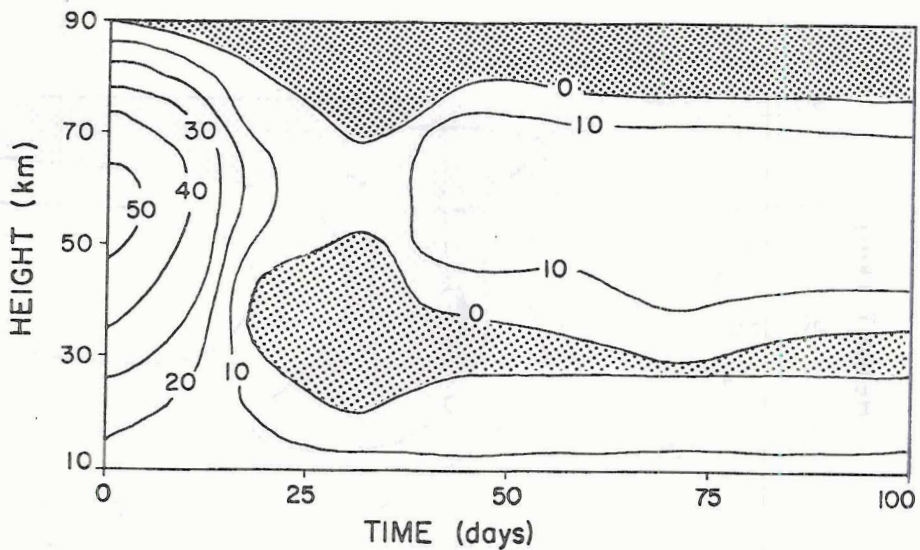
For the 100 m forcing a different picture emerges. Maximum amplitudes of nearly 1200 m do not occur until day 65. Since the forcing is weaker and in a sense therefore is less sudden (inasmuch as $\partial\Phi'/\partial t$ at the boundary is smallest for a 100 m forcing), the basic state zonal wind profile changes little in this time. Even after 100 days, there has been no sudden warming; the polar night jet maximum has actually

moved poleward, whilst weakening a little. At 100 days, the maximum wind of 47 ms^{-1} occurs at 70° and 47.5 km.

In Figure 19, we show for 100 m, 200 m and 300 m forcing; (i) the temporal development of the \bar{u} field as a function of latitude at 35 km, and (ii) the development of the \bar{u} field as a function of height at 60° . We choose 35 km, since it roughly corresponds to the 30 mb level, the level to which a circulation reversal must extend for a major SSW. For the 100 m wave, winds weaken at low latitudes and strengthen at high latitudes at 35 km (Figure 19 (a,i)), having first weakened there a little. However, at no time is the profile much changed from the original. Easterlies appear briefly at 30° after 50 days. At 60° (Figure 19(a,ii)) after 100 days the \bar{u} field is essentially unchanged from its initial form. For the 200 m wave at 35 km (Figure 19(b,i)) easterlies appear first at mid-latitudes after 30 days, then spread poleward. As the wave amplitude decays, the wind profile relaxes back to weak westerlies at all but high latitudes at 35 km. The relaxation is brought about by Newtonian cooling, relaxing the basic state temperature profile to its initial state. Note that as westerlies re-assert themselves, wave amplitude begins to increase again. At 60° (Figure 19(b,ii)), we see rapid deceleration as the zonal wind becomes easterly. The same sequence of events occurs for the 300 m forcing, except that the deceleration occurs sooner after the onset of forcing than for the 200 m wave. The easterlies appear almost simultaneously between 60° and the pole (Figure 19(c,i)). At 60° (Figure 19(c,ii)), the wind reversal never occupies the whole atmosphere, but winds are easterly throughout the atmosphere poleward of 60° . After 100 days, there is still a thin

(i) \bar{u} at 35 km.(ii) \bar{u} at 60°.

(i) \bar{u} at 35 km.(ii) \bar{u} at 60°.

(i) \bar{u} at 35 km.(ii) \bar{u} at 60°.

19 (c) 300 m

Figure 19 For (a) 100 m, (b) 200 m, and (c) 300 m forcing amplitudes, we show: (i) the development of the mean zonal wind field, \bar{u} , at 35 km as a function of latitude; and (ii) the development of the \bar{u} field at 60° as a function of height. Units are m/s, and stippled areas denote regions of easterly winds.

band of easterlies from pole to equator just below 35 km, which continues to block vertical wave propagation. Instead, at 60° , we see the redevelopment of wave amplitude after 70 days below this level, confined by the zero wind line.

In most of the solar-weather experiments reported in Chapter 4, we shall use the LH wind profile, since our upper boundary will be at 150 km and since Holton's wind data extend only to 90 km. We have run experiments, with the LH wind profile to 150 km, similar to those discussed above; viz, forcings of 100 m, 200 m, and 300 m to 100 days. The results follow along similar lines to those for profile H, and we have not shown them here. For a 100 m forcing, wave amplitudes never exceed 300 m and the basic state wind profile remains almost completely untouched, even after 100 days. For a 200 m forcing, the wave amplitude reaches 550 m between 10 and 20 days, declines and then increases again to a maximum of about 850 m after 50 days, declining thereafter. After 50 days, \bar{u} becomes negative at 60° in the lower stratosphere, but declines only slowly at all heights before this. For a 300 m forcing, the wave amplitude increases to over 800 m after 20 days, and then declines. A similar change in the \bar{u} profile at 60° is noted as for the 200 m forcing, except that low-level easterlies first appear after 25 days. We again note a quasi-bi-weekly periodicity in the fields.

Since the 300 m wave develops large amplitudes without creating large mean zonal wind changes before 25 days, we will use a forcing amplitude of 300 m in the solar-weather experiments, unless otherwise stated. The 25 day time span will be ample for the problem discussed in Chapter 4.

3.3 Sensitivity to static stability parameter

In Section 2.1, we mentioned that the static stability parameter, N^2 , is a constant in the model. This follows from an analysis of the energetics of the governing equations in Holton (1975, p. 33). Holton defined kinetic energy as:

$$K = \iiint_V \rho_0 \left(\frac{u^2 + v^2}{2} \right) dV,$$

where u is the total zonal wind ($= \bar{u} + u'$) and $v = \bar{v} + v'$. Holton (1975) then defined available potential energy as:

$$A = \iiint_V \frac{\rho_0}{2N^2} \left(\frac{\partial \Phi}{\partial z} \right)^2 dV,$$

where again $\Phi = \bar{\Phi} + \Phi'$. Now, in the absence of diabatic terms and boundary fluxes of energy, the equation

$$\frac{d}{dt} (A + K) = 0 \tag{3.25}$$

is only true if $N^2 = \text{constant}$. Otherwise, there is a residual term in (3.25). Note that by virtue of separating the geopotential field into two parts, Φ_0 and $\Phi (= \bar{\Phi} + \Phi')$, we had already constrained N^2 to be at most a function of height only. In order to define A , Holton made an approximation in the thermodynamic equation, neglecting the quantity wT as compared to wT_0 (T_0 is related to Φ_0). Stevens (1981, unpublished manuscript) has shown however, that this approximate system does not conserve total energy, $P + K$, where $P = \text{total potential energy}$.

Summarising, it is the splitting off of the Φ_0 field which determines that N^2 be a function of height only. With the approximate thermodynamic equation, the quantity A can be defined, but in order to satisfy (3.25), N^2 must now be constant. In addition now, total energy is not conserved, which would seem to be an important requirement for the model.

Since N^2 is certainly not constant in the real atmosphere and since the quantity $\partial\bar{q}/\partial\theta$ is a function of N^2 , as well as \bar{u} , it is of interest to see whether the SSW results are at all affected by the inclusion of a height-dependent N^2 . The SSW experiment of Section 3.1 with wind profile H and a 300 m forcing is therefore repeated but with N^2 determined from the U.S. Standard Atmosphere (1976) distribution of temperature. In Figure 20 we show the resulting distribution of N^2 with height, which should be compared with the constant value of $4 \times 10^{-4} \text{ s}^{-2}$ assumed before. The distribution is determined by (2.5) and T_0 is shown in Figure 1. We have not shown the results, since the development of the SSW is very similar to the case when N^2 is constant. However, we note the following: (a) the warming is retarded, the \bar{u} profile at 25 days with N^2 variable being about the same as that at 19 days with N^2 constant; (b) the wave does not attain as large an amplitude as when N^2 is constant, the maximum value being 900 m, compared to over 1000 m (Figure 7(a)).

Despite the radical departure of N^2 from its usually assumed value of $4 \times 10^{-4} \text{ s}^{-2}$, the two distributions of $\partial\bar{q}/\partial\theta$ differ little. It is interesting that Schoeberl and Strobel (1980), in a similar comparison between the SSW with constant and variable static stability, found that variable N^2 allowed the warming to proceed faster (by 4-5 days).

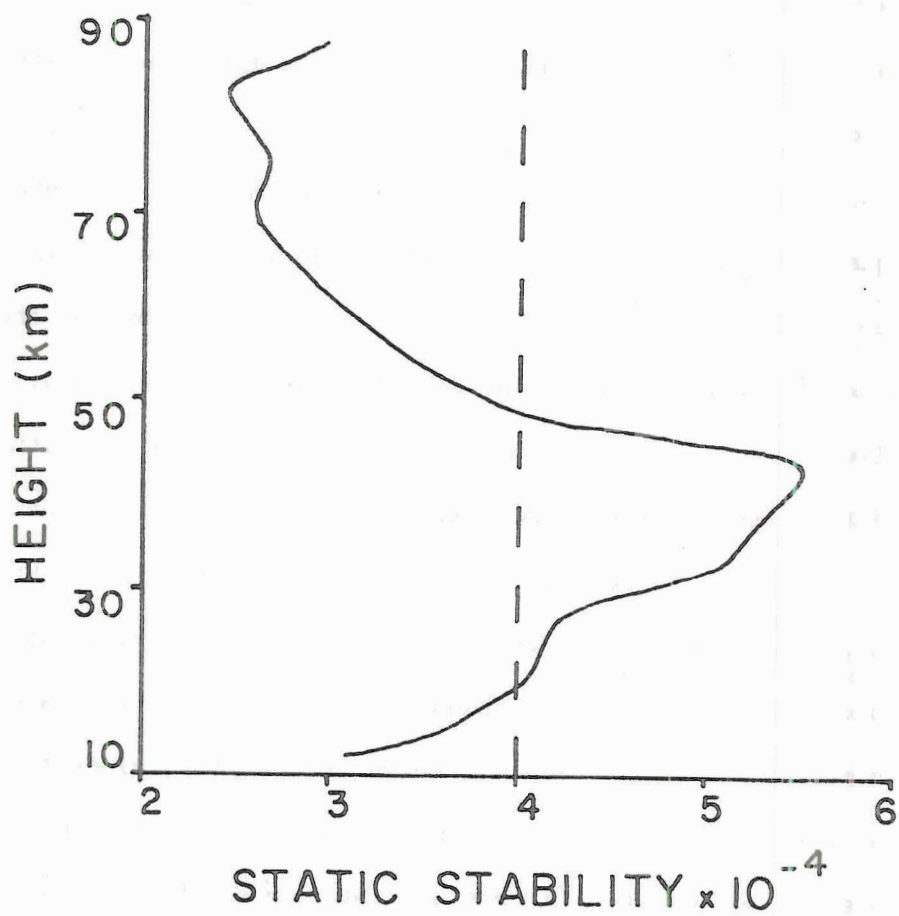


Figure 20 Distribution of static stability, $N^2 \times 10^{-4} \text{ s}^{-2}$, from the U.S. Standard Atmosphere (1976). Dashed line shows the constant value of $4 \times 10^{-4} \text{ s}^{-2}$ adopted in other calculations.

4. THE SOLAR-WEATHER PROBLEM

We turn now to the question of whether or not enhanced geomagnetic activity (EGMA) can influence long wave structure, and if so, can we notice any effects in the lower stratosphere or troposphere? As mentioned in the Introduction, we will impose a diabatic heating in the upper levels of the model. Hines' (1974) suggestion was that a solar disturbance might influence the reflection or absorption of planetary waves in the upper atmosphere. We will interpret this in terms of whether or not solar activity can alter the refractive index of the basic state atmosphere (i.e., $\partial\bar{q}/\partial\theta$ introduced in Chapter 3). Since the value of N^2 cannot change in the model, we are therefore asking whether or not solar activity can alter the basic state wind profile. If such a change can be brought about, we then ask whether or not the structure of planetary-scale waves in the lower atmosphere responds to the solar activity.

It should be mentioned from the outset that we have no hope of explaining apparent lower atmospheric responses to solar activity which occur within hours or even one or two days of the solar event. The vertical group velocity of the forced, stationary waves, with which we are dealing, is of the order of 6 km per day (Charney, 1949; Kanzawa, 1980). Thus it would take on the order of two weeks for an influence to propagate from the 100 km level to the surface. The question of sensitivity of tropospheric forced disturbances to upper atmospheric parameters is still, however, of general interest.

4.1 Some remarks on the model

The parameterized physics in the primitive equations of meteorology must be modified to be applicable in the thermosphere. Specifically, the effects of ion drag and viscous dissipation should be included in the thermodynamic equation. Ion drag results from the collision of neutral gas particles with charged particles and is a maximum during the day, when ionization is at its peak. The parameterization of ion drag used by Dickinson *et al.* (1975) indicates that one component of ion drag maximizes between 300 km and 400 km and is 0(10 - 100) smaller below 150 km, with a characteristic damping time of 1-4 days. A second component of ion drag maximizes at 150 km, having a damping time of about one day. However, this term, λ_{xy} , is incorporated through the term $(f - \lambda_{xy})(u, v)$ and since f exceeds λ_{xy} by a factor greater than 10, we feel justified in omitting ion drag up to 150 km, which will be the upper boundary in these calculations.

Below the turbopause, at which level (c. 110 km) turbulence dies away, eddy processes dominate molecular processes in diffusing heat and momentum. The coefficient of molecular viscosity grows rapidly with height above 110 km, to the extent that above c. 300 km, large horizontal and vertical shears cannot develop. The formulation of molecular viscosity implies that it will efficiently smooth out small-scale variations in wind. The linear drag term used in the model should, in principle, be replaced by molecular viscosity above the turbopause. However, we retain it up to the 150 km level, since we do not intend to accurately model the thermosphere; the region above the solar-induced forcing will simply act as a sponge to prevent false reflections at the

upper boundary from ruining the solution. Furthermore, a typical time scale associated with this dissipation mechanism does not decrease dramatically between 110 km and 150 km.

Molecular heat conduction also becomes important above the turbo-pause. Above about 150 km, the thermal structure is determined by a balance of heating by absorption of extreme ultraviolet radiation (EUV) and downward heat conduction. In the lower thermosphere, however, the importance of various terms in the thermodynamic equation has not been fully resolved. Infrared cooling becomes small above 110 km, but we retain it up to 150 km for the same reasons as above. We have therefore underestimated the thermal damping rate in the upper layers of the model atmosphere. It should be pointed out that the Newtonian cooling approximation is not good above c. 75 km, where local thermodynamic equilibrium breaks down.

We remark at this juncture, that the study is aimed at gauging the sensitivity of planetary-scale Rossby waves, to modulations at high levels. Physically, it seems reasonable that the longer the upper level field of, say, $\partial\bar{q}/\partial\theta$ is altered, the greater the chance of changing the lower-level wave structure. The duration of the upper-level changes depend upon (a) the amplitude of forcing (in the context of the model), (b) the duration of such forcing, and (c) the nature of the dissipation mechanisms prevailing. If, therefore, our thermal and mechanical dissipation rates are too small and yet even with prolonged, intense upper-level forcing we still see no large changes in long-wave structure, a more accurate representation of dissipation should not alter the basic outcome of our results. If, on the other hand, profound changes at lower levels are noted, we must re-examine the model's heat and momentum dissipation.

The variability of winds at thermospheric levels is such that it is more difficult to define a seasonal mean profile of zonal wind than is the case in the lower atmosphere. Diurnal and semi-diurnal tidal variations are observed to be important in the thermosphere, as indicated by Craig (1965; Tables 8.5 - 8.7). The amplitude of these oscillations is of the same order as the amplitude of the "mean" wind at this height (92 km) and observations indicate that tidal oscillations increase above this level. The initial mean zonal wind profile adopted initially in this study is the LH profile introduced in Chapter 3. Use of this scheme allows us to construct a wind profile up to 150 km. Whilst recognising the problem of whether or not a "mean" zonal wind profile has any meaning in the lower thermosphere (or indeed above), given the general, mechanistic nature of our study, it provides a reasonable starting point.

4.2 The nature of the forcing

The two forms of solar energy which drive the thermospheric circulation are electromagnetic radiation and the solar wind. Solar radiation with wavelengths greater than 200 nm passes through the thermosphere to be absorbed in the lower atmosphere, but at shorter wavelengths, EUV radiation is effectively absorbed within the thermosphere. At solstice, this drives a direct meridional circulation which involves ascent at summer hemisphere high latitudes, flow into the winter hemisphere and descent at high latitudes in the winter hemisphere (Roble, 1977). At equinox, there is equatorial ascent, poleward flow and descent at high latitudes of both hemispheres.

The charged flow from the sun, the solar wind, interacts with the earth's magnetic field to form the magnetopause, an imperfect shield

against the solar wind. Some energy associated with the solar wind continuously enters the magnetosphere and interacts with the upper atmosphere to produce aurorae, which are therefore always present in some form. The magnetosphere also stores energy from the solar wind and periodically releases it generating an auroral substorm. These occur, on average, five to six times daily. Finally, an event such as a solar flare can enhance the solar wind and create a geomagnetic storm, which typically lasts between one and five days. The storm does not involve a sustained, constant influx of energy, but rather an increased frequency and intensity of auroral substorms.

Energy from the solar wind is given to the upper atmosphere by particle precipitation and by the dissipation of induced electric currents. The particle precipitation gives rise to the familiar auroral displays at high latitudes. It occurs primarily within the auroral oval, an approximately circular region of radius c. 15° of latitude, centred on the geomagnetic pole. Figure 21 shows the distribution of the auroral oval in both hemispheres. The dissipation of electric currents (such as the auroral electrojet), and consequent heating, is also important in this region. During geomagnetic storms, the oval expands equatorward and thus so does the region of dissipative heating.

The dissipation of electric currents, which produces Joule heating, is the forcing mechanism which we use in this study. Although a geomagnetic storm can last for several days, the amount of energy deposition during this time is highly variable in time (and space) and thus intense heating occurs on much shorter time scales. We will approximate this temporally variable heating by a constant value, switched on and off with a time dependence given by:

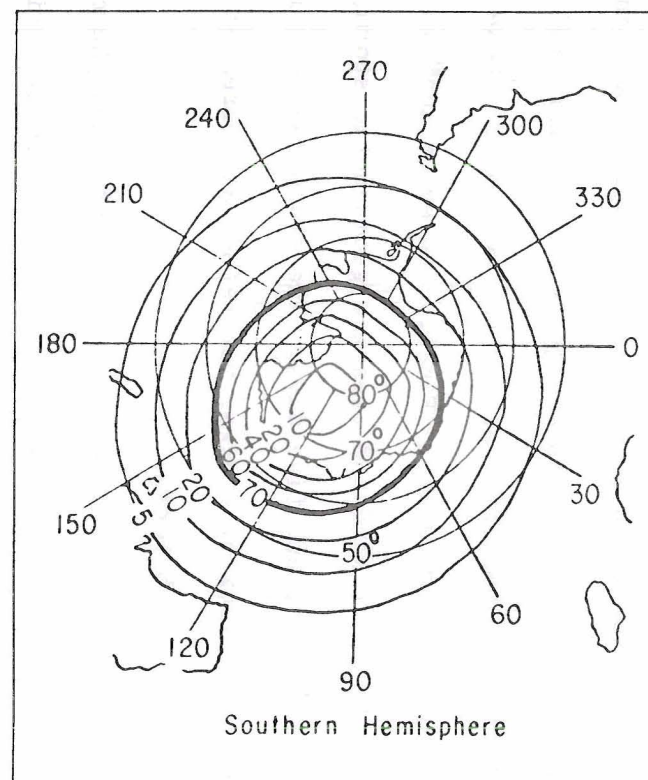
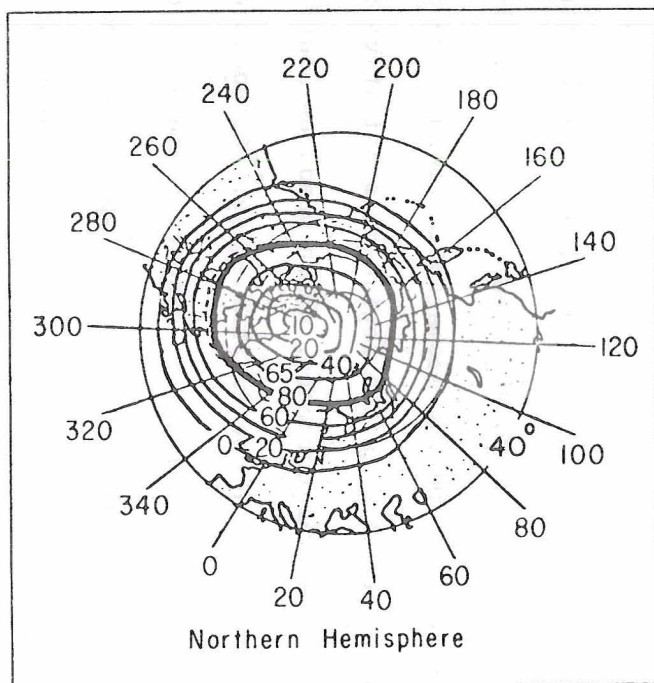


Figure 21 Isoaurorae of auroral appearance frequency. Units are percent. from: *Handbook of Geophysics and Space Environments*, 1965.

$$\left(1 - e^{-(t - t_B)/3600}\right) \left(1 - e^{-(t_E - t)/3600}\right), \quad (4.1)$$

where t_B and t_E are the times at which forcing begins and ends. The forcing therefore reaches e^{-1} of its maximum amplitude after about 30 minutes, (and decays over the same time scale). The forcing is left on for between two and five days.

Equation (2.41) shows the spatial distribution of the diabatic heating function assumed. It maximizes at height z_F km and at latitude $\theta_F \equiv \arcsin y_F$. We choose θ_F to be 60° , in accordance with the equatorward expansion of the auroral oval during disturbed conditions. The scale, over which the forcing decays, y_F , is determined from the distribution of auroral frequency (see Figure 21). In a full spherical model (i.e., one without our severe, spectral truncation), we would perhaps want to represent the forcing in the auroral oval by a double series, involving spherical harmonics in the meridional direction, and exponential functions (sines and cosines) in the latitudinal direction. In the truncated model, we take the forcing to be projected onto wavenumber one and onto the zonally averaged flow ($s = 0$), which gives maximum net heating at some longitude, λ , with no net heating at $\lambda \pm 180^\circ$. This is equivalent to assuming that at all longitudes, maximum heating occurs at the same latitude (θ_F), which is obviously an approximation, but for the purposes of this study, it will suffice.

The greatest unknown in the present study is the amplitude of the forcing. There are very few references in the literature to a heating rate, in terms of degrees per day, associated with Joule heating. There are, however, quotes of energy deposition rates into the thermosphere (or part of it). Cole (1962) derived a heating rate of $10^{-5} \text{ erg cm}^{-3} \text{ s}^{-1}$

at 150 km due to a moderate geomagnetic storm. Ching and Chiu (1973) arrived at a rather lower figure of 10^{-7} erg cm⁻³ s⁻¹, but this applies to heating averaged over a greater depth of the thermosphere than considered by Cole. Banks (1977) found a value for dissipative heating from observations to be as large as 10^{-5} erg cm⁻³ s⁻¹ at 120 km. According to Roble (1977), the energy input to the thermosphere during geomagnetically "quiet" conditions is 5×10^{17} to 10^{18} erg s⁻¹, and is ten times as large during a geomagnetic storm. Referring back to Table 1, Willis' (1976) estimate of the energy associated with a storm lasting between two and three hours agrees with this figure.

If we take a value of dissipative heating rate at 150 km to be 10^{-5} erg cm⁻³ s⁻¹, we arrive at a heating rate of:

$$\begin{aligned} \frac{dT}{dt} &= \frac{10^{-6}}{\rho(150 \text{ km})c_p} && \text{(S.I. units)} \\ &= 0.35 \text{ K s}^{-1} \end{aligned}$$

This is obviously an extremely large heating rate if it applies continuously over a period of several days, and is more applicable to heating on a relatively short time-scale (minutes rather than days). Although during an intense storm the rate of energy deposition may be as high as 10^{19} erg s⁻¹, averaged over a matter of days it is smaller.

Consider Willis' estimate of 10^{18} erg s⁻¹, acting over 10^4 s. We adopt this value as being representative over two to five days, and note that it is a factor of 10 smaller than the peak value quoted by Roble (1977). The rate is equivalent to the deposition of 10^{15} J during the time span. Instead, let this energy be deposited over two days,

so that the heating rate becomes $5.8 \times 10^9 \text{ J s}^{-1}$. Let this energy be deposited in a volume of the atmosphere bounded by latitude circles 55° and 65° around the globe, and by the levels 110 km and 130 km. The volume of this box is $4.45 \times 10^{17} \text{ m}^3$. Taking the density at 120 km, $3.54 \times 10^{-8} \text{ kg m}^{-3}$ to be representative of the volume, we find that over the two days the temperature increase of the atmosphere in the "box" is 63.8 K, equivalent to a heating rate of 31.9 K day^{-1} .

Calculations of Joule heating rates show that a maximum occurs between 110 km and 120 km, falling off above and below (see, for example: Banks, 1977; Hays et al. 1973). In addition, Banks (1979) has indicated that Joule dissipation may lead to heating rates of 1 - 10 K day^{-1} in the upper mesosphere.

On the basis of these (limited) arguments, we choose a heating rate of 15 - 30 K day^{-1} , centred mostly in the lower thermosphere ($z_F = 110 - 120 \text{ km}$) but we also report on experiments with the heating maximizing at 70 km in the mesosphere. It is noted that only about 50% of energy deposited in the thermosphere during a storm goes into Joule heating; the rest is associated with particle precipitation (Banks, 1977).

Despite the limited areal nature of the forcing, it can at times locally exceed the heating due to absorption of EUV radiation, and Dickinson et al. (1975) have shown that this in turn is sufficient to cause a reversal of the thermospheric meridional circulation cell, either at high latitudes or occasionally throughout the hemisphere.

4.3 The effect of the heating on the basic state atmosphere

It is obviously impracticable to run tens of experiments to gauge the effect of the forcing on the basic state atmosphere, each one with a different latitude or height of maximum forcing, amplitude or duration of forcing. We have performed only a few such experiments and hope that they provide sufficient illumination on the subject.

We first apply a forcing (diabatic heat source) of amplitude 15 K day^{-1} in the model. The heating is switched on at the start of the integration, and for all experiments discussed in this section, there is no wave forcing at the lower boundary. The forcing parameters are $(y_F, z_F) = (60^\circ, 115 \text{ km})$ and the duration of heating (in both the zonally averaged flow and wavenumber one) is two days. We let $(y_E, z_E) = (5.4^\circ, 9 \text{ km})$; these parameters will remain fixed in all cases. For reference, we show in Figure 22 the initial distribution of \bar{u} up to 150 km. The initial distribution of $\partial\bar{q}/\partial\theta$ up to 150 km is shown in Figure 9(b).

After two days, when the heating ceases, a fairly large deceleration of winds has occurred centred at 45° and 125 km. The mean zonal wind change $(\bar{u}(t) - \bar{u}(0))$ after two days is shown in Figure 23. The mean zonal wind has decreased by up to -23.2 ms^{-1} , so that an area of easterlies now appears in the high-level mid-latitudes. At the same elevation but at around 70° , mean zonal winds have increased. Wind changes below the 90 km level do not exceed $\pm 1 \text{ ms}^{-1}$ at any time, which we expect from the exponential increase of density with decreasing height. The heat source initially induces a meridional flow away from the region of forcing, as the geopotential surfaces are distorted.

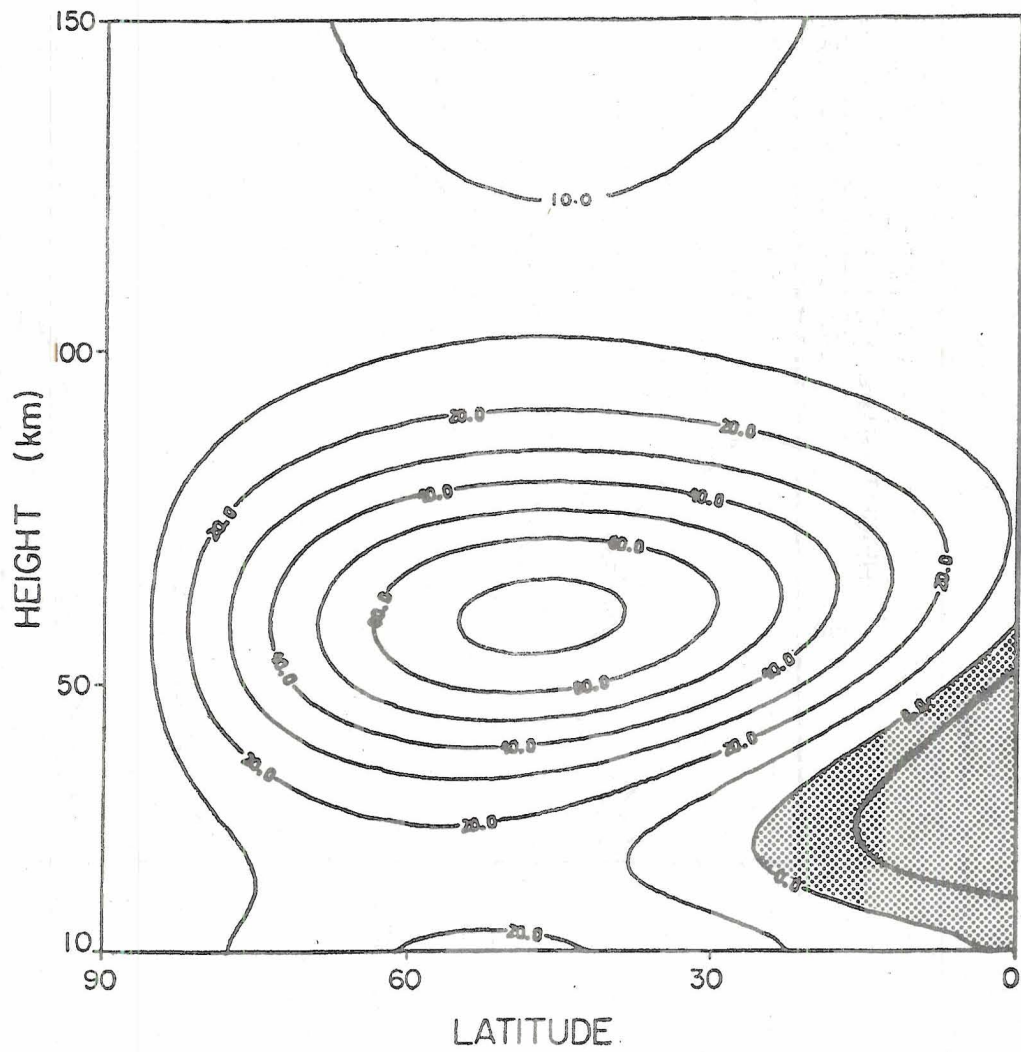


Figure 22 Initial mean zonal wind profile for the solar-weather experiments. From: Lindzen and Hong (1974). Stippled area denotes region of easterly wind.

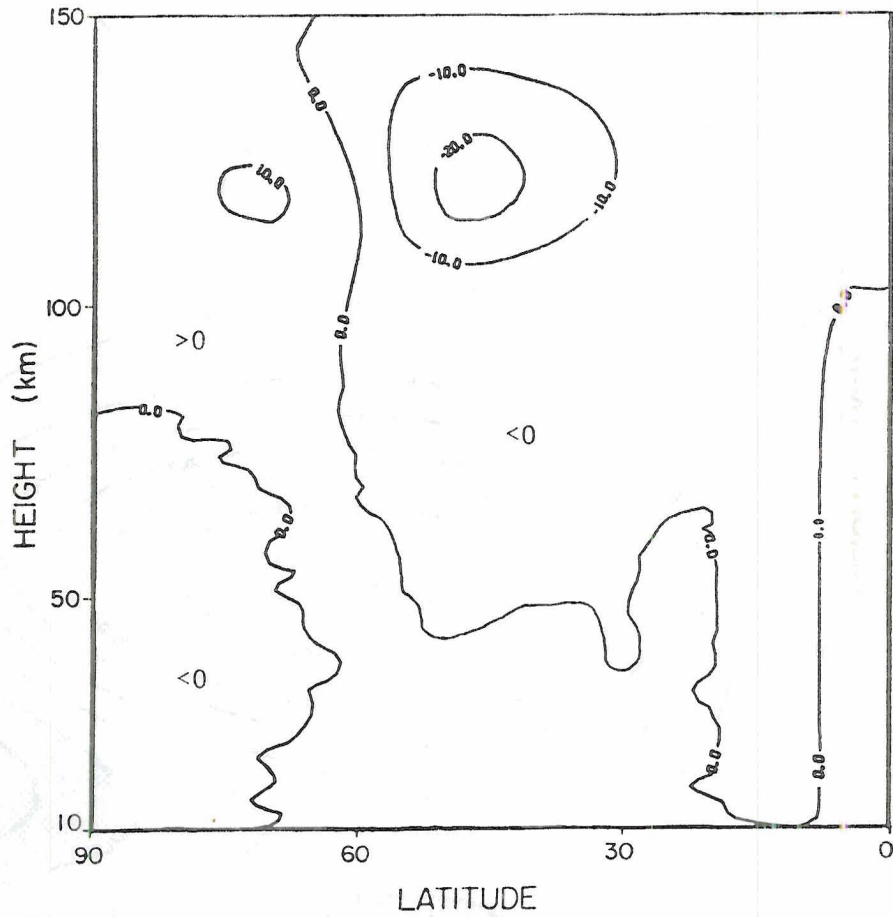


Figure 23 Mean zonal wind change after two days, i.e., $(\bar{u}(2d) - \bar{u}(0))$ with upper-level heating but no lower boundary forcing. The heating amplitude is 15 K day^{-1} , the duration is two days, and $(y_F, z_F) = (60^\circ, 115 \text{ km})$.

After one day, \bar{v} has attained a value of -1.5 ms^{-1} at 45° . This in itself gives an instantaneous value for $\partial\bar{u}/\partial t$ of -13.3 ms^{-1} per day. At the same time the eddy momentum flux convergence here gives an acceleration an order of magnitude smaller; so the mean zonal wind change is principally due to the coriolis torque. The sudden onset (and decay) of heating will give rise to gravity wave motion. This and the induced larger-scale motion will tend to redress the imbalance between the mean temperature and wind fields, which the heating causes. In addition, the damping mechanisms will act to return both the perturbation and mean flows to their initial state.

There are two unrealistic aspects of this simulation. First, there is the problem of underestimated dissipation, mentioned above. In addition, the mean wind field is not subject to explicit dissipation, only implicitly through Newtonian cooling. The addition of this would, of course, lead to a more rapid return of the basic state to its initial value after the cessation of forcing. Second, Dickinson et al. (1975) noted that a high-latitude storm generated upward motion above the storm, with equatorward flow above 150 km, although it should be pointed out that their forcing was at a higher altitude, the maximum forcing per unit mass occurring at 220 km. It is certainly possible that the lid at 150 km is causing the meridional flow noted above 100 km. To test the effect of the lid, we have made two trial runs. The initial mean zonal wind is set to zero everywhere and a heating of 15 K day^{-1} is imposed at $(60^\circ, 115 \text{ km})$ for two days. In the first case, the lid is at 150 km; in the second case it is at 250 km. The resulting change of \bar{u} at 125 km is almost the same in the two cases after two days. The mean meridional wind field is also almost unchanged by putting the lid

up higher. We were unable to set the lid any higher than 250 km since the calculation in this case "blows up" before one day, presumably due to the combined effect of very low density and inefficient damping at high altitudes. The experiment however lends some credence to the results discussed above.

In Figure 24, we show the mean zonal wind change at latitudes 50° and 70° as a function of height after 2, 6 and 10 days. Both poleward and equatorward of the forcing, the maximum changes are at the same altitude, although are of different amplitudes, presumably because of geometrical constraints at high latitudes (\bar{v} must be zero at the pole). The disturbance decays rather slowly, although we can change this by changing the model damping mechanisms.

The induced wind shears produce a large change in the field of $\partial\bar{q}/\partial\theta$, which we show for day two in Figure 25. An area of large values (> 3) has developed around 65° and 117.5 km, whilst negative values have developed equatorward. The area of large, positive $\partial\bar{q}/\partial\theta$ is conducive to wave energy propagation (locally), but we note that the two regions of high, positive $\partial\bar{q}/\partial\theta$ (in the lower thermosphere and lower stratosphere) are separated by a region of very small $\partial\bar{q}/\partial\theta$. Thus we would expect any wave energy emanating from the lower atmosphere to be guided away from the region of storm effects; so we can anticipate little change of planetary wave structure in the lower atmosphere due to the storm. The field of $\partial\bar{q}/\partial\theta$ relaxes to its "pre-storm" distribution after about six days.

Obviously, if we increase the amount of energy deposition into the lower thermosphere, either by an increased storm duration or by an increased amplitude of heating, we increase both the intensity and

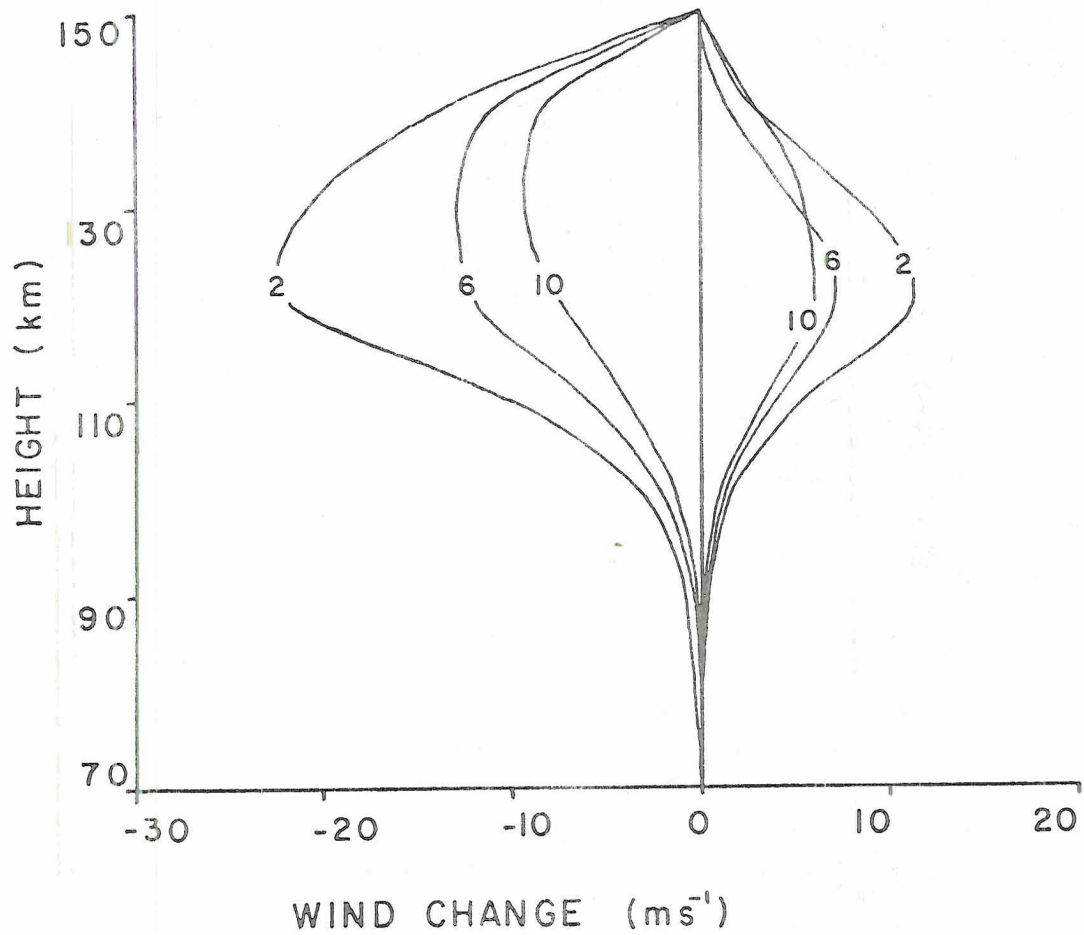


Figure 24 Change of basic state zonal wind, $(\bar{u}(t) - \bar{u}(0))$, at 50° (left, negative) and at 70° (right, positive) after 2, 6, and 10 days. Forcing amplitude is 15 K day^{-1} applied between days 0 and 2 at $(y_F, z_F) = (60^\circ, 115 \text{ km})$.

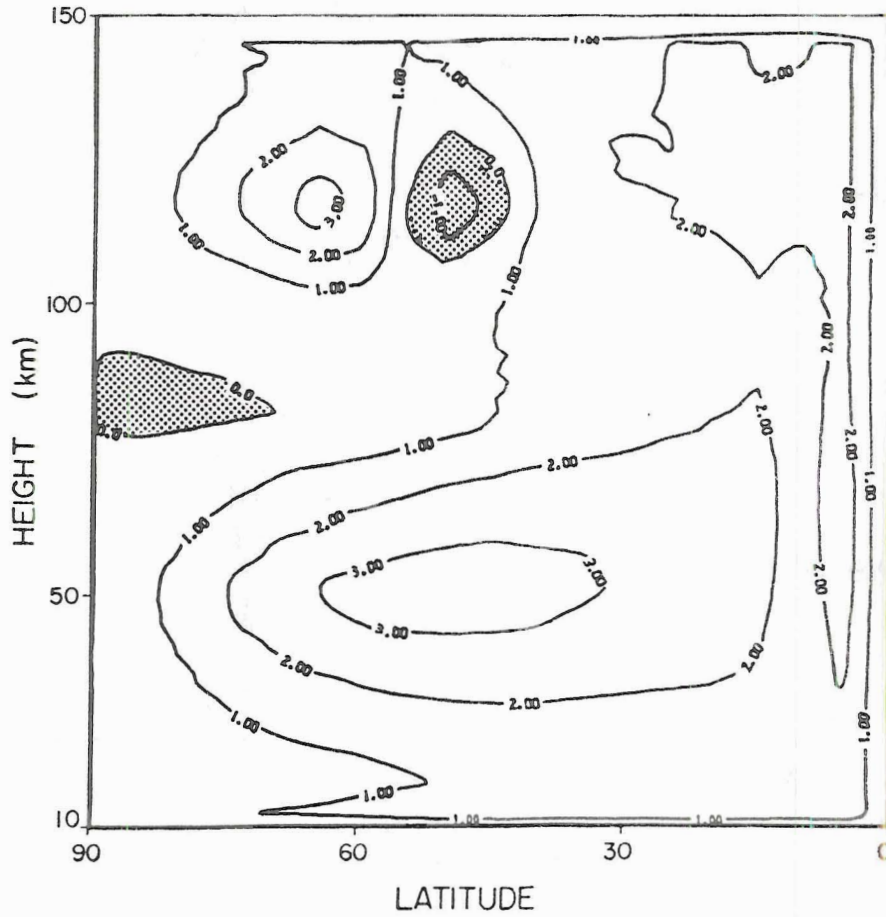


Figure 25 Latitude-height distribution of $\partial \bar{q} / \partial \theta$ after two days with upper-level heating but no lower boundary forcing. The heating amplitude is 15 K day^{-1} , the duration is two days, and $(y_F, z_F) = (60^\circ, 115 \text{ km})$. Areas of negative $\partial \bar{q} / \partial \theta$ are stippled.

duration of upper-level, basic state changes. In one experiment, we have allowed the storm to persist for five days. At this time, winds have decreased by over 45 ms^{-1} at $(45^\circ, 125 \text{ km})$ and have increased by 16.3 ms^{-1} at $(75^\circ, 120 \text{ km})$. Also the distribution of $\partial\bar{q}/\partial\theta$ after five days is about the same as it was after two days with a two day heating, but again there is a region of low $\partial\bar{q}/\partial\theta$ in the mesosphere. If we return to a two day forcing, but with a maximum amplitude of 30 K day^{-1} , the effect is very similar to a five day forcing of 15 K day^{-1} , with similar changes in \bar{u} and $\partial\bar{q}/\partial\theta$ being noted.

Following the observations of Banks (1979) that Joule dissipation may cause heating in the upper mesosphere, we have performed a second set of experiments, with heating maximizing at 70 km. The assumed heating rate is larger than that quoted by Banks (1979) and may be at a rather low altitude; thus the results should be viewed as something of an upper bound on expected behaviour. For a 15 K day^{-1} heating for two days at $(y_F, z_F) = (60^\circ, 70 \text{ km})$, we show in Figure 26 the mean zonal wind change after two days. In Figure 27 we show the same field at 50° and 70° as a function of height at selected times, and in Figure 28 we show the latitudinal gradient of potential vorticity after two days. These should be compared with Figures 23-25.

As expected, the major changes now occur at a lower elevation, about 10 km above z_F . There are also mean zonal wind changes induced in the lower thermosphere and we note the broad latitudinal effect of the heating. Again, in the immediate vicinity of the heating, a meridional flow away from y_F occurs. The field of $\partial\bar{q}/\partial\theta$ is increased poleward of the heat source and there is now a band of uniformly high values of

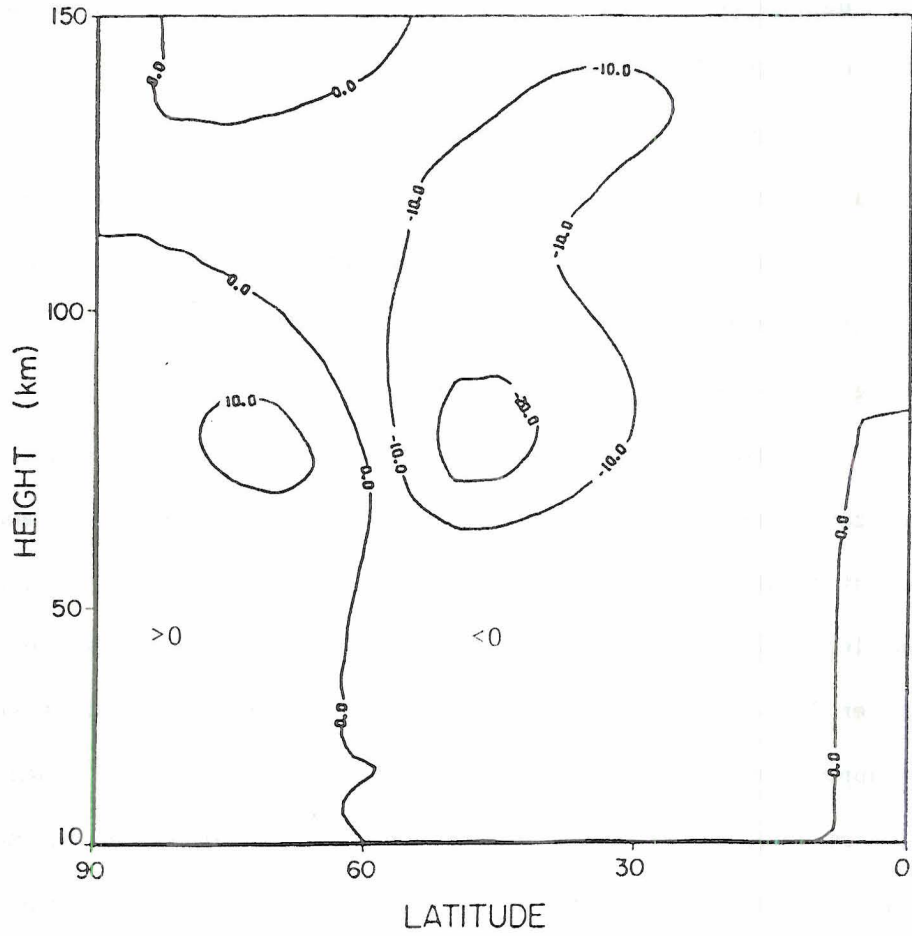


Figure 26 As Figure 23 but with $(y_F, z_F) = (60^\circ, 70\text{km})$.

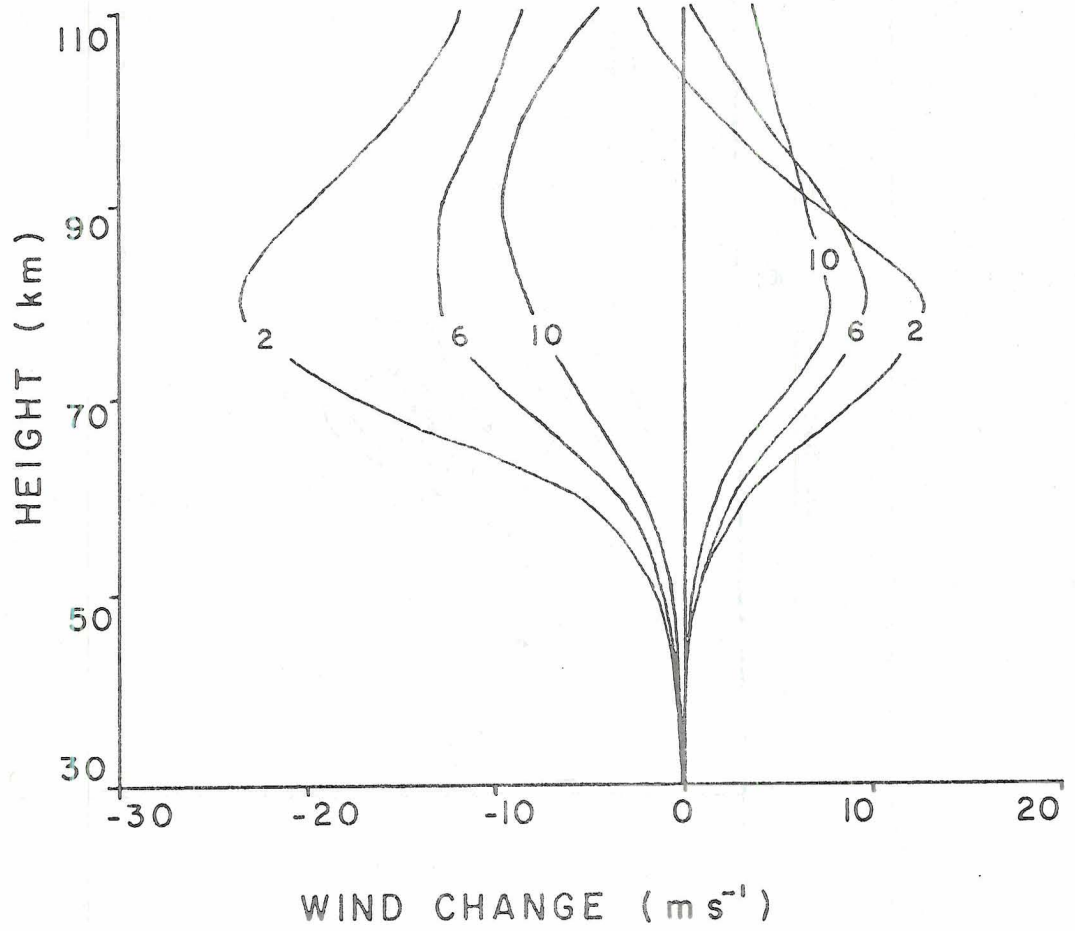


Figure 27 As Figure 24 but for $(y_F, z_F) = (60^\circ, 70\text{km})$.

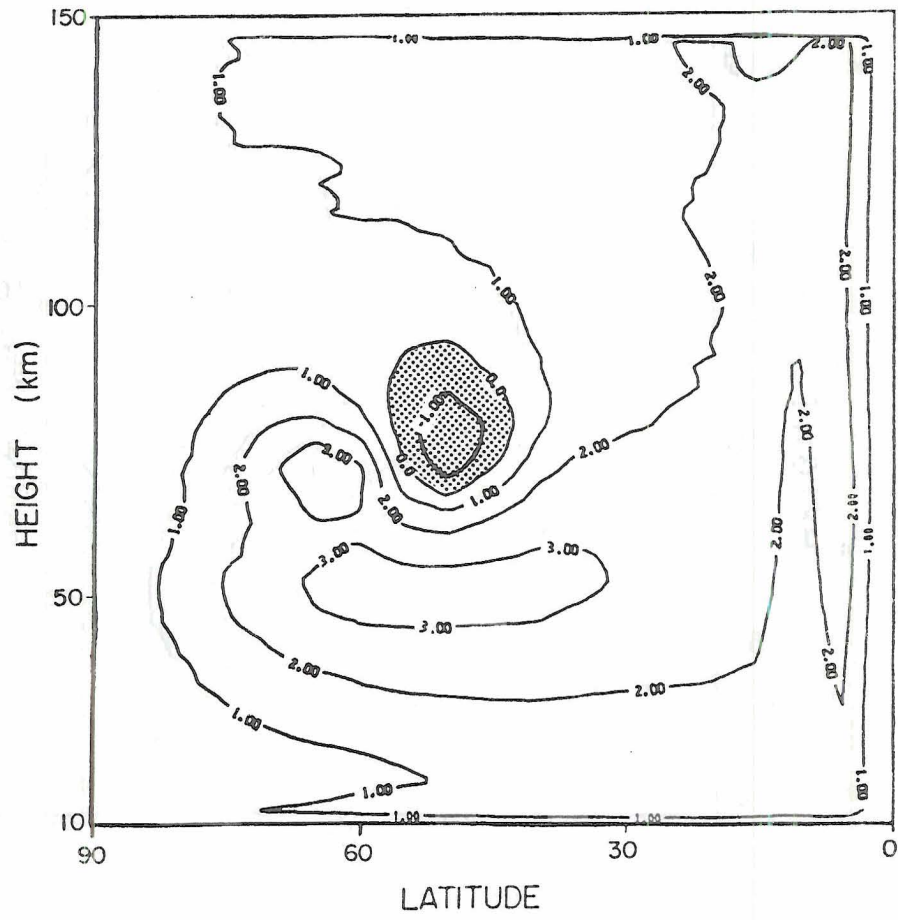


Figure 28 As Figure 25 but with $(y_F, z_F) = (60^\circ, 70\text{km})$.

$\partial \bar{q} / \partial \theta$ extending through the middle atmosphere. The region of negative $\partial \bar{q} / \partial \theta$ around 90 km at polar latitudes, which was present initially (Figure 9(b)), has now vanished and has not been re-established after 10 days.

We may therefore expect to be more hopeful, regarding a modification of planetary wave structure, when the forcing is located at a lower level. This follows simply by inspection of the $\partial \bar{q} / \partial \theta$ fields.

4.4 Joule heating and planetary wave structure

We come finally to the major question of the thesis: can upper-level heating influence lower atmosphere planetary wave structure? By wave structure we mean both wave amplitude and phase. The input of heat in the upper atmosphere must create local changes in wave structure, since we are forcing both the zonally averaged flow and wavenumber one, but this need not imply that any such changes will extend beyond the immediate vicinity of the forcing. Also, any changes which do occur may be quite short lived, since the heating does not persist for long.

Our procedure is to force a wave of maximum amplitude 300 m at the lower boundary (10 km), as we did in the SSW experiments, and allow the forcing to proceed for some time, in order that the planetary wave becomes well established. At some time after the lower boundary wave forcing has begun, we introduce an upper level heat source, as specified in Section 4.3, i.e., we use the same amplitudes, durations and locations of maximum forcing as discussed above. We can then examine the planetary wave structure to see what effect the heating has had.

Our first experiment will serve as a control. The lower level wave is forced but there is no upper level forcing. Figure 29 shows the time-height development of wave geopotential amplitude from day zero to day 24 (solid lines). The wave amplitude grows to over 600 m at 10 days, declines and then rises again to over 750 m around 22 days. The figure differs a little from Figure 7(b) because of the Rayleigh friction parameterization (see Section 3.2). During the 24 day period of integration, the mean zonal winds gradually weaken below the mesopause, but only become easterly in a very small region of the mid-latitude lower stratosphere at day 24. In the lower thermosphere, a region of easterly mean zonal winds begins to develop at high latitudes after 14 days.

In our second experiment, we turn on the diabatic heat source at $(y_F, z_F) = (60^\circ, 115 \text{ km})$ between days 14 and 16. We choose this time since it is approximately the amount of time required for the wave's influence to reach the lower thermosphere. In Figure 30, we show the distribution of \bar{u} and $\partial\bar{q}/\partial\theta$ at the onset of forcing. They are not quite the same as in Figures 22 and 9(b) because of the wave forcing from below. The behaviour of the mean fields at upper levels following the forcing is very much as described in Section 4.3. The easterlies, which in the absence of forcing were developing at high latitudes around 110 km, are replaced by westerlies, whilst equatorward of 60° , an easterly flow develops. A region of relatively large $\partial\bar{q}/\partial\theta$ develops poleward of the forcing, somewhat reducing the extent of the area of negative $\partial\bar{q}/\partial\theta$ at the polar mesopause. The wave amplitude grows to over 400 m at 65° and 125 km at 16 days, but the effect is very localised. The dashed lines in Figure 29 represent the development of the

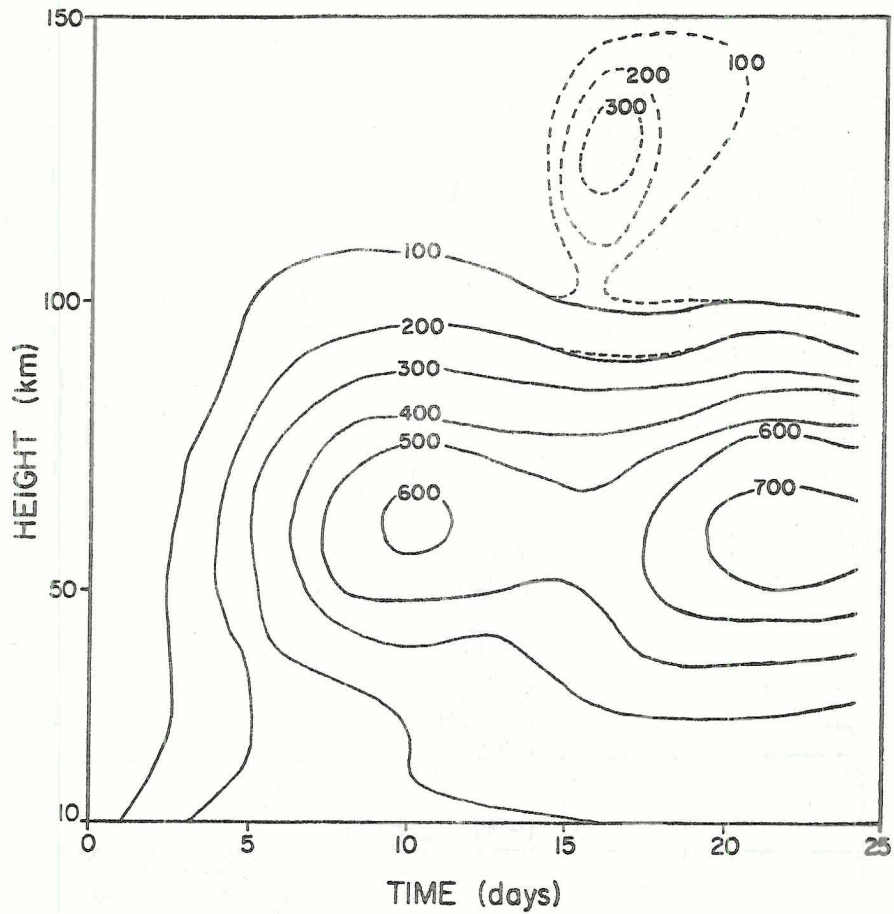


Figure 29 Time-height development of wave geopotential amplitude at 60° . Solid lines: lower boundary forcing only; dashed lines: lower boundary forcing and upper-level heating of 15 K day^{-1} between days 14 and 16 with $(y_F, z_F) = (60^\circ, 115 \text{ km})$.

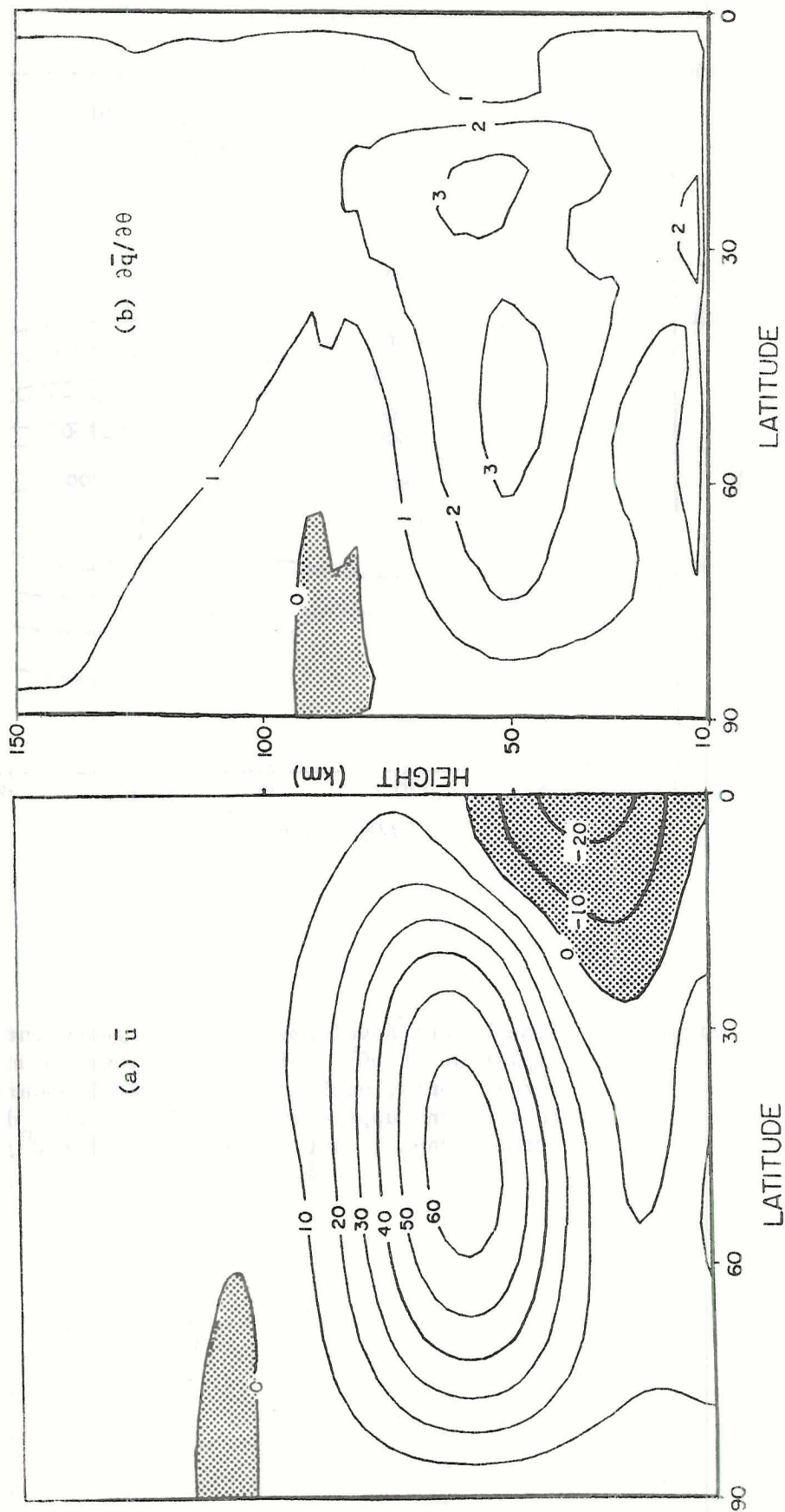
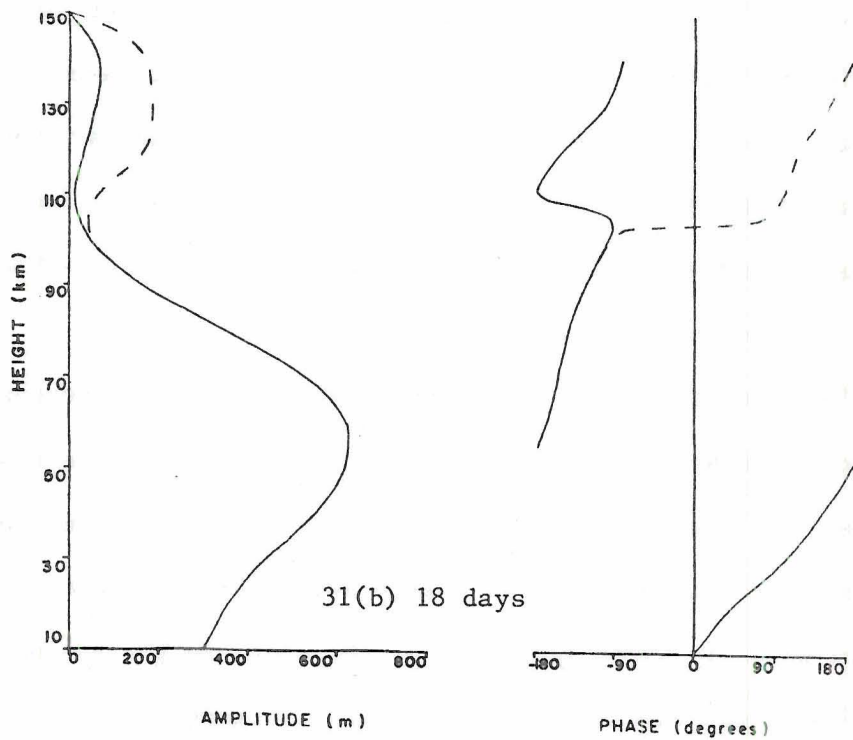
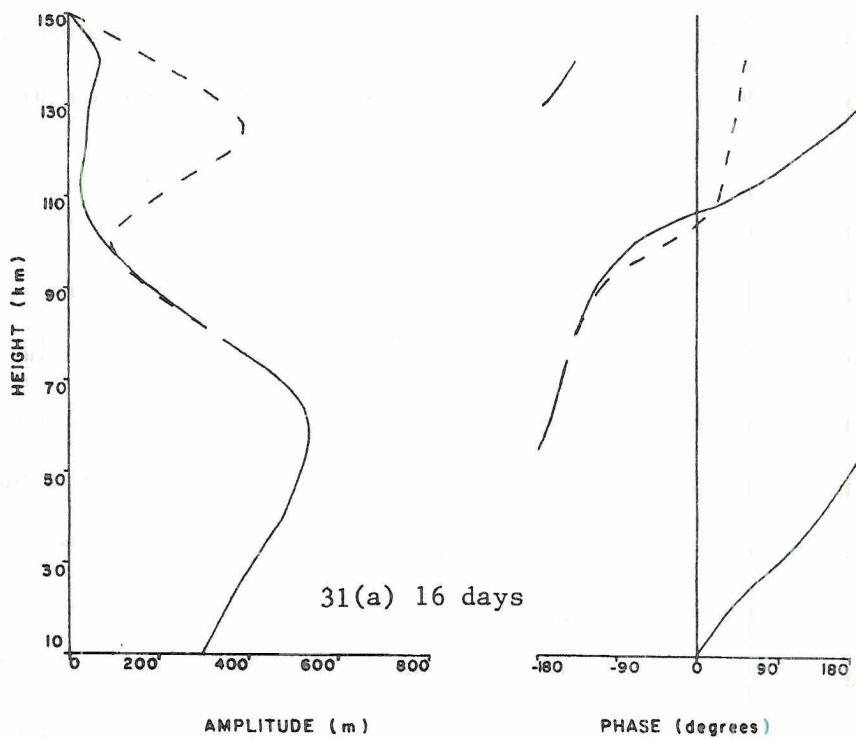


Figure 30 Latitude-height distribution of (a) \bar{u} , and (b) $\frac{\partial \bar{q}}{\partial \theta}$ at 14 days, just before upper-level heating is switched on. Stippled areas denote regions of negative \bar{u} and $\frac{\partial \bar{q}}{\partial \theta}$, respectively.

wave geopotential field between days 16 and 20 at 60° when diabatic heating is added. Below 80 km, changes in geopotential amplitude are of the order of 1 m, and even at 100 km they do not exceed 20 m. Furthermore the changes decay rapidly with time after the heating is switched off.

In Figure 31 we show the wave amplitude and phase at 60° , with and without forcing at days 16, 18 and 20. Below about 80 km, differences in wave amplitude are too small to be of significance. The same is true for the phase structure of the wave. In their study of wave sensitivity to changes in basic state zonal wind, Geller and Alpert (1980) noted that changes in wave structure were seen only up to three scale heights below the level of forcing, and at all levels above (see their Figures 9-11). Using our representative scale height, $H = 7$ km, means that according to them, we should see no change in wave structure below about 95 km. In fact, we do see changes about 30 km below the forcing level, but they are only small. If we consider either an increased duration of forcing (from days 14 to 19) or an increased amplitude of forcing (30 K day^{-1} for two days), we find very similar results. The wave amplitude forced at 115 km in this case is bigger than shown in Figure 31, but the difference between forced and unforced wave structure again becomes very small below 90 km.

The presence of the zero wind line in the lower thermosphere guides wave energy away from the location of the storm. At the onset of forcing, the region of low $\bar{\partial q} / \partial \theta$ at high latitudes around 80-90 km guides lower atmospheric wave energy away from the region of the storm, and the easterly winds generated by the storm in the thermosphere continue to divert wave energy equatorward. Figure 32 shows the distribu-



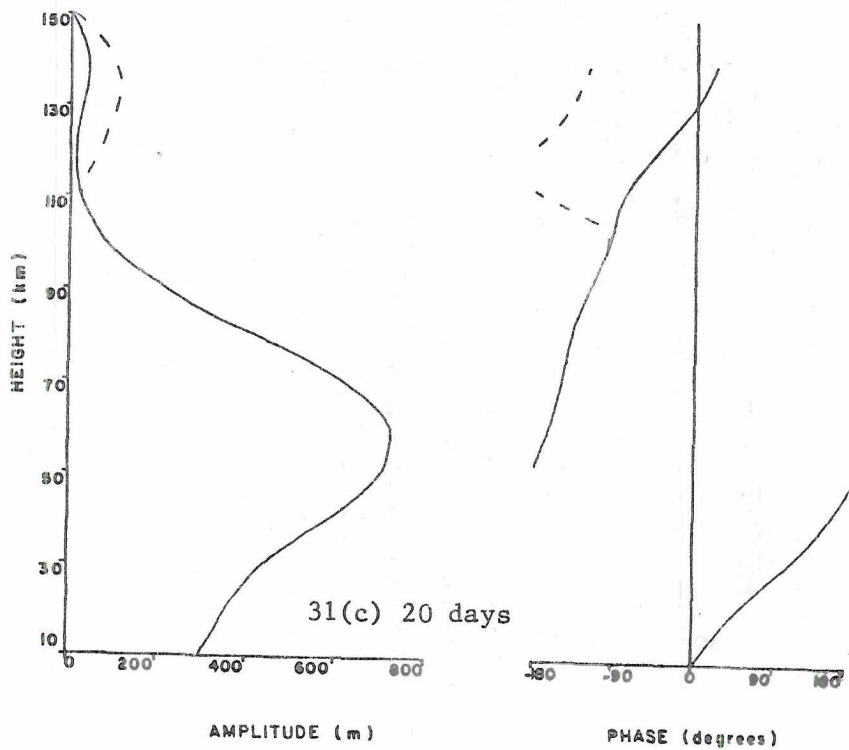


Figure 31 Variation with height of wave geopotential amplitude and phase at 60° with lower boundary forcing, and without (solid lines) and with (dashed lines) upper-level forcing at (a) 16 days, (b) 18 days, and (c) 20 days. Forcing amplitude is 15 K day^{-1} between days 14 and 16, and $(y_F, z_F) = (60^\circ, 115 \text{ km})$.

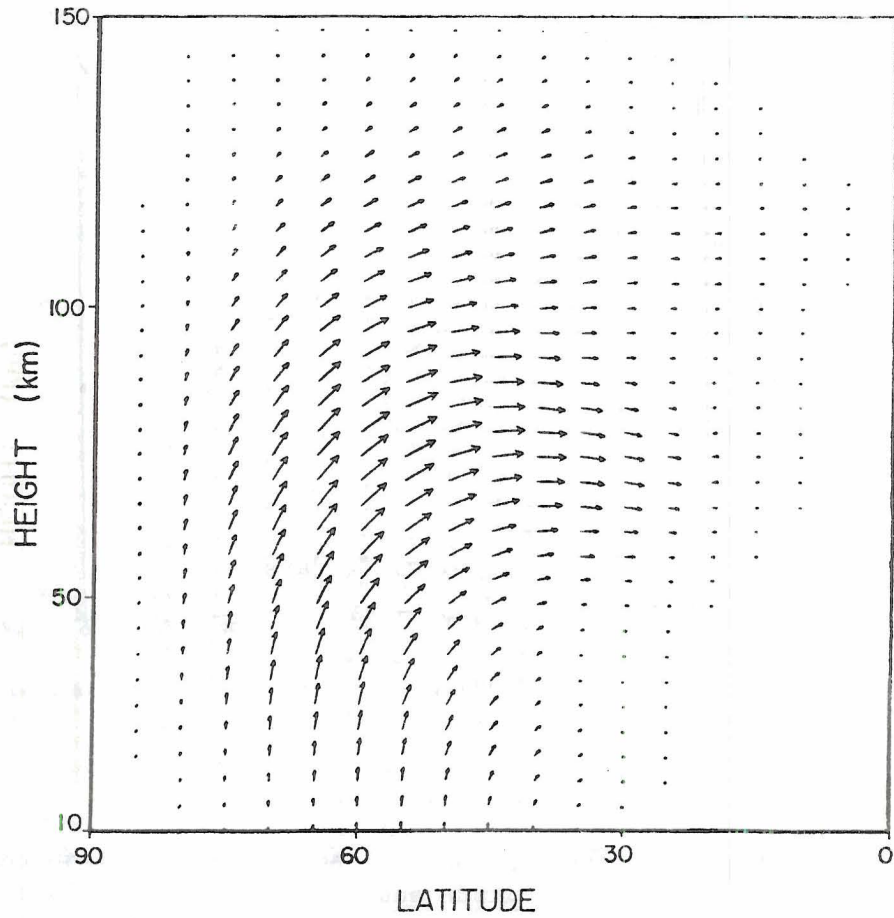


Figure 32 Latitude-height distribution of \bar{F} at day 16 with lower boundary forcing but without upper-level heating.

tion of the vector quantity \underline{F} at day 16 without diabatic heating. There is convergence of wave energy flux above the polar night jet and little wave energy flux up into the thermosphere; the vectors are almost horizontal above the polar night jet. The field of \underline{F} after 16 days is unaltered by the impact of the heating (whichever duration and amplitude we choose). For a 15 K day^{-1} forcing for two days, the heat and momentum fluxes generated do not noticeably alter the wave energy flux field.

In our next experiment, we lower the level of maximum forcing to 70 km, with $y_F = 60^\circ$ and a forcing of 15 K day^{-1} is applied now between days 10 and 12. The basic state zonal wind field at 10 days is very much like that shown in Figure 30(a), except that the upper level region of easterlies has yet to form. The field of $\partial\bar{q}/\partial\theta$ is also very similar to that shown in Figure 30(b). In Figure 33 we show the time-height development of the wave geopotential amplitude field, with and without heating; and in Figure 34 we show the wave geopotential amplitude distribution at 14 days, again with and without forcing. There is a more sizeable impact on the wave structure when the forcing is at 70 km than when it is at 115 km; this is not entirely unexpected, since the forcing is now much closer to the polar night jet, the area in which the wave amplitude maximizes. The effect of the heating at 70 km is more prolonged than with heating at 115 km. The lowest level at which changes in wave geopotential amplitude are seen is 30 km, but changes here are only about 1 m. Changes of up to 10 m are seen at 40 km. In Figure 35 we show the wave structure at 60° for days 12, 14 and 16. The height of maximum wave amplitude is raised by the heating for about five days after its initiation, but by day 16 is almost where it would be without

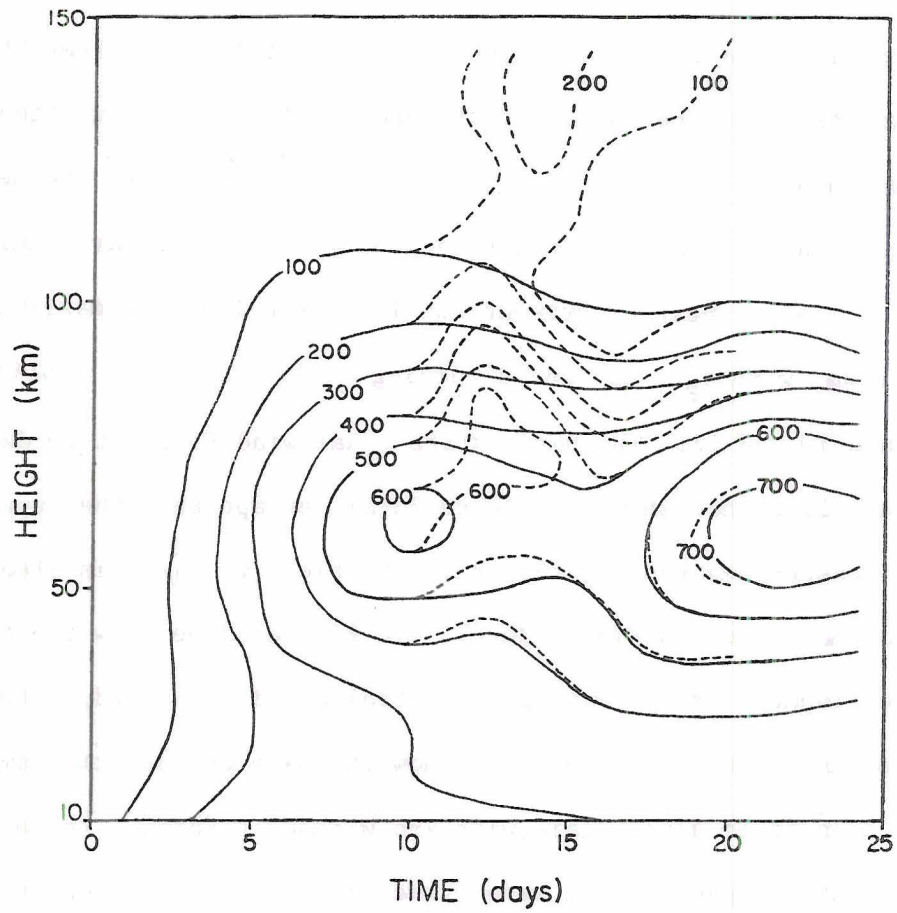


Figure 33 As Figure 29 but with a forcing of 15 K day^{-1} between days 10 and 12, and with $(y_F, z_F) = (60^\circ, 70 \text{ km})$.

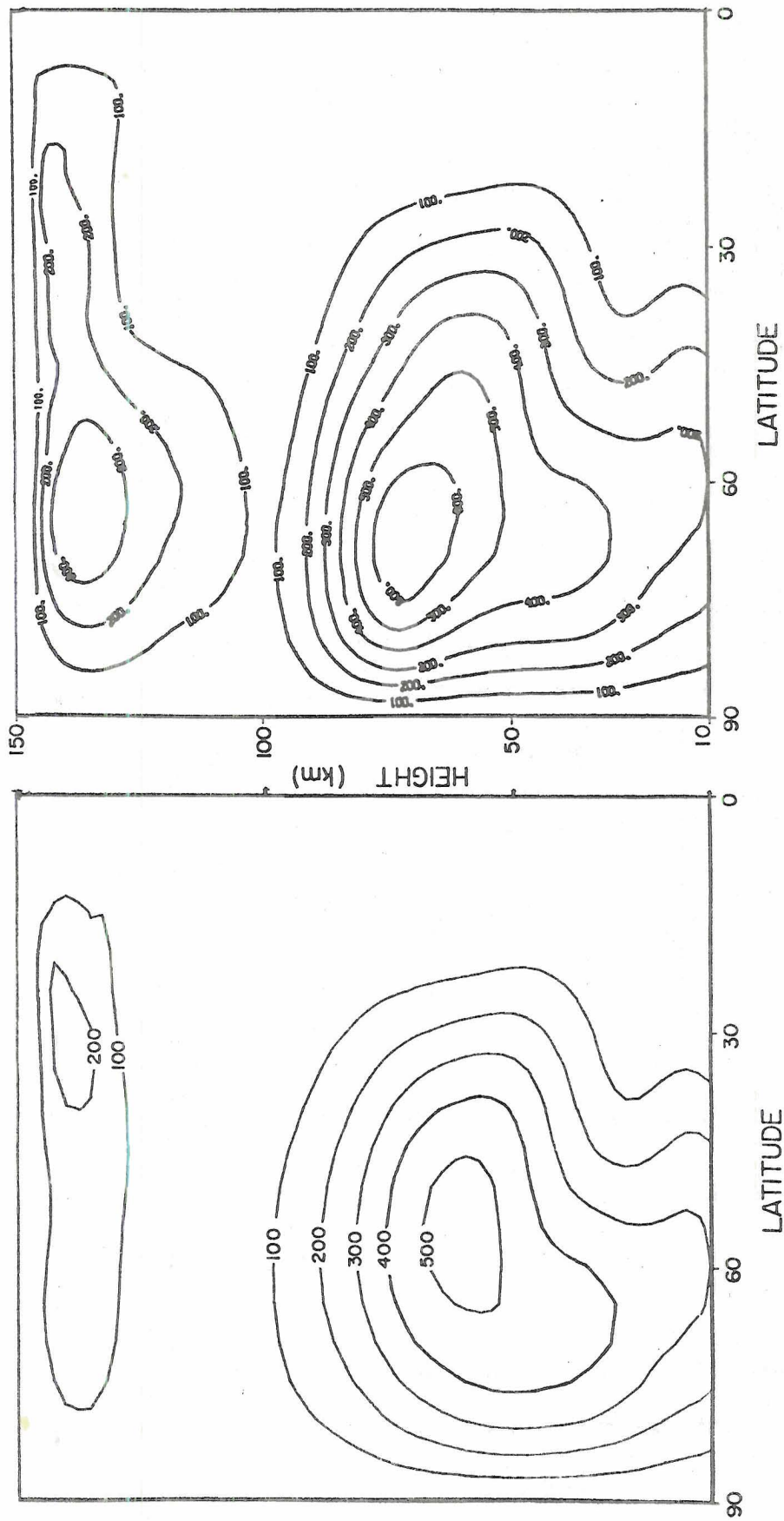
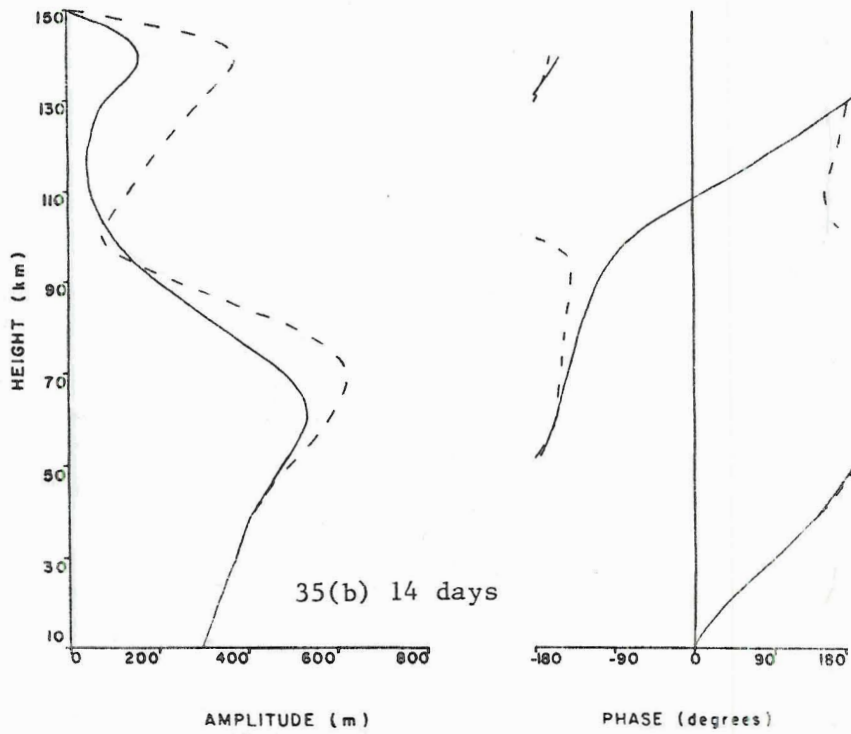
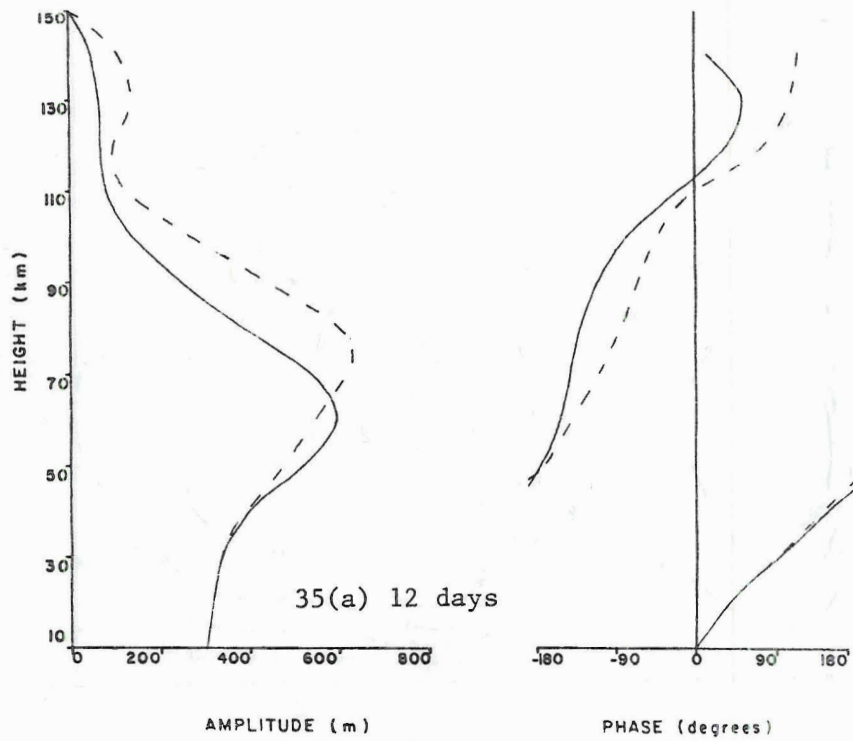


Figure 34 Latitude-height distribution of wave geopotential amplitude at 14 days with lower boundary forcing, and with (right) and without (left) upper-level heating of 15 K day^{-1} between days 10 and 12 at $(y_F, z_F) = (60^\circ, 70\text{km})$.



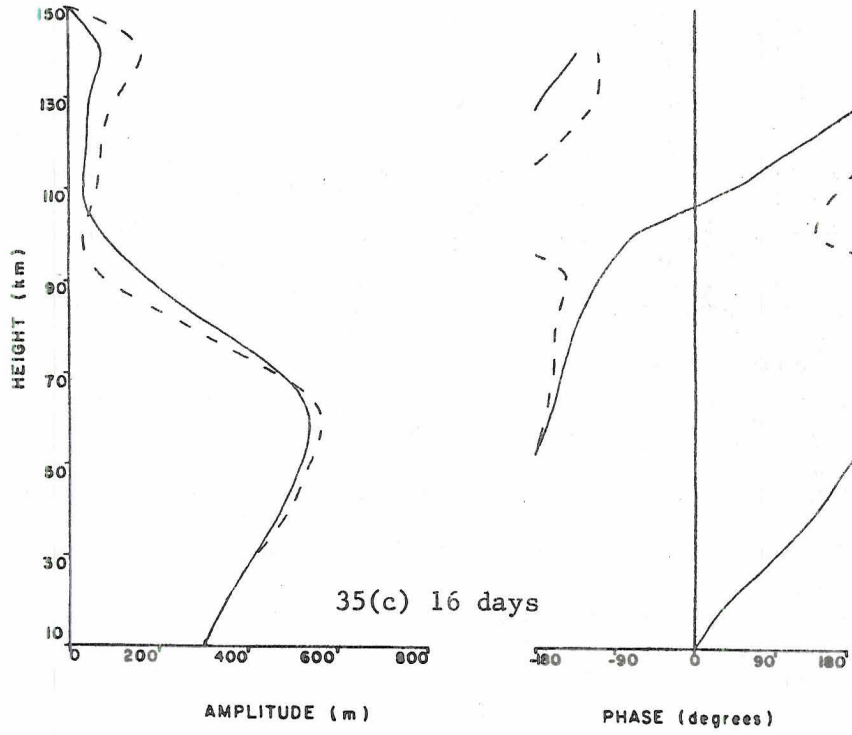


Figure 35 As Figure 31 but at (a) 12 days, (b) 14 days, and (c) 16 days, with a heating of 15 K day^{-1} between days 10 and 12 at $(y_F, z_F) = (60^\circ, 70 \text{ km})$.

the heating. Again, the depth to which changes are created by the storm are in agreement with the results of Geller and Alpert (1980).

The wave energy flux vectors at day 12 are significantly modified by the storm. As Figure 36(a) shows, wave energy is normally guided through the polar night jet maximum towards the equator, being deflected away from the region of negative $\partial\bar{q}/\partial\theta$ at the polar mesopause. The storm causes these values to become positive (the distribution of $\partial\bar{q}/\partial\theta$ at day 12 is very similar to that shown in Figure 28) and consequently wave energy can be guided up through the high latitude mesosphere. Figure 36(b) shows the field of \underline{F} after 12 days of forcing. The increased vertical orientation of the vectors reflects the fact that eddy heat flux is doubled in amplitude by the storm with its maximum around 70 km. By day 14, there is still enhanced vertical wave energy flux above 70 km at middle and high latitudes after the storm has passed, but it is decaying as values of $\partial\bar{q}/\partial\theta$ return to be small or negative between 80 km and 90 km at high latitudes.

Summarizing, the effect of the storm is quite localized in both space and time. With a high level storm, the low values of $\partial\bar{q}/\partial\theta$ between the lower and upper atmosphere (large upper level values being induced by the storm) largely prevents the flow of wave energy to the region of forcing, as we anticipated in Section 4.3. For a storm-induced heating at 70 km, the effect on planetary wave structure is more pronounced and also more sustained. In both cases however, there is little or no modification of wave structure below about ($z_F - 30$ km) and thus there can be no modification of wave structure in the lower

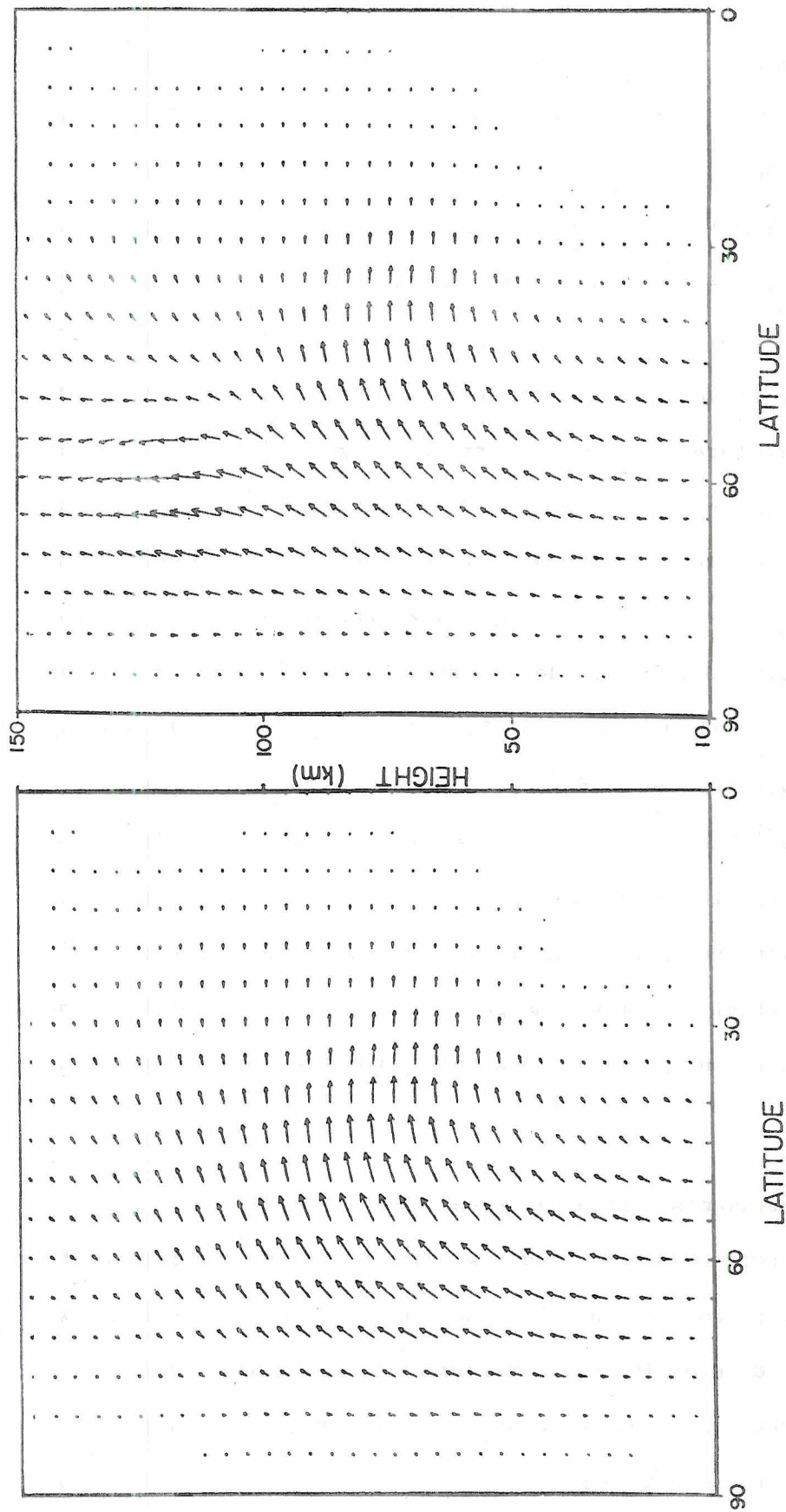


Figure 36 Latitude-height distribution of F at day 12 with lower boundary forcing, and with (right) and without (left) upper-level heating of 15 K day^{-1} between days 10 and 12 at $(y_F, z_F) = (60^\circ, 70 \text{ km})$.

stratosphere or troposphere. The pre-existing distribution of $\overline{\partial q/\partial \theta}$ and the distribution induced by the storm are obviously of importance, when considering the extent of changes caused by a storm.

We finally consider briefly whether or not the time at which an upper level storm occurs, in relation to the amplification of the large-scale wave below, is a determining factor in the storm's influence. We noted above that a storm at 70 km had a more pronounced effect on wave structure than did a storm at 115 km. The lower level storm was applied at an earlier stage of the large-scale wave's development, simply because we used the time for the wave's influence to reach the level z_F as a convenient temporal marker for switching on the forcing. Examination of the wave development in Figure 29 shows that amplitudes dip after about two weeks of forcing, and are at their peak at 10 days and between 20 and 25 days. We have repeated the experiment with a 15 K day^{-1} heating at $(y_F, z_F) = (60^\circ, 115 \text{ km})$, but with heating applied between (a) 10 and 12 days, and (b) 20 and 22 days. The timing of the storm, with respect to the large-scale wave development, is found to be immaterial. We find changes below 100 km to be of the same order as those shown in Figure 31, and they penetrate to similar atmospheric depths.

4.5 Experiments with a different wind profile

In both Chapters 3 and 4 we have noted the importance of the basic state wind profile, and thus the basic state refractive index distribution, in determining the development of planetary-scale wave structure and thereafter of either a stratospheric sudden warming or of the atmosphere's response to a geomagnetic storm. In Chapter 3 it was shown that

Holton's wind profile allowed a larger wave to develop than did wind profile LH. We used Lindzen and Hong's (1974) scheme to generate a basic state wind field, because it can easily produce such a profile up to any desired height. In the light of the results of Chapter 3 however, we have constructed a second wind profile based on Holton's data. An interpolation routine was used to fit a smooth curve to the wind data between 47.5 km and 67.5 km and to the value $\bar{u} = 0$ at 150 km. Values at 2.5 km spacings are then produced for our initial mean zonal wind profile, which is shown in Figure 37. Below 67.5 km, the profile is the same as in Figure 4(a). The profile has the benefit of enhanced wave propagation in high latitude regions, because of the "tongue" of high values of $\bar{\partial q} / \partial \theta$ extending to high latitudes at low levels (see Section 3.1).

As with the experiments reported in Section 4.3, we first apply a heating of 15 K day^{-1} at $(y_F, z_F) = (60^\circ, 115 \text{ km})$ for two days without a lower boundary wave forcing. We again see the development of easterly winds, centred at 50° and 125 km, and there is some acceleration of mean zonal winds at 70° at the same altitude. The response is very similar to that with the LH wind profile.

Next, we introduce the lower boundary wave, with the same heating characteristics as above applied between days 14 and 16. In Figure 38, we show the structure of the wave at 60° after 16 days, with and without forcing. As before, there are no significant changes in wave structure below 70 km. We can attribute this finding to the efficiency of the mean wind field for guiding wave energy upward, which is such that winds in the entire thermosphere become easterly after 10-12 days. Thus a critical level has already formed at the mesopause when the upper level

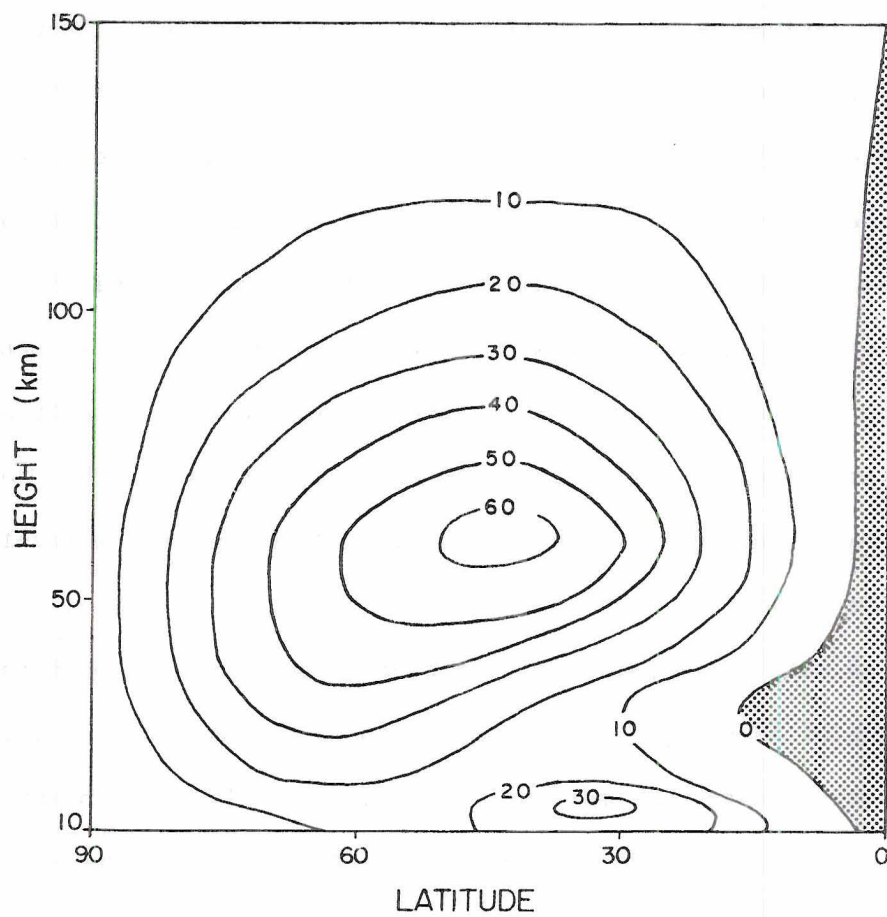


Figure 37 Latitude-height distribution of initial mean zonal wind profile given by Holton's wind data, interpolated to give $\bar{u}=0$ at $z=150\text{km}$. Winds are easterly in stippled area.

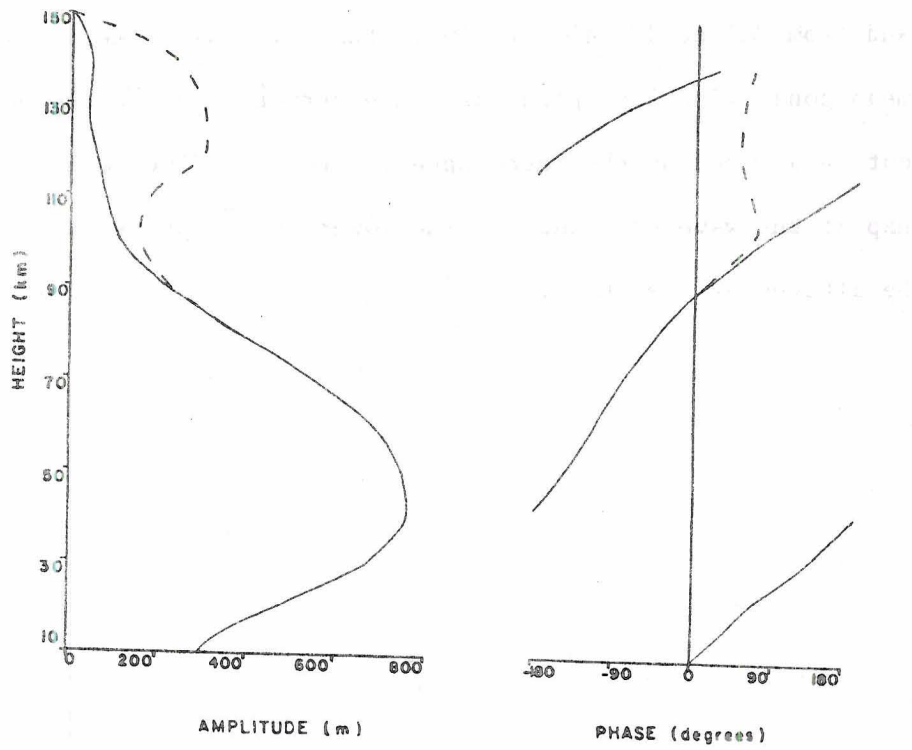


Figure 38 As Figure 31, at day 16, but with the initial mean zonal wind profile shown in Figure 37.

storm occurs. Nevertheless, we can infer from the work presented here and from Geller and Alpert (1980) that even with the initial profile of mean zonal wind, the planetary wave structure below the mesopause would not be altered by the thermospheric storm, and we would certainly not expect the wave structure in the lower stratosphere or troposphere to be altered by the storm.

5. SUMMARY AND CONCLUSIONS

A limited review of the literature concerning solar-weather effects on time scales on the order of one month or less, has revealed that the atmosphere may indeed respond to anomalous solar activity, i.e., that we may see changes in atmospheric pressure, temperature and wind following, say, a solar flare or in response to the 27 day solar rotation period. Such responses have been clearly demonstrated in the thermosphere, but the evidence is rather more tenuous below the mesopause. Caution is advised in interpreting the results, since in some cases (e.g., Hicks and Justus (1970)), correlations have been made between atmospheric parameters and parameters which supposedly reflect the behaviour of the sun in some sense, but which in fact may be modulated by the atmosphere's behaviour (e.g., Hines' (1973) discussion, regarding the index Kp). In other instances, different interpretations of the statistical results have been put forward (e.g., King et al. (1977); Schäfer (1979)).

The work of Wilcox et al. (1973), relating atmospheric vorticity to solar magnetic sector crossings, has added impetus to the field, because the sector crossings are unquestionably related to the behaviour of the sun. However, even if a connection between the atmosphere's behaviour and that of the sun has been proven (which many believe is not the case), a physical basis for the linkage has yet to be established. Comparisons between the energy associated with the General Circulation of the atmosphere and that associated with such solar-related events as a geomagnetic storm, even an intense one, (e.g., Willis (1976)), preclude the idea that atmospheric variations can be induced by a direct deposition of energy into the lower atmosphere. Consequently, some

indirect means have been sought to connect solar-induced changes at upper levels with atmospheric variations at lower levels.

Of the mechanisms put forward, we have chosen to investigate that suggested by Hines (1974). This holds that changes in the atmosphere's structure at upper levels may influence the development and resulting structure of planetary-scale waves in the lower atmosphere. In the nomenclature of dynamic meteorology, a solar-related event may induce changes in the basic state (i.e., zonally averaged) wind and static stability structure of the atmosphere, and thereby alter the ability of planetary-scale waves to propagate through the atmosphere. This follows, because from quasi-geostrophic theory, the equation governing the structure of a planetary-scale wave can be couched in the form of an equation representing the propagation of the wave through an atmosphere with a variable index of refraction. This index of refraction in turn is a function of the basic state wind and static stability.

The sensitivity of wave structure to the distribution of basic state wind (and therefore to the distribution of refractive index) has been shown by Schoeberl and Geller (1976). In the course of this study, we have made similar findings, and thus we are in a position to question the sensitivity of planetary-scale wave structure to modulations in refractive index, induced by solar events at relatively high altitudes.

We have constructed a numerical model to test Hines' hypothesis. The model is based on the primitive equations of meteorology within a hemisphere, and is time-dependent. The atmospheric fields are split into a zonally averaged part and a zonally varying part, which is severely truncated to allow only one wave. In this study, we have

considered only wavenumber one. The model is a slightly different version of that developed by Holton (1976) to study the stratospheric sudden warming (SSW). We have examined the sensitivity of the model response to various factors (initial basic state wind, static stability, amplitude of forcing and, by accident, mechanical dissipation) in the context of the SSW and have found that considerable variations occur. The wind profile originally used by Holton (1976) leads to a SSW, which appears to come within the definition of a "major" warming. On the other hand, experiments with two different wind profiles, which are qualitatively similar to Holton's, produce warmings which might be termed "minor". The differences arise because of the differing initial distributions of the latitudinal gradient of basic state potential vorticity ($\overline{\partial q / \partial \theta}$), which to a first approximation is the same as the refractive index (in quasi-geostrophic theory). A larger wave (in the sense of geopotential amplitude) is allowed to develop with Holton's wind profile, than in the other two cases, and thus there are larger eddy heat and momentum fluxes and flux convergences. It is these flux convergences, and the counter effects of adiabatic warming or cooling and coriolis torques, which drive the SSW.

Following Holton (1980, 1981) and Holton and Wehrbein (1980), the combined effects of eddy heat and momentum fluxes is examined through the distribution of the vector quantity \underline{F} , which is analagous to the Eliassen-Palm wave energy flux. The distribution of \underline{F} at selected times reveals how wave energy is "guided" away from regions with negative refractive index, and similarly is "guided" toward regions with large, positive values of refractive index.

It perhaps has not been stressed sufficiently to this point that the wave structure responds to the distribution of refractive index (the quantity Q_s in (3.3)). We have throughout the study referred only to the distribution of $\overline{\partial q / \partial \theta}$, but in fact there are two other terms which comprise Q_s , and examination of (3.3) reveals that the distribution of $\overline{\partial q / \partial \theta}$ is a somewhat liberal guide to expected wave energy propagation and thus to wave structure. The sensitivity of wave structure to the model's mechanical dissipation parameterization was noted in Section 3.2. There is undoubtedly mechanical dissipation of wave energy at high levels of the atmosphere, since the forced, large-scale, quasi-stationary waves are observed to decay in amplitude above the polar night jet. The distribution of this dissipation is uncertain, however, and we have therefore used a simple expression for its vertical variation, in common with other workers. We have also used a simple parameterization of thermal damping, despite the availability of more reasonable schemes for including Newtonian cooling (e.g., Dickinson (1973)).

We have been concerned here only with the sensitivity of wave structure (in both the SSW and the solar-weather studies) to changes in basic state wind. As discussed in Chapter 3, the static stability parameter, N^2 , must remain fixed during the calculations. However, wave structure is also sensitive to the static stability distribution. It would be interesting to pursue the effect that variable static stability had on the development of the SSW, as discussed in Section 3.3. Specifically, the development of the SSW may be altered by allowing N^2 to be determined by the complete basic state temperature field (rather

than a part of it, as is the case here), with its spatial and temporal variability.

Our experiments concerning the solar-weather problem have indicated that we should not expect to see tropospheric or lower-stratospheric wave structure respond to solar effects at high altitudes. These results are in agreement with earlier work of Geller and Alpert (1980), who simply prescribed changes in the mean flow, rather than calculating such changes as a response to solar variability. The identification of diabatic heating in the model with Joule dissipation heating in the atmosphere is useful in terms of being able to cite a reason for imposing such a heating in the model. However, the uncertainty attached to the observed distribution, amplitude and duration of Joule dissipation heating in the atmosphere, and our crude methods of representing the distribution and rather liberal estimates of heating amplitudes and locations (not to mention the simplified atmospheric model used), mean that we are only providing an estimate of what we may expect to happen in the real atmosphere.

Nevertheless, and despite the large heating rates and low levels of maximum forcing we have assumed in some experiments (e.g., a 30 K day^{-1} heating of both the zonally averaged flow and wavenumber one at 70 km), we have been unable to induce a lower-atmospheric response to an upper level "storm". The concepts introduced in Chapter 3, namely the distribution of $\overline{\partial q / \partial \theta}$ and of \underline{F} , prove useful in diagnosing the experiments. Heating in the lower thermosphere produces changes in values of $\overline{\partial q / \partial \theta}$, which are conducive to wave propagation. However, the changes are of a sufficiently local nature, that middle atmospheric refractive indices are unchanged, and thus wave energy flux is diverted away from the

"storm" region. For a "storm" at lower altitudes, the effect on wave structure is quite considerable in the upper stratosphere and mesosphere, but still no effects are noticed in the lower stratosphere.

We have examined the consequences of upper atmospheric effects on the lower atmosphere, since this was Hines' original suggestion. To perform similar experiments, but with solar-induced changes at lower altitudes, could imply that a mechanism other than Joule heating would have to be invoked to explain the basic state atmospheric changes. As noted in Chapter 1, the solar proton event of August 1972 produced considerable changes in the distribution of atmospheric ozone, and yet the findings of Schoeberl and Strobel (1978) seem to indicate that this too has a negligible effect on the lower atmosphere.

In the context of this model therefore, and in the light of other studies, it appears that we have no hope of explaining lower atmospheric responses to solar variations (i.e., solar-weather effects) through the intermediary effect of planetary-scale waves.

BIBLIOGRAPHY

- Asselin, R., 1972: Frequency filter for time integrations. Mon. Wea. Rev., 100, 487-490.
- Banks, P.M., 1977: Observations of Joule and particle heating in the auroral zone. J. Atmos. Terr. Phys., 39, 179-193.
- Banks, P.M., 1979: Joule heating in the high-latitude mesosphere. J. Geophys. Res., 84, 6709-6712.
- Bates, J.R., 1980: On the interaction between a radiatively damped planetary wave and the zonally averaged circulation in the middle atmosphere. Pageoph., 118, 266-283.
- Charney, J.G., 1949: On a physical basis for numerical prediction of large-scale motions in the atmosphere. J. Meteor., 6, 371-385.
- Charney, J.G. and P.G. Drazin, 1961: Propagation of planetary scale disturbances from the lower into the upper atmosphere. J. Geophys. Res., 66, 83-109.
- Ching, B.K. and Y.T. Chiu, 1973: Global distribution of thermospheric heat sources: EUV absorption and Joule dissipation. Planet Space Sci., 21, 1633-1646.
- Cole, K.D., 1962: Joule heating of the upper atmosphere. Austr. J. Phys., 15, 223-235.
- Craig, R.A., 1965: The Upper Atmosphere Meteorology and Physics. Academic Press, 509 pp.
- Dickinson, R.E., 1968: On the exact and approximate linear theory of vertically propagating planetary Rossby waves forced at a spherical lower boundary. Mon. Wea. Rev., 96, 405-415.
- Dickinson, R.E., 1968a: Planetary Rossby waves propagating vertically through weak westerly wind wave guides. J. Atmos. Sci., 25, 984-1002.
- Dickinson, R.E., 1969: Vertical propagation of planetary Rossby waves through an atmosphere with Newtonian cooling. J. Geophys. Res., 74, 929-938.
- Dickinson, R.E., 1973: Method of parameterization for infrared cooling between altitudes of 30 and 70 kilometers. J. Geophys. Res., 78, 4451-4457.
- Dickinson, R.E., E.C. Ridley, and R.G. Roble, 1975: Meridional circulation in the thermosphere. I: Equinox conditions. J. Atmos. Sci., 32, 1737-1754.

- Ebel, A., and W. Bätz, 1977: Response of stratospheric circulation at 10 mb to solar activity oscillations resulting from the sun's rotation. Tellus, 29, 41-47.
- Eliassen, A. and E. Palm, 1961: On the transfer of energy in stationary mountain waves. Geofys. Publ., 22, No. 3, 1-23.
- Geller, M.A. and J.C. Alpert, 1980: Planetary wave coupling between the troposphere and the middle atmosphere as a possible sun-weather mechanism. J. Atmos. Sci., 37, 1197-1215.
- Green, J.S.A., 1972: Large-scale motion in the upper stratosphere and mesosphere: an evaluation of data and theories. Phil. Trans. Roy. Soc. London, 271, 577-583.
- Handbook of Geophysics and Space Environments, 1965. Air Force Cambridge Research Laboratories.
- Hays, P.B., R.A. Jones, and M.H. Rees, 1973: Auroral heating and the composition of the neutral atmosphere. Planet Space Sci., 21, 559-573.
- Heath, D.F., A.J. Krueger, and P.J. Crutzen, 1977: Solar proton event: influence on stratospheric ozone. Science, 197, 886-888.
- Herman, J.R. and R.A. Goldberg, 1978: Sun, Weather, and Climate. NASA publication #SP-426, 360 pp.
- Hicks, J.E. and C.G. Justus, 1970: Response of winds in the 90- to 140- km altitude region to variations in solar activity. J. Geophys. Res., 75, 5565-5570.
- Hines, C.O., 1973: Comments on "A test of an apparent response of the lower atmosphere to solar corpuscular radiation." J. Atmos. Sci., 30, 739-738.
- Hines, C.O., 1974: A possible mechanism for the production of sun-weather correlations. J. Atmos. Sci. 31, 589-591.
- Hirota, I., 1968: Planetary waves in the upper stratosphere in early 1966. J. Met. Soc. Jap., 46, 418-430.
- Hirota, I. and J.J. Barnett, 1977: Planetary waves in the winter mesosphere-preliminary analysis of Nimbus 6 PMR results. Quart. J. Roy. Met. Soc., 103, 487-498.
- Holton, J.R., 1975: The dynamic meteorology of the stratosphere and mesosphere. Meteor. Monogr., No. 37, Amer. Meteor. Soc., 218 pp.
- Holton, J.R., 1976: A semi-spectral numerical model for wave-mean flow interactions in the stratosphere: Application to sudden stratospheric warmings. J. Atmos. Sci., 33, 1639-1649.

- Holton, J.R., 1980: The dynamics of sudden stratospheric warmings. Ann. Rev. Earth Planet. Sci., 8, 169-190.
- Holton, J.R., 1981: The dynamics of sudden stratospheric warmings. Abstracts of the Third Conference on the Meteorology of the Upper Atmosphere, San Diego, p. 63.
- Holton, J.R. and C. Mass, 1976: Stratospheric vacillation cycles. J. Atmos. Sci., 33, 2218-2225.
- Holton, J.R. and W. Wehrbein, 1979: A semi-spectral numerical model for the large scale stratospheric circulation. Middle Atmosphere Project, Report #1, Dept of Atmospheric Sciences, University of Washington, 41 pp.
- Holton, J.R. and W. Wehrbein, 1980: The role of forced planetary waves in the annual cycle of the zonal mean circulation of the middle atmosphere. J. Atmos. Sci., 37, 1968-1983.
- Jacchia, L.G., 1963: Variations in the Earth's upper atmosphere as revealed by satellite drag. Rev. Mod. Phys., 35, 973-991.
- Kanzawa, H., 1980: The behaviour of mean zonal wind and planetary-scale disturbances in the troposphere and stratosphere during the 1973 sudden warming. J. Met. Soc. Jap., 58, 329-356.
- King, J.W., A.J. Slater, A.D. Stevens, P.A. Smith and D.M. Willis, 1977: Large-amplitude standing planetary waves induced in the troposphere by the sun. J. Atmos. Terr. Phys., 34, 1357-1367.
- Lindzen, R.S. and S.-S. Hong, 1974: Effects of mean winds and horizontal temperature gradients on solar and lunar semidiurnal tides in the atmosphere. J. Atmos. Sci., 31, 1421-1446.
- Lordi, N.J., A. Kasahara, and S.K. Kao, 1981: Numerical simulation of stratospheric sudden warmings with a primitive equation spectral model. To appear in J. Atmos. Sci.
- Madden, R.A., 1978: Further evidence of traveling planetary waves. J. Atmos. Sci., 35, 1605-1618.
- Matsuno, T., 1970: Vertical propagation of stationary planetary waves in the winter northern hemisphere. J. Atmos. Sci., 27, 871-883.
- Matsuno, T., 1971: A dynamical model of the stratospheric sudden warming. J. Atmos. Sci., 28, 1479-1494.
- McInturff, R.M., 1978: Stratospheric warmings: Synoptic, dynamic, and general circulation aspects. NASA publication #1017, 166 pp.
- Nastrom, G.D. and A.D. Belmont, 1978: Preliminary reports on the 27 day solar rotation variation in stratospheric zonal winds. Geophys. Res. Lett., 5, 665-668.

- Noonkester, V.R., 1967: An apparent response of 100-millibar winds to increases in geomagnetic activity. J. Geophys. Res., 72, 1275-1282.
- O'Neill, A., 1981: A diagnostic analysis of stratospheric warmings during a northern hemisphere winter based on Eliassen-Palm fluxes, their convergence, and residual mean-meridional circulations. Abstracts of the Third Conference on the Meteorology of the Upper Atmosphere, San Diego, p. 64.
- Ramakrishna, S. and R. Seshamani, 1973: The effect of solar activity on temperatures in the equatorial mesosphere. J. Atmos. Terr. Phys., 35, 1631-1641.
- Ramakrishna, S., and R. Seshamani, 1976: Day-night dependence of geomagnetic activity effects on mesospheric temperature. J. Geophys. Res., 81, 6173-6176.
- Ramanathan, V., L.B. Callis, and R.E. Boughner, 1976: Sensitivity of surface temperature and atmospheric temperature to perturbations in the stratospheric concentration of ozone and nitrogen dioxide. J. Atmos. Sci., 33, 1092-1112.
- Richmond, A.D., 1979: Thermospheric heating in a magnetic storm: dynamic transport of energy from high to low latitudes. J. Geophys. Res., 84, 5259-5266.
- Roberts, W.O., and R.H. Olson, 1973: Geomagnetic storms and wintertime 300-mb trough development in the north Pacific-north America area. J. Atmos. Sci., 30, 135-140.
- Roble, R.C., 1977: The Thermosphere. In: The upper atmosphere and magnetosphere. NRC publication, 168 pp.
- Sato, Y., 1980: Observational estimates of Eliassen and Palm flux due to quasi-stationary planetary waves. J. Met. Soc. Jap., 58, 430-435.
- Schäfer, J., 1979: The evaluation of solar induced planetary waves at the 500 mb level. Geophys. Astrophys. Fluid Dynamics, 13, 263-272.
- Schmitz, G. and N. Greiger, 1980: Model calculations on the structure of planetary waves in the upper troposphere and lower stratosphere as a function of the wind field in the upper stratosphere. Tellus, 32, 207-214.
- Schoeberl, M.R., 1978: Stratospheric warmings: Observations and theory. Rev. Geoph. Sp. Phys., 16, 521-538.
- Schoeberl, M.R. and M.A. Geller, 1976: The structure of stationary planetary waves in winter in relation to the polar night jet intensity. Geophys. Res. Lett., 3, 177-180.

- Schoeberl, M.R. and D.F. Strobel, 1978: The response of the zonally averaged circulation to stratospheric ozone reductions. J. Atmos. Sci., 35, 1751-1757.
- Schoeberl, M.R. and D.R. Strobel, 1980: Numerical simulation of sudden stratospheric warming. J. Atmos. Sci., 37, 214-236.
- Schuermans, C.J.E., 1979: Effects of solar flares on the atmospheric circulation. Solar-Terrestrial Influences on Weather and Climate, D. Reidel Publ. Co., 105-118.
- Shapiro, R., 1973: Reply to: Comments on "A test of an apparent response of the lower atmosphere to solar corpuscular radiation." J. Atmos. Sci., 30, 741-744.
- Simmons, A.J., 1974: Planetary-scale disturbances in the polar winter stratosphere. Quart. J. Roy. Met. Soc., 100, 76-108.
- Somerville, R.C.J., J.E. Hansen, P.H. Stone, W.J. Quirk, and A.A. Lacis, 1973: Numerical experiments on short-term meteorological effects of solar variability. NASA publication #SP-366, pp. 199-211.
- Tung, K.K. and R.S. Lindzen, 1979: A theory of stationary long waves. Part II: Resonant Rossby waves in the presence of realistic vertical shears. Mon. Wea. Rev., 107, 735-750.
- U.S. Standard Atmosphere, 1976: NOAA publication, 227 pp.
- Volland, H., 1979: Possible mechanisms of solar activity-weather effects involving planetary waves. Solar-terrestrial Influences on Weather and Climate, D. Reidel Publ. Co., 263-274.
- Volland, H., and J. Schäfer, 1979: Cause and effect in some types of sun-weather-relationships. Geophys. Res. Lett., 6, 17-20.
- Wilcox, J.M. 1973: Solar activity and the weather. NASA publication #SP-366, pp. 25-38.
- Wilcox, J.M., P.H. Scherrer, L. Svalgaard, W.O. Roberts, R.H. Olson, and R.L. Jenne, 1974: Influence of solar magnetic sector structure on terrestrial atmospheric vorticity. J. Atmos. Sci., 31, 581-588.
- Willis, D.M., 1976: The energetics of sun-weather relationships: magnetospheric processes. J. Atmos. Terr. Phys., 38, 685-698.

APPENDIX I LIST OF SYMBOLS

A	available potential energy
D	typical depth scale; diffusion operator
\underline{F}	analog of wave energy flux (see (3.20))
H	scale height (= 7 km)
J'	diabatic heating function
K	diffusion coefficient ($K/\Delta y^4 = 5 \times 10^{-7} \text{ m}^4 \text{ s}^{-1}$); kinetic energy
L	typical length scale
N^2	static stability parameter ($= 4 \times 10^{-4} \text{ s}^{-2}$)
P	total potential energy
\bar{P}	analog of quasi-geostrophic potential vorticity flux (see (3.19))
Q', \bar{Q}	perturbation and zonally averaged diabatic heat source
Q_s	(refractive index) ²
R	gas constant for dry air
R_o	Rossby number $\equiv (U/2\Omega L)$
S', \bar{S}	diabatic terms in perturbation and mean potential vorticity equations
T	temperature
U	typical velocity scale; zonally averaged zonal wind ($\equiv \bar{u} e^{-z/2H}$)
V	zonally averaged meridional wind ($\equiv \bar{v} e^{-z/2H}$)
Z	vertical structure function (Appendix III)

a	earth's radius
c_p	specific heat of dry air at constant pressure
f	coriolis parameter
g	gravitational acceleration
h_T	maximum amplitude of forcing wave
i	latitudinal index in numerical model (regular grid)
j	latitudinal index in numerical model (staggered grid)
k	vertical index in numerical model
ℓ	$2\Omega a/N$
m	longitudinal wavenumber ($\equiv s/a\cos\theta$)
n	temporal index in numerical model
n^2	(refractive index) ²
p	pressure
q', \bar{q}	perturbation and zonally averaged potential vorticity
$\partial\bar{q}/\partial\theta$	latitudinal gradient of basic state potential vorticity
s	longitudinal wavenumber
t	time
$u'(\text{or } u), \bar{u}$	perturbation and zonally averaged zonal wind
$v'(\text{or } v), \bar{v}$	perturbation and zonally averaged meridional wind
\bar{v}^*	residual meridional velocity
w', \bar{w}	perturbation and zonally averaged vertical wind
\bar{w}^*	residual vertical velocity
x	longitudinal coordinate ($= a \cos\theta \cdot \lambda$)
y	latitudinal coordinate ($= a\theta$)
y_F, y_E	latitude of maximum diabatic heating and e-folding scale of forcing

z	vertical coordinate ($= H \ln(p_0/p)$)
z_F, z_E	height of maximum diabatic heating and e-folding scale of forcing
A	amplitude of diabatic heating
F_x, F_y, F	momentum flux divergence
H, \mathcal{G}	heat flux and its divergence
$\mathcal{L}_y, \mathcal{L}_z$	horizontal, vertical operators
α_R, α_N	coefficients of Rayleigh friction and Newtonian cooling
β	df/dy
θ	latitude
θ'	potential temperature
κ	R/c_p
λ	longitude
μ	$\cos\theta$ (Appendix III)
ν	parameter in Asselin time filter ($= .02$)
ρ_0	globally averaged density ($\equiv \rho_0(z)$)
σ	dissipative (e-folding time) $^{-1}$; frequency (Appendix III)
$\bar{\omega}$	angular velocity ($\bar{u}/a \cos\theta$)
ω	dp/dt
$\Delta y, \Delta z, \Delta t$	horizontal, vertical, temporal increments in numerical model
ϕ' (or ϕ), $\bar{\phi}$	perturbation and zonally averaged geopotential
ϕ_0	globally averaged geopotential $\equiv \phi_0(z)$
$\bar{\phi}^*$	zonally averaged initial geopotential ($\equiv \psi^* e^{z/2H}$)
ψ	zonally averaged geopotential ($\equiv \bar{\phi} e^{-z/2H}$)
Ω	frequency of earth's rotation

APPENDIX II INDICES OF GEOMAGNETIC ACTIVITY

- C: A value of between 0 and 2 is assigned to the fluctuation in the Earth's magnetic field strength and direction at one location. 0 = quiet; 1 = moderately disturbed; 2 = greatly disturbed.
- Ci: A daily average of C values at all observatories. 0.0 = quiet; 2.0 = most disturbed, on a global basis.
- K: An index of the largest excursion of magnetic field strength in all three directions over a three hour period at one station. 0 = quiet; 9 = most disturbed.
- Kp: A "planetary" version of K, in which values of K at 12 stations between geomagnetic latitudes 48° and 63° in both hemispheres are averaged.
- Cp: Global value of Kp, derived from eight consecutive values of Kp. 0.0 = quiet; 2.0 = most disturbed. The value of Cp is approximately logarithmically proportional to the range of values defining Kp.
- Ap: As Cp, but the values are approximately linearly proportional to the range of values defining Kp.
- Dst: A measure of equatorial geomagnetic activity due to ring currents. Variations in ring current at equal longitude spacings are taken at latitudes away from the region of the auroral and equatorial electrojet.

AE: A measure of activity in the auroral zone, derived from differences around a latitude circle of the horizontal electric current over short time intervals.

Solar magnetic sector structure:

The solar magnetic field is divided into four sectors. In each, the magnetic field polarity is fixed, but oppositely directed from that in neighbouring sectors. The polarity is either toward or away from the sun, as Figure A1 schematically indicates. The pattern rotates with the sun, once every 27 days (approximately). Thus, as the sun rotates, the polarity of the solar magnetic field switches (from "toward" to "away from") four times in each solar rotation.

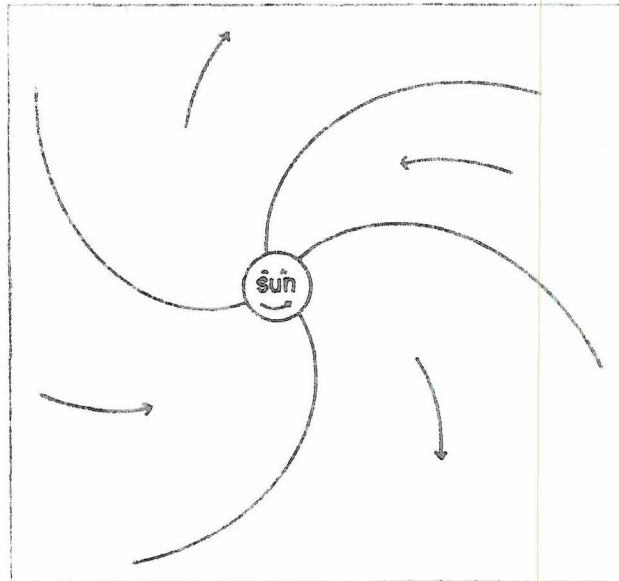


Figure A1 Observed solar magnetic sector structure, from Herman and Goldberg (1978). Arrows denote 3-hour measurements of interplanetary magnetic field direction.

APPENDIX III ANALYSIS FOR BOUNDARY FORCING FUNCTION

Matsuno (1970) and Holton (1976) used different forcing functions at their model lower boundaries. The two correspond to the function given by (2.39) with $s = 2$ and 1 , respectively. Holton (1976) used a \sin^2 profile at the lower boundary, in order to satisfy the condition $\partial\phi'/\partial y = 0$ at the pole for wavenumber two. However, as we show below, we must also have $\partial^2\phi'/\partial y^2 = 0$ at the pole for wavenumber one. Holton's (1976) function does not meet this requirement, whereas (2.39) does.

Consider the perturbation equations of motion, linearised about a motionless, adiabatic, isothermal basic state, in spherical geometry:

$$\frac{\partial u'}{\partial t} - fv' = -\frac{\partial\phi'}{\partial x} \quad (\text{III.1})$$

$$\frac{\partial v'}{\partial t} + fu' = -\frac{\partial\phi'}{\partial y} \quad (\text{III.2})$$

$$\frac{\partial}{\partial t} \left(\frac{\partial\phi'}{\partial z} \right) + N^2 w' = 0 \quad (\text{III.3})$$

$$\frac{\partial u'}{\partial x} + \frac{1}{\cos\theta} \frac{\partial(v' \cos\theta)}{\partial y} + \left(\frac{\partial}{\partial z} - \frac{1}{H} \right) w' = 0, \quad (\text{III.4})$$

where $x = a\cos\theta.\lambda$ and $y = a\theta$ (θ is latitude).

We eliminate w' between (III.3) and (III.4) and, assuming

$$\begin{pmatrix} u' \\ v' \\ \phi' \end{pmatrix} = \begin{pmatrix} u(y) \\ v(y) \\ \phi(y) \end{pmatrix} Z(z) e^{i(\sigma t + s\lambda)}, \quad (\text{III.5})$$

we have:

$$i\sigma u - fv = -\frac{is\phi}{a\cos\theta} \quad (\text{III.6})$$

$$i\sigma v + fu = -\frac{d\phi}{ad\theta} \quad (\text{III.7})$$

$$\frac{isu}{a\cos\theta} + \frac{1}{a\cos\theta} \frac{d(v\cos\theta)}{d\theta} + \frac{i\sigma}{gh} \phi = 0. \quad (\text{III.8})$$

Equations (III.6) - (III.8) are the horizontal equations, which can be reduced to Laplace's Tidal Equation. The separation constant, h , is called the equivalent depth. The Vertical Structure Equation in Z is not used here.

We define $\mu = \cos\theta$ and expand all variables in power series in μ , where we assume μ to be small (i.e., we are near the pole).

Thus, for example,

$$u = u_0 + u_1\mu + u_2\mu^2 + \dots \quad (III.9)$$

Substituting the expanded variables into (III.6) - (III.8) yields:

$$\begin{aligned} i\sigma (u_0 + u_1\mu + u_2\mu^2 + \dots) - 2\Omega \left(1 - \frac{\mu^2}{2} - \dots\right) (v_0 + v_1\mu + v_2\mu^2 + \dots) \\ = -\frac{is}{a\mu} (\phi_0 + \phi_1\mu + \phi_2\mu^2 + \dots) \end{aligned} \quad (III.10)$$

$$\begin{aligned} i\sigma (v_0 + v_1\mu + v_2\mu^2 + \dots) + 2\Omega \left(1 - \frac{\mu^2}{2} - \dots\right) (u_0 + u_1\mu + u_2\mu^2 + \dots) \\ = \frac{1}{a} \left(1 - \frac{\mu^2}{2} - \dots\right) (\phi_1 + 2\phi_2\mu + 3\phi_3\mu^2 + \dots) \end{aligned} \quad (III.11)$$

$$\begin{aligned} \frac{is}{a\mu} (u_0 + u_1\mu + u_2\mu^2 + \dots) - \frac{1}{a\mu} \left(1 - \frac{\mu^2}{2} - \dots\right) (v_0 + v_1\mu + v_2\mu^2 + \dots) \\ - \frac{1}{a} \left(1 - \frac{\mu^2}{2} - \dots\right) (v_1 + 2v_2\mu + 3v_3\mu^2 + \dots) \\ + \frac{i\sigma}{gh} (\phi_0 + \phi_1\mu + \phi_2\mu^2 + \dots) = 0. \end{aligned} \quad (III.12)$$

In (III.10) - (III.12), we have used $\sin\theta = (1 - \mu^2)^{\frac{1}{2}}$. Since we are interested in the behaviour of the fields u , v , and ϕ as $\mu \rightarrow 0$, we multiply (III.10) and (III.12) by μ and first examine the zeroth order equations (terms involving μ^0).

$$(III.10) \quad \Rightarrow \quad \frac{is}{a} \phi_0 = 0 \quad (III.13)$$

$$(III.11) \Rightarrow i\sigma v_0 + 2\Omega u_0 = \frac{\phi_1}{a} \quad (III.14)$$

$$(III.12) \Rightarrow \frac{isu_0}{a} - \frac{v_0}{a} = 0. \quad (III.15)$$

Referring back to (III.9) and comparing the expansion with the usual Taylor series expansion of a function, say Ψ , we can regard Ψ_0 , Ψ_1 and Ψ_2 as the values of the function and its first and second derivatives, evaluated at the pole ($\mu = 0$). Thus (III.13) implies that $\Phi'(\theta = \pi/2) = 0$ for $s \neq 0$.

Looking now at the first order equations (terms involving μ) we have:

$$(III.10) \Rightarrow i\sigma u_0 - 2\Omega v_0 = -\frac{is}{a} \phi_1 \quad (III.16)$$

$$(III.11) \Rightarrow i\sigma v_1 + 2\Omega u_1 = \frac{2\phi_2}{a} \quad (III.17)$$

$$(III.12) \Rightarrow \frac{isu_1}{a} - \frac{2v_1}{a} + \frac{i\sigma\phi_0}{gh} = 0. \quad (III.18)$$

From (III.15), we have

$$v_0 = isu_0.$$

Substituting this into (III.16) gives:

$$i(\sigma - 2\Omega s) u_0 = -\frac{is}{a} \phi_1 \quad (III.19)$$

but (III.14) states that

$$i(\sigma s^2 - 2\Omega s) u_0 = -\frac{is}{a} \phi_1. \quad (III.20)$$

Equations (III.19) and (III.20) are only consistent if $s = 1$. Otherwise, we must have the trivial solution $(u_0, v_0, \phi_1) = \underline{0}$. Thus:

$$\text{for } s > 1, \quad \left(u', v', \frac{\partial \Phi'}{\partial y} \right)_{\text{pole}} = 0 \quad (\text{III.21})$$

$$\text{for } s = 1, \quad \left(u', v', \frac{\partial \Phi'}{\partial y} \right)_{\text{pole}} \neq 0 \text{ is allowed.} \quad (\text{III.22})$$

Equation (III.21) is a familiar result, and is invoked by Holton (1976) to produce his forcing function, Φ_B .

Proceeding to the second order equations,

$$\text{(III.10)} \Rightarrow i\omega u_1 - 2\Omega v_1 = -\frac{is}{a} \Phi_2 \quad (\text{III.23})$$

$$\text{(III.11)} \Rightarrow i\omega v_2 + 2\Omega u_2 - \Omega u_0 = \frac{3\Phi_3}{a} - \frac{\Phi_1}{2a} \quad (\text{III.24})$$

$$\text{(III.12)} \Rightarrow \frac{isu_2}{a} - \frac{3v_2}{a} + \frac{v_0}{a} + \frac{i\sigma\Phi_1}{gh} = 0 \quad (\text{III.25})$$

From (III.18), using (III.13), we have

$$v = \frac{isu_1}{2};$$

so that (III.23) gives us

$$i(\omega - s\Omega) u_1 = -\frac{is}{a} \Phi_2, \quad (\text{III.26})$$

whilst (III.17) gives

$$i \left(\frac{\sigma s^2}{4} - s\Omega \right) u_1 = -\frac{is}{a} \Phi_2. \quad (\text{III.27})$$

Again for consistency therefore, we must have either $s = 2$ or $u_1 = v_1 = \Phi_2 = 0$. So:

$$\text{for } s = 2 \quad \left(\frac{\partial u'}{\partial y}, \frac{\partial v'}{\partial y}, \frac{\partial^2 \Phi'}{\partial y^2} \right)_{\text{pole}} \neq 0 \text{ is allowed} \quad (\text{III.28})$$

$$\text{for } s \neq 2 \quad \left(\frac{\partial u'}{\partial y}, \frac{\partial v'}{\partial y}, \frac{\partial^2 \Phi'}{\partial y^2} \right)_{\text{pole}} = 0. \quad (\text{III.29})$$

Equation (III.29) represents the result we have been seeking, since it tells us that for wavenumber one, $\partial^2\phi'/\partial y^2$ must be zero at the pole. Hence, we require the forcing function at the lower boundary to satisfy this condition, and thus we use the form given by (2.39).

THE UNIVERSITY OF CHICAGO
LIBRARY
540 EAST 57TH STREET
CHICAGO, ILL. 60637
TEL: 773-936-3200
WWW.CHICAGO.EDU

THE UNIVERSITY OF CHICAGO
LIBRARY
540 EAST 57TH STREET
CHICAGO, ILL. 60637
TEL: 773-936-3200
WWW.CHICAGO.EDU

THE UNIVERSITY OF CHICAGO
LIBRARY
540 EAST 57TH STREET
CHICAGO, ILL. 60637
TEL: 773-936-3200
WWW.CHICAGO.EDU